Research Report 2016-02
Civil & Natural Resources Engineering

UNIVERSITY OF CANTERBURY
Te Whare Wānanga o Waitaha
CHRISTCHURCH NEW ZEALAND

THE SIMPLE LATERAL MECHANISM ANALYSIS (SLAMA) FOR THE SEISMIC PERFORMANCE ASSESSMENT OF A CASE STUDY BUILDING DAMAGED IN THE 2011 CHRISTCHURCH EARTHQUAKE

Dr. Ciro Del Vecchio
Eng. Roberto Gentile
Prof. Stefano Pampanin

ISSN 1172-9511

UC ENGINEERING

June 2017

University of Canterbury
Civil and Natural Resources Engineering

Research report N. 2016-2

The Simple Lateral Mechanism Analysis (SLaMA) for the seismic performance assessment of a case study building damaged in the 2011 Christchurch earthquake

By:

Dr. Ciro Del Vecchio
Eng. Roberto Gentile
Prof. Stefano Pampanin

2017

ISSN 1172-9511

Table of Contents

1. INTRODUCTION

This report presents the simplified seismic assessment of a case study reinforced concrete (RC) building following the newly developed and refined NZSEE/MBIE guidelines on seismic assessment (NZSEE/MBIE, semi-final draft 26 October 2016).

After an overview of the step-by-step 'diagnostic' process, including an holistic and qualitative description of the expected vulnerabilities and of the assessment strategy/methodology, focus is given, whilst not limited, to the implementation of a Detailed Seismic Assessment (DSA) (NZSEE/MBIE, 2016c).

The DSA is intended to provide a more reliable and consistent outcome than what can be provided by an initial seismic assessment (ISA). In fact, while the Initial Seismic Assessment (ISA), of which the Initial Evaluation Procedure is only a part of, is the more natural and still recommended first step in the overall assessment process, it is mostly intended to be a coarse evaluation involving as few resources as reasonably possible.

It is thus expected that an ISA will be followed by a Detailed Seismic Assessment (DSA) not only where the threshold of 33%NBS is not achieved but also where important decisions are intended that are reliant on the seismic status of the building.

The use of %NBS (% New Building Standard) as a capacity/demand ratio to describe the result of the seismic assessment at all levels of assessment procedure (ISA through to DSA) is deliberate by the NZSEE/MBIE guidelines (Part A) (NZSEE/MBIE 2016a). The rating for the building needs only be based on the lowest level of assessment that is warranted for the particular circumstances. Discussion on how the %NBS rating is to be determined can be found in Section A3.3 (NZSEE/MBIE 2016a), and, more specifically, in Part B for the ISA (NZSEE/MBIE 2016b) and Part C for the DSA (NZSEE/MBIE 2016c).

As per other international approaches, the DSA can be based on several analysis procedures to assess the structural behaviour (linear, nonlinear, static or dynamic, force or displacement-based). The significantly revamped NZSEE 2016 Seismic Assessment Guidelines strongly recommend the use of an analytical (basically 'by hand') method, referred to the Simple Lateral Mechanism Analysis (SLaMA) as a first phase of any other numerically-based analysis method. Significant effort has thus been dedicated to provide within the NZSEE 2016 guidelines (NZSEE/MBIE 2016c) a step-by-step description of the procedure, either in general terms (Chapter 2) or with specific reference to Reinforced Concrete Buildings (Chapter 5).

More specifically, extract from the guidelines, NZSEE *"recommend using the Simple Lateral Mechanism Analysis (SLaMA) procedure as a first step in any assessment. While SLaMA is essentially an analysis technique, it enables assessors to investigate (and present in a simple form)*

the potential contribution and interaction of a number of structural elements and their likely effect on the building's global capacity. In some cases, the results of a SLaMA will only be indicative. However, it is expected that its use should help assessors achieve a more reliable outcome than if they only carried out a detailed analysis, especially if that analysis is limited to the elastic range

For complex structural systems, a 3D dynamic analysis may be necessary to supplement the simplified nonlinear Simple Lateral Mechanism Analysis (SLaMA)."

This report presents the development of a full design example for the the implementation of the SLaMA method on a case study buildings and a validation/comparison with a non-linear static (pushover) analysis.

The step-by-step-procedure, summarized in Figure 1, will be herein demonstrated from a component level (beams, columns, wall elements) to a subassembly level (hierarchy of strength in a beam-column joint) and to a system level (frame, C-Wall) assuming initially a 2D behaviour of the key structural system, and then incorporating a by-hand 3D behaviour (torsional effects).

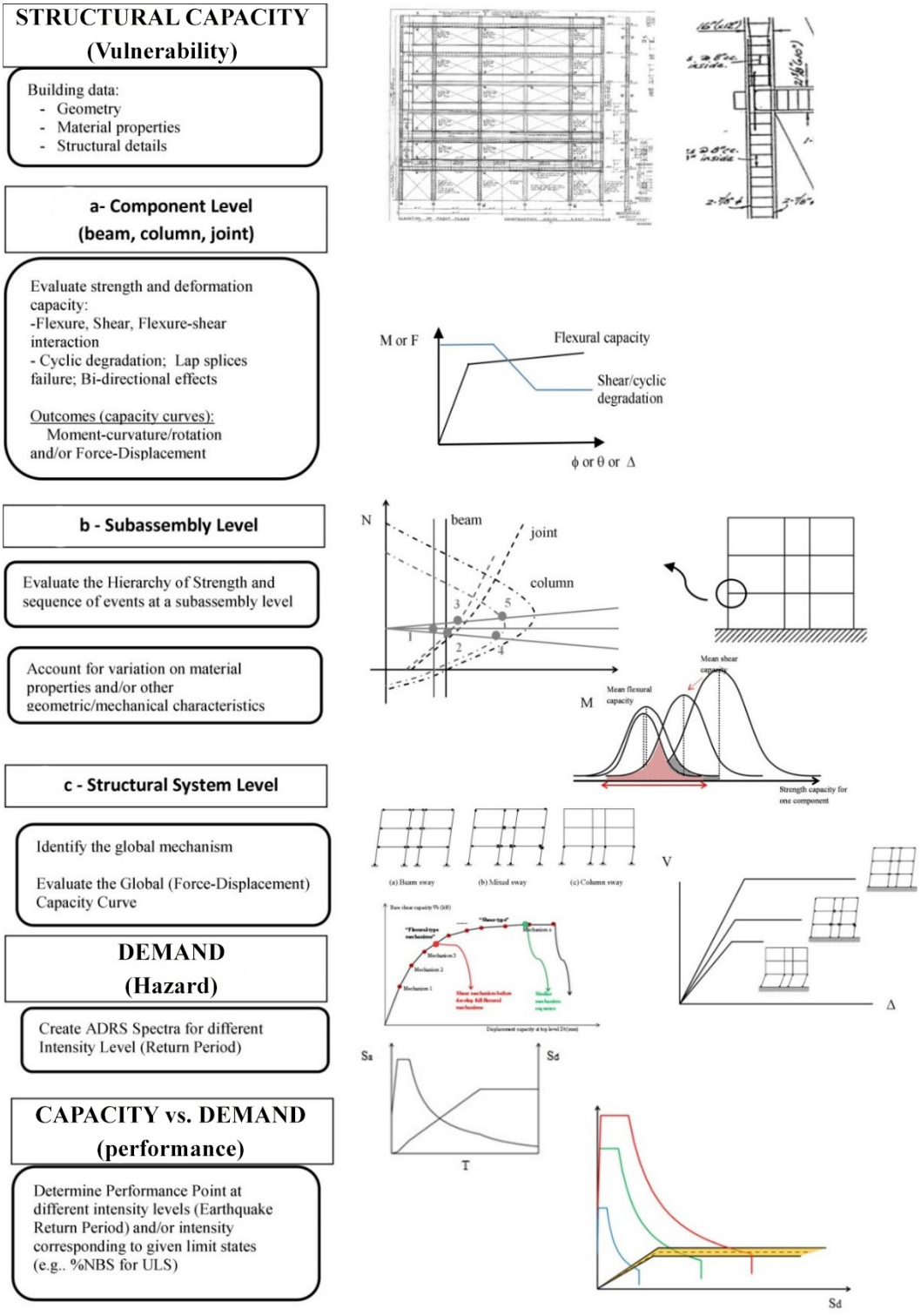

Figure 1: Flow-Chart of Performance Evaluation of RC Structures: from local (material-component) to Global (system) level.

While providing a complete demonstration of the overall procedure, few examples of detailed analytical calculations for selected structural components will be given. Results of key parameters (strength and deformations) of all elements, necessary to derive the global mechanism, are also provided.

The effectiveness of the SLaMA approach (and the related approximations) is this then demonstrated through a comparison with a refined 2D numerical pushover analyses, using a lumped plasticity model for each lateral resisting system.

The case study building is one of the RC buildings severely damaged during the Christchurch earthquake 2011 (Pampanin et al. 2012). In order to show the ability of the adopted assessment procedure to capture the actual observed failure mechanism and the relevant structural damage, a comparison with the damage detected in the aftermath of the Christchurch (2011) earthquake is also provided.

More specifically, references will be made to NZSEE/MBIE guidelines (NZSEE/MBIE 2016c), version 10 October 2016: Chapters C1-C2 for the overall approach, Chapter C5 – Concrete for the main structural systems, Chapter C7 –infills frame to consider the effect of spandrel beams (included in the architectural drawings, but not in the structural ones), Chapter C4 geotechnical aspects, but also on the general holistic description of the expected vulnerability (Sections C1-C2).

Furthermore, in order to convey the importance of structural detailing, a controlled variation of the structural details (e.g. stirrups spacing in the joints, contribution of wall flanges, non-ductile RC column for interior gravity frames) has been considered as potential alternative scenarios and the effect on the structural response qualitatively (or briefly quantitatively) described.

In particular:

- Structural Capacity (Vulnerability): Assessing the lateral capacity of the building in terms of capacity curve (push-over) by using the procedure descried at C5 of the NZSEE/MBIE guidelines (NZSEE/MBIE 2016c). This goal can be achieved starting from the building data collection (geometry, material properties and structural details, key structural elements and potential structural weaknesses) which allows the estimation of the probable component capacity (a) in terms of moment-drift accounting for all the possible failure modes (flexural, shear, lap splice, etc.). At subassembly level (b), the probable inelastic behaviour of elements is evaluated by comparing probable member capacities with the hierarchy of strength.
  At the structural system level (c), a fuse of capacity curves can be obtained considering the beam sidesway and column sidesway (they represent the upper and lower bound of the actual frame capacity, respectively) and the mixed sidesway mechanisms (which consider the strength hierarchy at subassembly level). The probable strength and the variability of material properties (uncertainties) should be also properly accounted for. Once that the capacity curves of the lateral resisting systems are estimated, they can be combined to assess the 2D building lateral capacity in each of the principal directions. The (3D) torsional effects are also considered with a simplified approach.

- Demand (Hazard): Evaluate the seismic demand (Hazard) through the acceleration-displacement response spectrum (ADRS) accounting for site effects (C3 of the NZSEE/MBIE 2017);

- Capacity vs. Demand (Performance): Performance point evaluation through comparison of Capacity vs. Demand to assess the %NBS (C2 of the NZSEE/MBIE 2017).

2. BUILDING DESCRIPTION

2.1. **Overview**

The case study building is an 8-storey RC building (Securities House, located at 221 Gloucester Street) which was used as commercial office before February 2011, when the Canterbury Earthquake occurred. It was built in 1974 and designed when Capacity design and seismic details had not been introduced yet. Although the capacity design was officially introduced in the New Zealand code in 1976 (MOW 1976), already improved detailing were included in some by-laws (early 1970s) and this design example reflects somehow an example of good practice of the day. Well-detailed columns and beam-column joints and capacity design (by requiring flexural strengths of columns at a beam column joint to exceed the corresponding sum of the beam flexural strengths) were introduced (MOW 1968).

Basic information on the building characteristics and its location is reported in Table 1 and Figure 2.

Table 1: Building information

	INFORMATION
BUILDING NAME	Securities House
BUILDING LOCATION	221 Gloucester Street
NUMBER OF STOREY ABOVE GROUND	8
STOREY HEIGHT	3.05m
AGE	1974 (built year), designed in the pre-70's
STRUCTURAL TYPE	RC Frames with C-shaped Wall and gravity columns
BUILDING TYPOLOGY	Pre-70s RC Mid-to-High Rise
OCCUPANCY TYPE	Commercial office
SOIL TYPE	D (soft soil)

Figure 2: Aerial view of the building (Pampanin et al. 2012).

The selected building is part of the ensemble of buildings inspected in the aftermath of the Christchurch 2011 earthquake. A general overview of the building performances grouped in building classes is reported in Pampanin et al. (2012) along with a discussion on the common structural weaknesses. Details on the building geometry, structural configuration, reinforcement details and detected damage are reported in Pampanin et al. (2012).

2.2. **Structural system**

As shown in Figure 3 and Figure 4, where basic plan and elevation views are reported, the building structural systems consist of:

- reinforced concrete frame in the longitudinal direction (N-S or Y-direction, indicated as Frame 1);
- reinforced concrete perimeter frame systems in the transverse direction (E-W or X-direction, indicated as Frame A and Frame D);
- a C-shaped reinforced concrete structural wall and an inner L-shaped singly reinforced concrete walls with mesh on the east side of the building (where staircases are located);
- The Floor system consists of a cast-in-situ 5 in. or 10in. thick depending on location;
- Interior gravity columns are adopted in the central part of the building.

The building, thus, presents a combination of frames and a core wall located on the east side (staircase), leading to strength-stiffness eccentricity and potential inelastic torsion effects.

In the Y-direction, the wall web is connected to exterior columns by framing beams creating a symmetric dual system. Even though the two wall flanges in the X-directions have the role to supports the flat slab, their contribution to the lateral building stiffness cannot be neglected.

As a first step in this design example, it is assumed to decouple the behaviour of the C-wall in the two main directions.

The foundation system consists of single footings with piles for columns, connected by slender foundation beams/strips and foundation deep beams with piles for the walls. The footings are all connected via shallow foundation beams.

Plan and elevation view of the critical structural systems are shown in Figure 3 and Figure 4. The building has a regular shape but unbalanced resisting system due to the location of the C-shape wall (staircase) on the east side with no counterpart on the west facade.

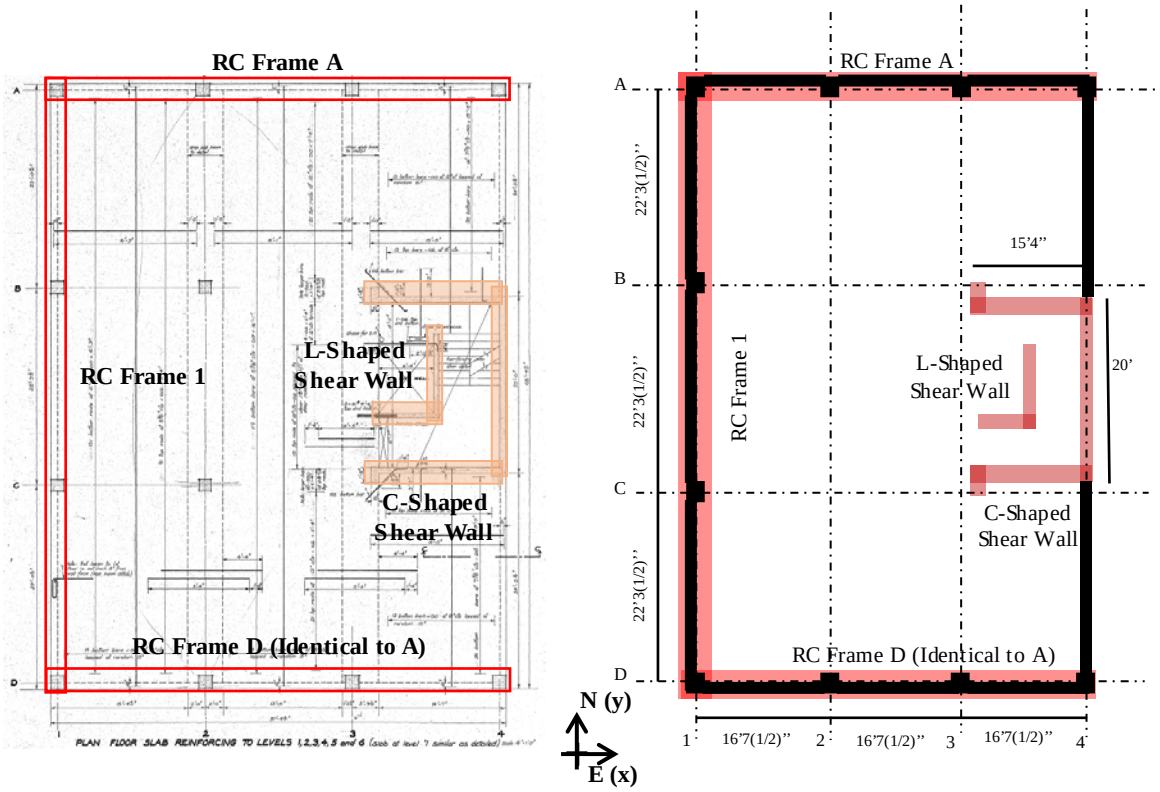

Figure 3: Ground floor plan view of the case study building with illustration of structural systems (Chen 2015).

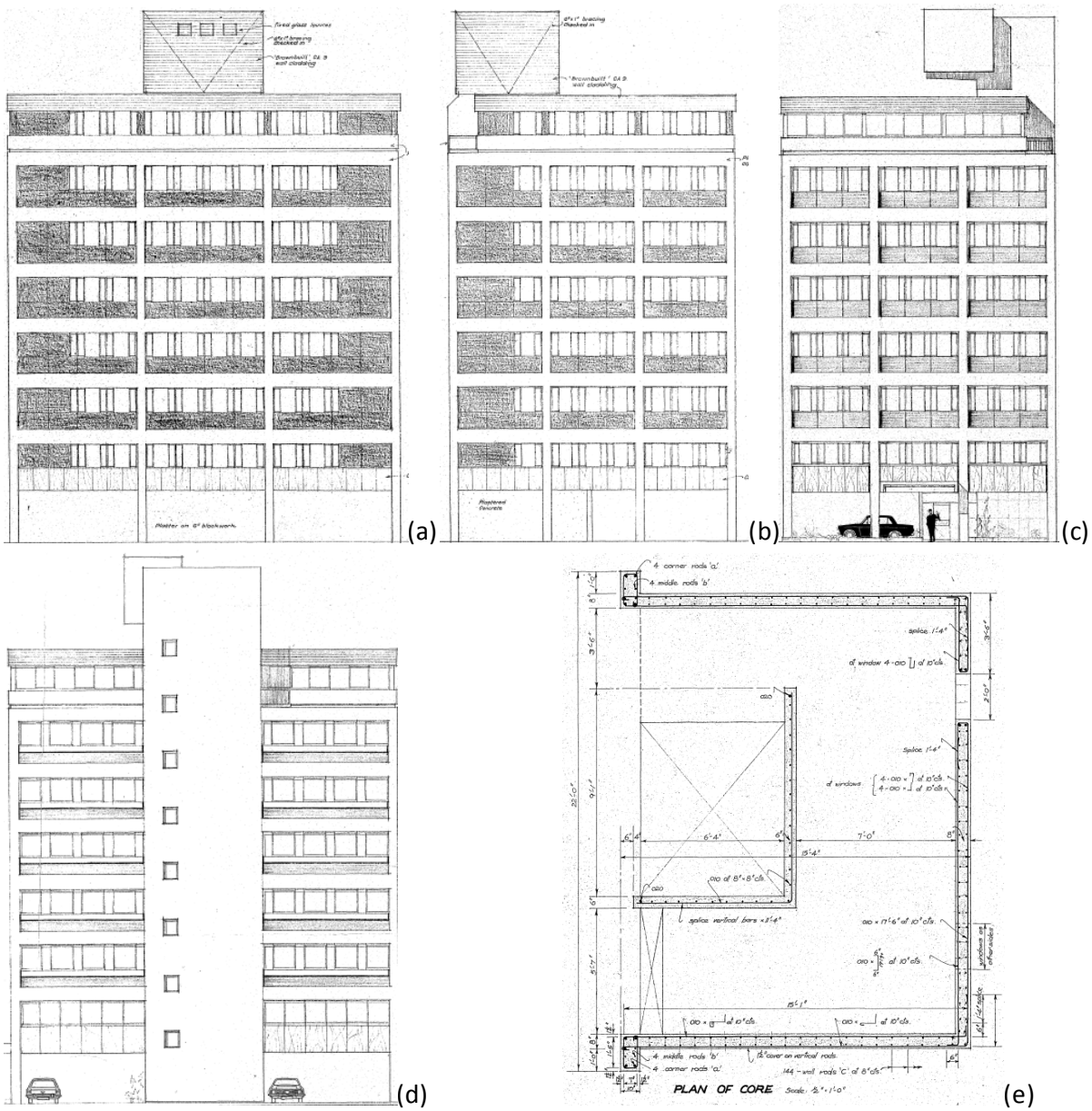

Figure 4: Frame systems elevation view (a) Longitudinal Frame 1 (west elevation view); (b) Transverse Frame A (north elevation view); (c) Transverse Frame D (south elevation view); (d) C-shaped shear walls (east elevation view); (e) C-shaped shear wall and inner L-shaped wall (plan view).

Table 2: Summary of the main structural systems and other components

Structural System	*Type*	*Load*
Frame 1	Seismic resistant RC frame	Resist lateral load in longitudinal direction Resist gravity load
Frame A	Seismic resistant RC frame	Resist lateral load in transverse direction Resist gravity load
Frame D	Same as Frame A	Same as Frame A
C-shaped Shear Wall	Seismic resistant RC shear wall	Resist gravity load from stairs, slabs or building equipment Resist lateral load from both longitudinal and transverse directions
L-shaped Wall	Gravity-load wall	Resist gravity load from stairs or building equipment
Interior Frames	Gravity-load columns	Resist gravity load
Foundation System	Single footings on piles for columns and deep beams on piles for walls. Standard Franki cast in-situ piles.	Footings are connected using slender foundation beams.

NOTE: "Gravity load" in the table is a general term describing load from vertical direction, including live load, etc.

The pre-stressed 5" (127 mm) RC flat slab was casted in-situ. In correspondence of the inner line connecting interior columns (lines 2 and 3), the slab thickness was increased to 10" (254 mm) for a width about 1 m. Perimeter frames resist the lateral seismic actions. For instance, Frame 1 and the dual system (wall + frame) resist the lateral force in the longitudinal direction, Y, and frames A and D resist the lateral force coming along the transverse direction, X. The C-shaped reinforced concrete wall, thus, contributes to lateral resistance in both directions.

2.3. **Material Properties**

As indicated in section C5.4.1, as a starting point and in the absence of further direct information, default values on the mechanical properties of the reinforcing steel can be assumed in accordance with standards at the time of construction.

In this case the structural drawings report (specified) material properties, as shown in Figure 5.

The concrete compressive strength used for the design is about 3500 lb sq/in = 24.1MPa.

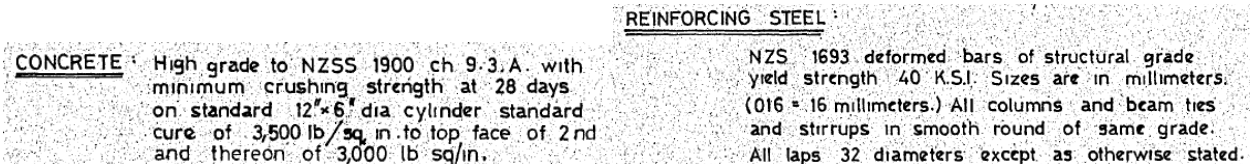
CONCRETE : High grade to NZSS 1900 ch 9.3.A. with minimum crushing strength at 28 days on standard 12"×6" dia cylinder standard cure of 3,500 lb/sq. in. to top face of 2nd and thereon of 3,000 lb sq/in.

REINFORCING STEEL :
NZS 1693 deformed bars of structural grade yield strength 40 K.S.I. Sizes are in millimeters. (016 = 16 millimeters.) All columns and beam ties and stirrups in smooth round of same grade. All laps 32 diameters except as otherwise stated.

Figure 5: Material strength stated in structural drawings (Pampanin et al. 2012).

As mentioned in Section C5.4.2.2, an aging coefficient of 1.5 could be used to evaluate the probable compressive strength of the concrete.

However, in the absence of more direct information on the material at the time of construction and/or at the time of the assessment, it is herein felt than using a probable compression strength f'_c=30MPa for the DSA procedure would possibly be on the higher and non-conservative side.

In real practice, it would be highly suggested to retrieve more reliable information from on-site material testing, specifically if/when shear failure in elements/subassemblies can be triggered when considering low-strength concrete values.

In order to account for the high variability of concrete material properties commonly found in pre-70's cast-in-situ buildings due to a lower quality control checks/measurements when compared to today's requirement, an upper bound for the probable strength of concrete is herein taken as 25MPa.

This would correspond to either a -20% variation from the probable value calculated as $1.5 \cdot f'_c$ or to the assumption of a lower but still realistic class of concrete (concrete compressive strength 17.2 MPa, see table C5.3) and same aging coefficient.

According to the drawings, deformed bars Grade 275 (40 ksi) were adopted.

Probable material properties herein used for the assessment are summarised in Table 3.

They are computed multiplying the nominal strength by the coefficients 1.5 and 1.08, as suggested at C5.4.2.2 and C5.4.3.3 for concrete and steel, respectively, and applying the aforementioned judgement on the concrete strength.

The other basic concrete material properties are computed: concrete tensile strength (Table. C5A.2, $f_{ct}=0.36(f'_c)^{1/2}=1.83$) and concrete elastic modulus (NZS 3101:2006 5.2.3, $E_c=3320(f'_c)^{1/2}+6900$).

Table 3*:* Summary of probable material properties

Materials	*Properties*	*Values*
Concrete	Strength (f'_c) (MPa)	17.2*1.5=25.8
	Tensile Strength (f_{ct}) (MPa)	1.83
	Elastic Modulus (E_c) (MPa)	23763
	Crushing Strain (ε_{cu})	0.004 for unconfined concrete
Reinforcing Steel	Yield Strength (f_{sy}) (MPa)	275*1.08=300
	Elastic Modulus (E_s) (MPa)	200000
	Yield Strain (ε_y)	0.0015 computed as f_{sy}/E_s
	Ultimate Strength (f_{su}) (MPa)	1.25*300=375
	Ultimate Strain (ε_{su})	0.15

Furthermore, as suggested in the C5.4.1, the effects of variation of material strength on the hierarchy of strength should be considered. The variations considered in this study are ± 20% of the probable value of concrete strength.

At this stage, no additional variability of member strength due to geometry and details uncertainty is considered, assuming that the geometry and structural member details, clearly reported in the structural drawings, have been correctly executed and implemented.

2.4. **Reinforcement details**

The reinforcement details were identified using the original drawings available (see Figure 6-Figure 9) for the selected case study. It is worth noting that the building was designed according to pre 1970's design practice when, in principle, capacity design and modern seismic details had not been officially introduced yet in the concrete codes (NZS 3101P 1970). However, already improved detailing were included in some by-laws (early 1970s) and this design example reflects somehow an example of good practice of the day. Well-detailed columns and beam-column joints and capacity design (by requiring flexural strengths of columns at a beam column joint to exceed the corresponding sum of the beam flexural strengths) were introduced (MOW 1968).

The beam longitudinal reinforcements consist of ϕ24 and ϕ20 bars anchored 90° in the joint core. The reinforcement amount significantly varies floor-to-floor to account for the shear demand reduction along the building height. The ratios of longitudinal reinforcement and the stirrups spacing comply with the NZS3101P (1970) and the limitations summarized in Table C5D.2 of the NZSEE/MBIE guidelines (NZSEE/MBIE 2016c). The longitudinal reinforcement ratio, computed considering tension bars only, is in the range 0.006-0.013. The beam transverse reinforcement consists of ϕ10 bars 178 mm spaced, which is significantly lower than the maximum spacing suggested by the code (450 mm, see Table C5D.2 of the guidelines). The reinforcement details are summarised in Table 4, and compared with the limitations of the NZS3101P.

The seismic resistant columns are square columns with 457.2 mm sides at all the building levels. Significant variations for longitudinal and transverse reinforcements can be observed along the building height, in particular at level 4. At this level, the hierarchy of strengths should be properly checked to assess the possibility of a soft-storey mechanism. The total longitudinal reinforcement ratio in the seismic resistant columns, ρ_l, ranges between 0.012 and 0.035, which is in agreement with minimum and maximum prescribed values, 0.01 and 0.08, respectively (see Table 5, summarizing the relevant reinforcement limitations of Table C5D.3 of the guidelines). The amount of transverse reinforcement is the same for all the columns ϕ10 bars, 228 mm spaced with 135° hooks (this is compliant with the minimum requirement of $12d_b$, see Table C5D.3 of the guidelines). Furthermore, a reduced spacing, about 76mm, was adopted in the plastic hinge regions at both column ends for a length about 500mm.

The gravity columns are characterized by the same amount of longitudinal and transverse reinforcements. However, the stirrups spacing reduction in the plastic hinge regions was not provided. This may led to a reduced displacement capacity of those columns. This aspect should be properly checked assessing the building capacity.

Beam bars bent into the joint panel and ϕ10 stirrups about 100 mm spaced characterize the joint subassemblies. At the time of construction, no joint stirrups were required, see NZS 3101P (1970).

The C-shaped shear wall has double layer longitudinal reinforcement consisting of 22 bars per layer 200 mm spaced on each flange (X direction) and 30 bars per layer on the web (Y direction). The diameter of the bars is variable along the building height (ϕ20 at the ground floor up to ϕ10 to the last four floors). The ϕ10 transverse reinforcements are 254mm spaced. The ratios of longitudinal reinforcement (ρ_{min}=0.003 and ρ_{max}= 0.015) are compliant with the limitations suggested by the NZS3101P (1970) summarized in Table C5D.3. More details on the wall reinforcement layout are reported in Figure 14 and Table 6.

Table 4*:* Reinforcement limitations for beams

Parameter	*Case study building*	*Limitation in NZS3101P*
$\rho_{l,\,min}$	0.006	> 0.005
$\rho_{l,\,max}$	0.013	< 0.033
spacing	178mm	< 450mm
A_v	157mm^2	> 54mm^2

Table 5*:* Reinforcement limitations for columns

Parameter	*Case study building*	*Limitation in NZS3101P*
$\rho_{l,\,min}$	0.012	> 0.01
$\rho_{l,\,max}$	0.035	< 0.08
spacing	228mm	< 448mm
A_v	157mm^2	> 54mm^2

Table 6*:* Reinforcement limitations for walls

Parameter	*Case study building*	*Limitation in NZS3101P*
L_n/t	14	< 35
$\rho_{l,\,min}$	0.003	> 0.002
$\rho_{l,\,max}$	0.015	-
spacing	254mm	< 457mm

The member dimensions and the reinforcement details are summarized in the following figures for the structural systems analysed in this report. In-situ inspections are suggested to verify the correspondence with the reinforcements used in the construction.

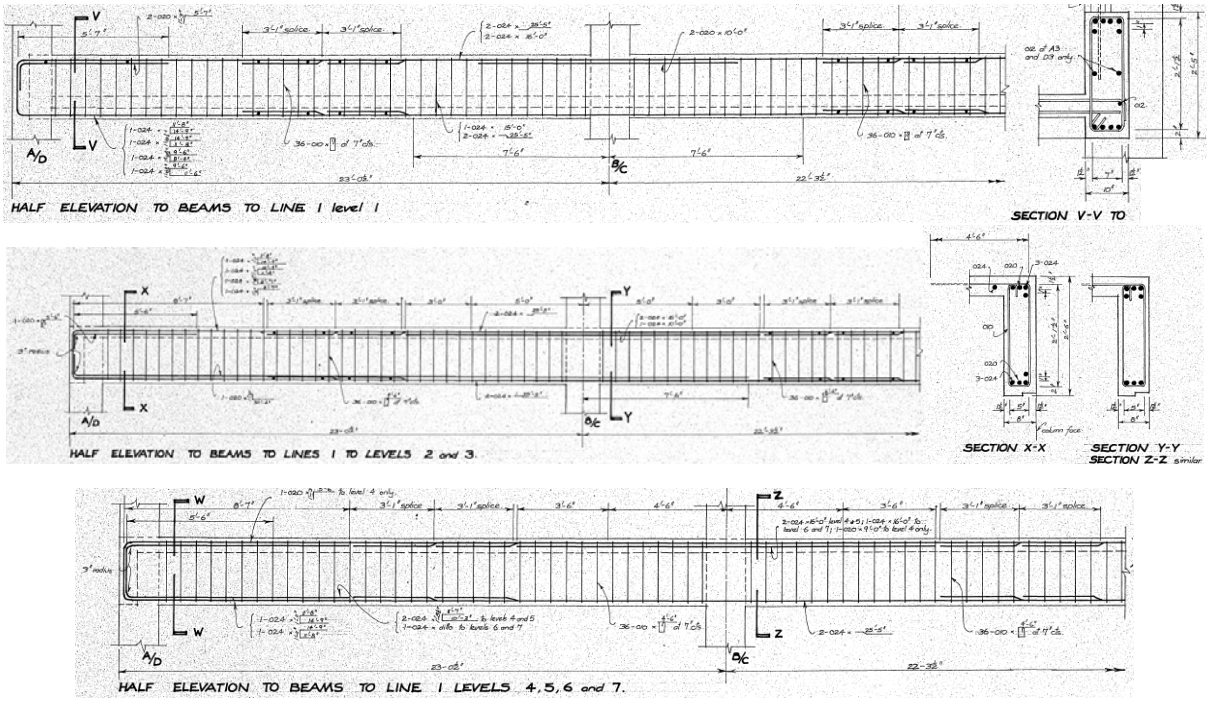

Figure 6: Example of beam reinforcement details in the Longitudinal Frame 1.

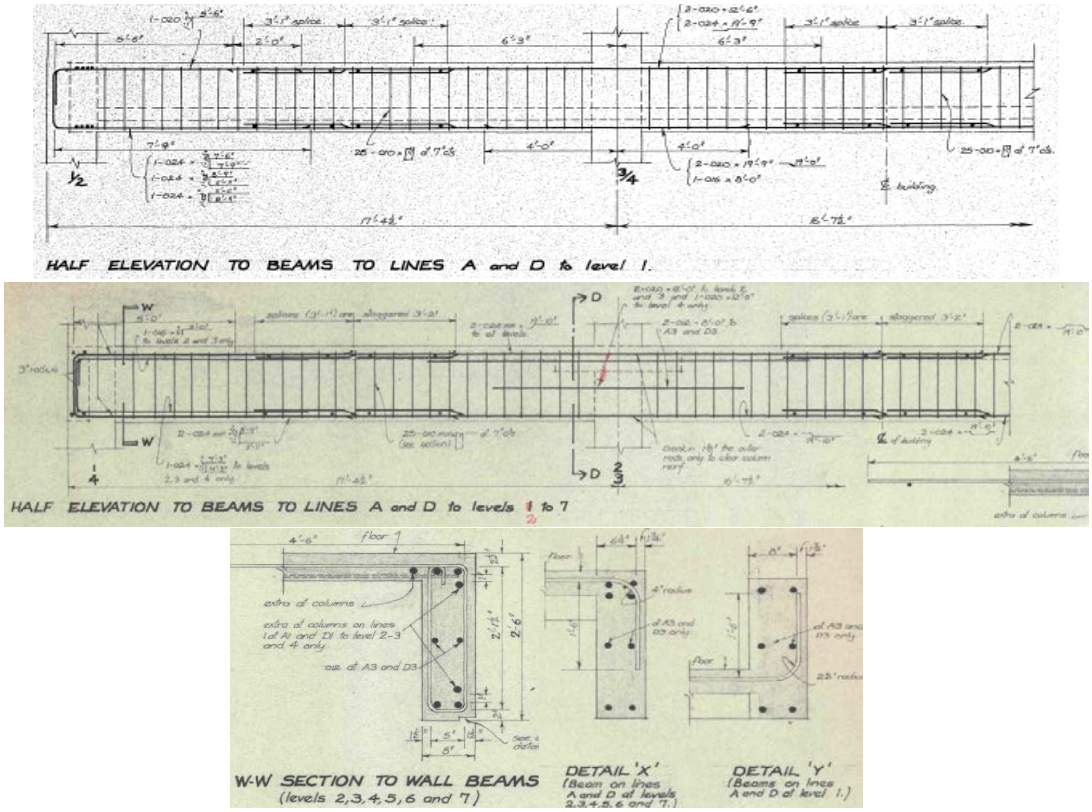

Figure 7: Example of beam reinforcement details in Frame A and D

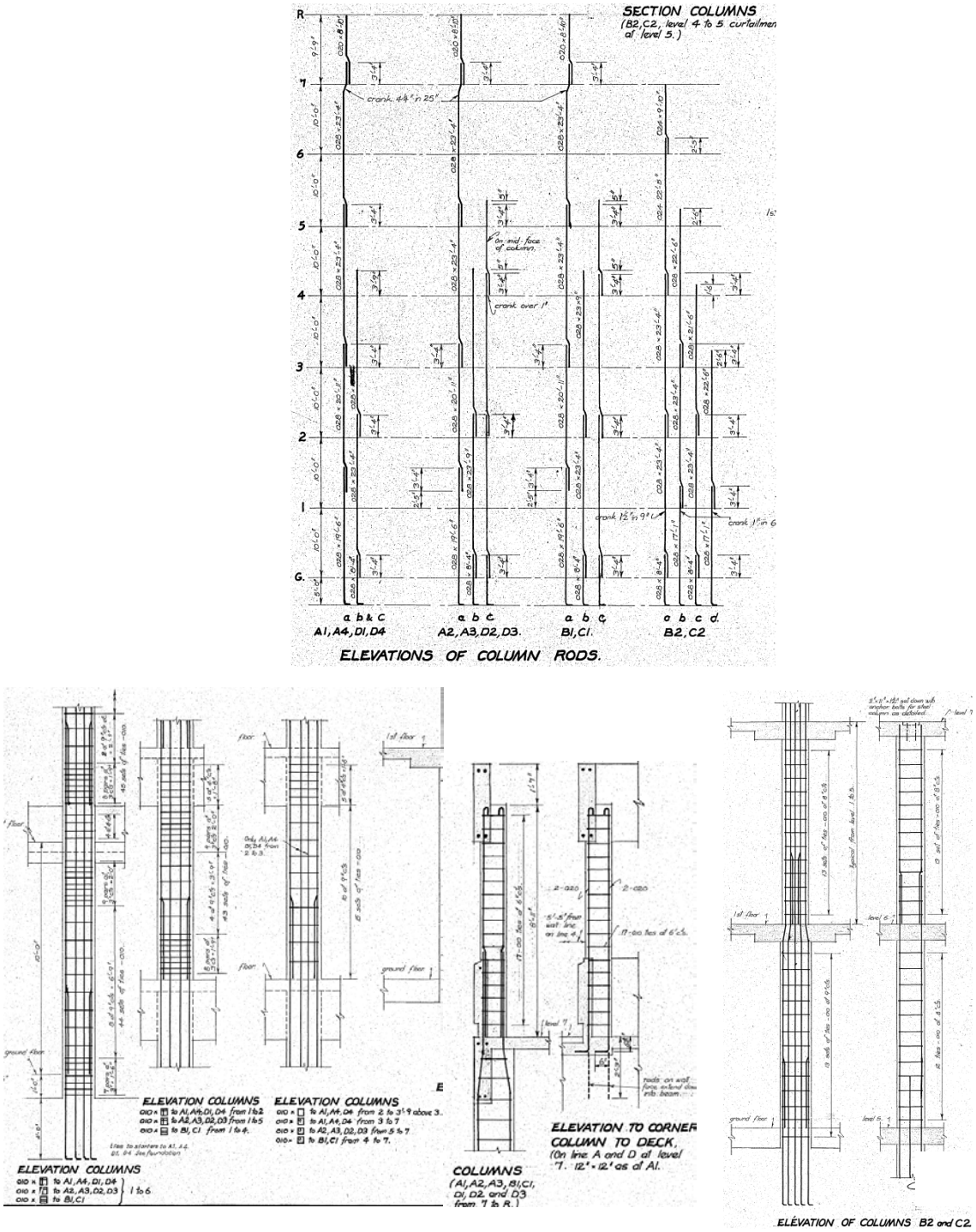

Figure 8: Elevation scheme of column reinforcements in Frame 1, A and D.

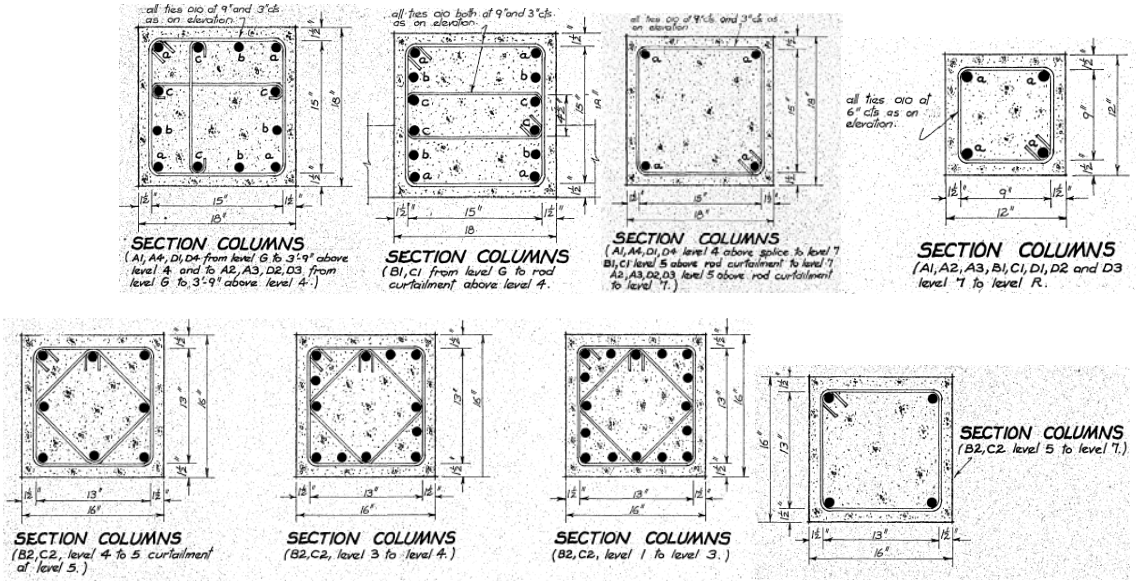

Figure 9: Example of column reinforcement details in Frame 1, A and D.

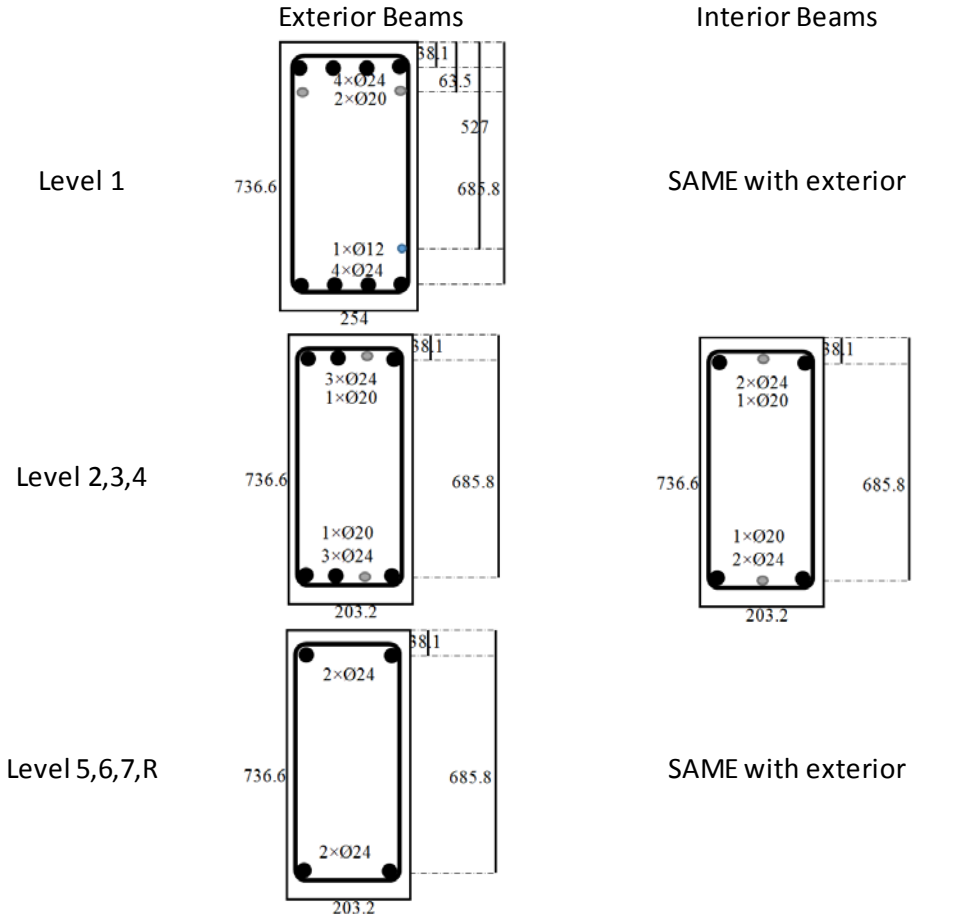

Figure 10: Beam details in Frame 1 (redrawn, Chen 2015).

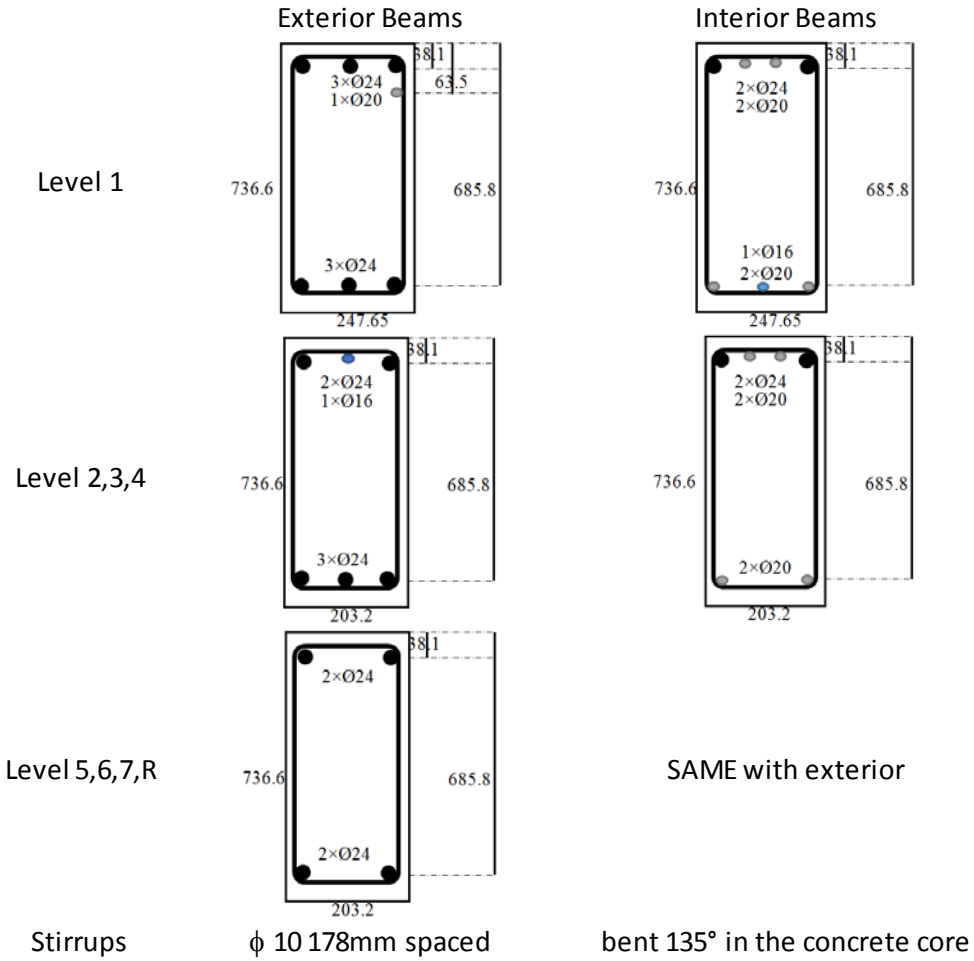

Figure 11: Beam details in Frame A/D (redrawn, Chen 2015).

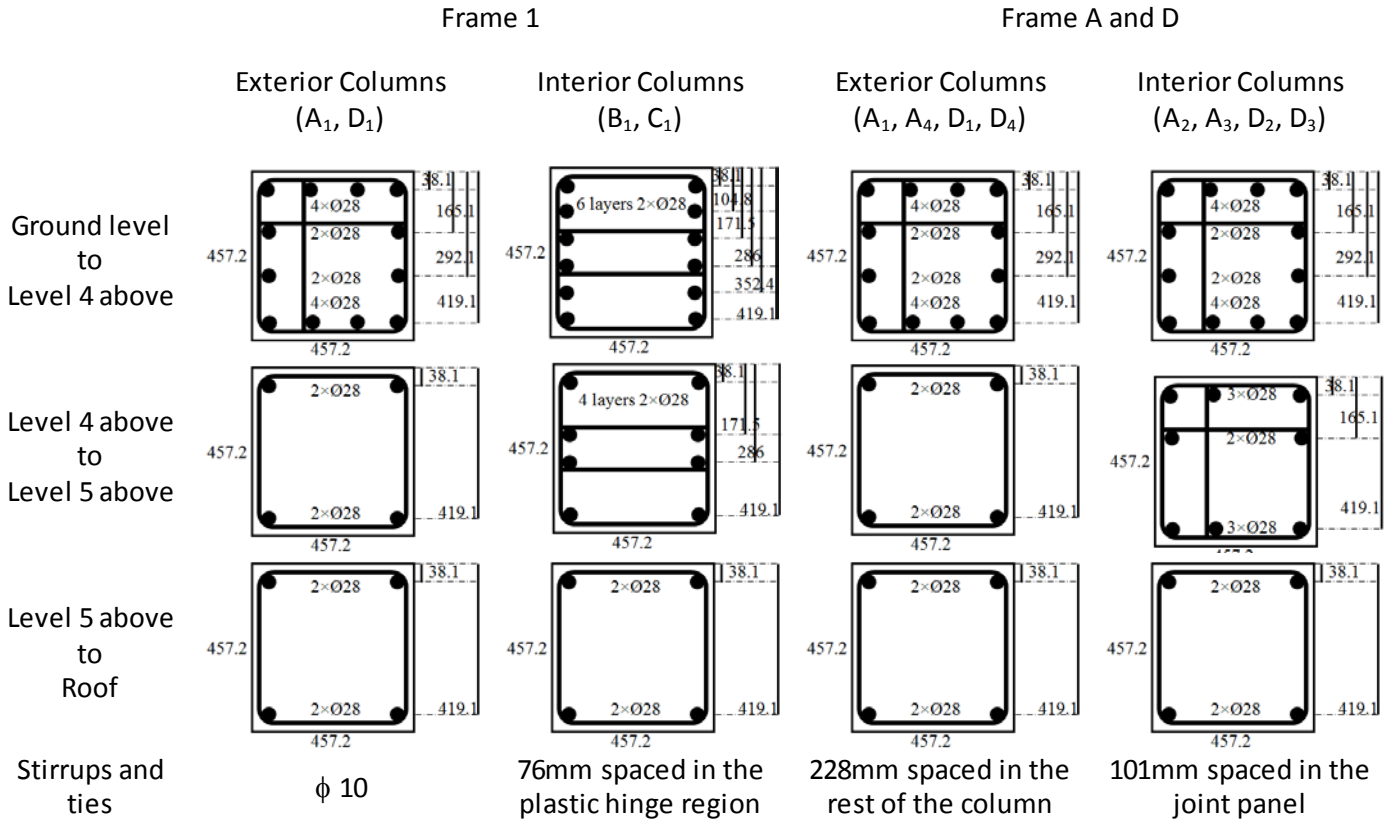

Figure 12: Column details (redrawn, Chen 2015).

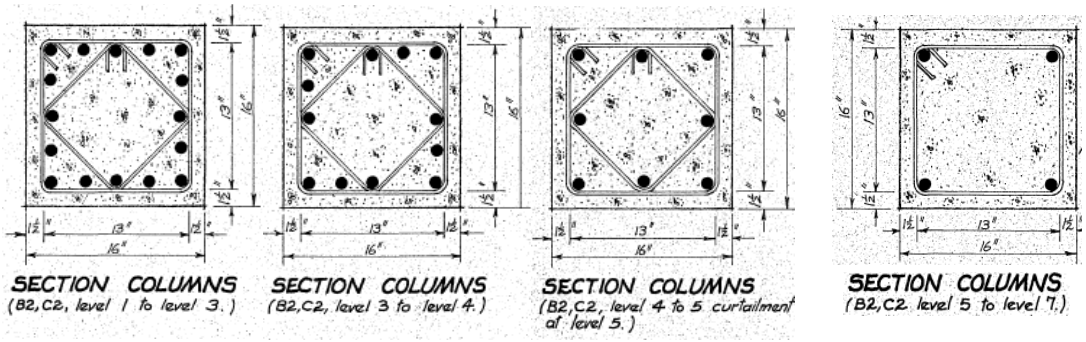

Figure 13: Reinforcement details of gravity columns.

As outlined in Figure 8, the lap length of longitudinal reinforcements is always higher than 20db (about 1m in all columns and beams), thus, according to section C5.5.3.2, the nominal bending moment capacity can be attained.

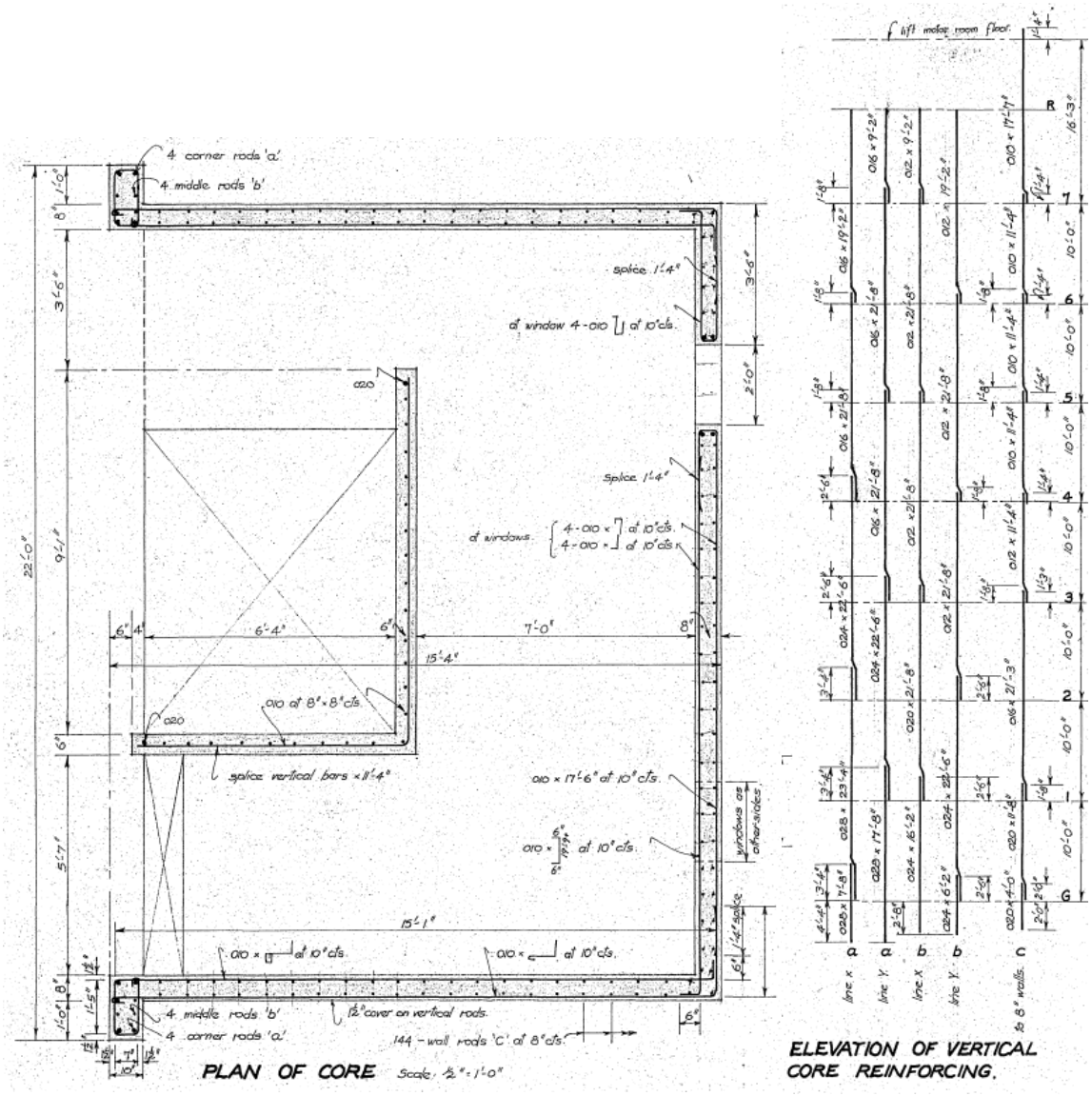

Figure 14: RC shear wall details.

2.5. **Observed damage**

A description of the observed damage to the building following the 22 Feb 2011 Christchurch earthquake can be found in Pampanin et al. (Pampanin et al. 2012). The building suffered for

severe structural damage and, in the aftermath of the Canterbury sequence, it was RED tagged and consequently demolished (see Table 7).

As shown in Figure 15 and Table 8, the damage was mostly concentrated in the frames, with limited damage to the structural walls. The overall mechanism in the frame was a mixed sway, comprising, in general, a combination of beam flexural hinging in the exterior beam-column joints, shear damage in the interior joints and shear failure in some columns at the level 1 (first suspended floor) due to the interaction with the deep spandrel/frame beams.

Table 7: General damage information of Building No.21 – Securities House

INSPECTION	GENERAL DAMAGE INFORMATION
TAGGING	Red
BUILDING DAMAGE RATIO	11-30%
USABILITY RATE	R2: Severe damage demolition likely

Table 8: Summary of observed structural damage

STRUCTURAL DAMAGE	DAMAGE DESCRIPTION
BEAMS	Plastic hinge formations in external beam ends in all storeys except top floor
COLUMNS	Severe short column damage on 1st floor
JOINTS	Joint hinging in internal joints in all storeys except top floor
FOUNDATION	Minor/ None
ROOF FLOOR	Minor/ None

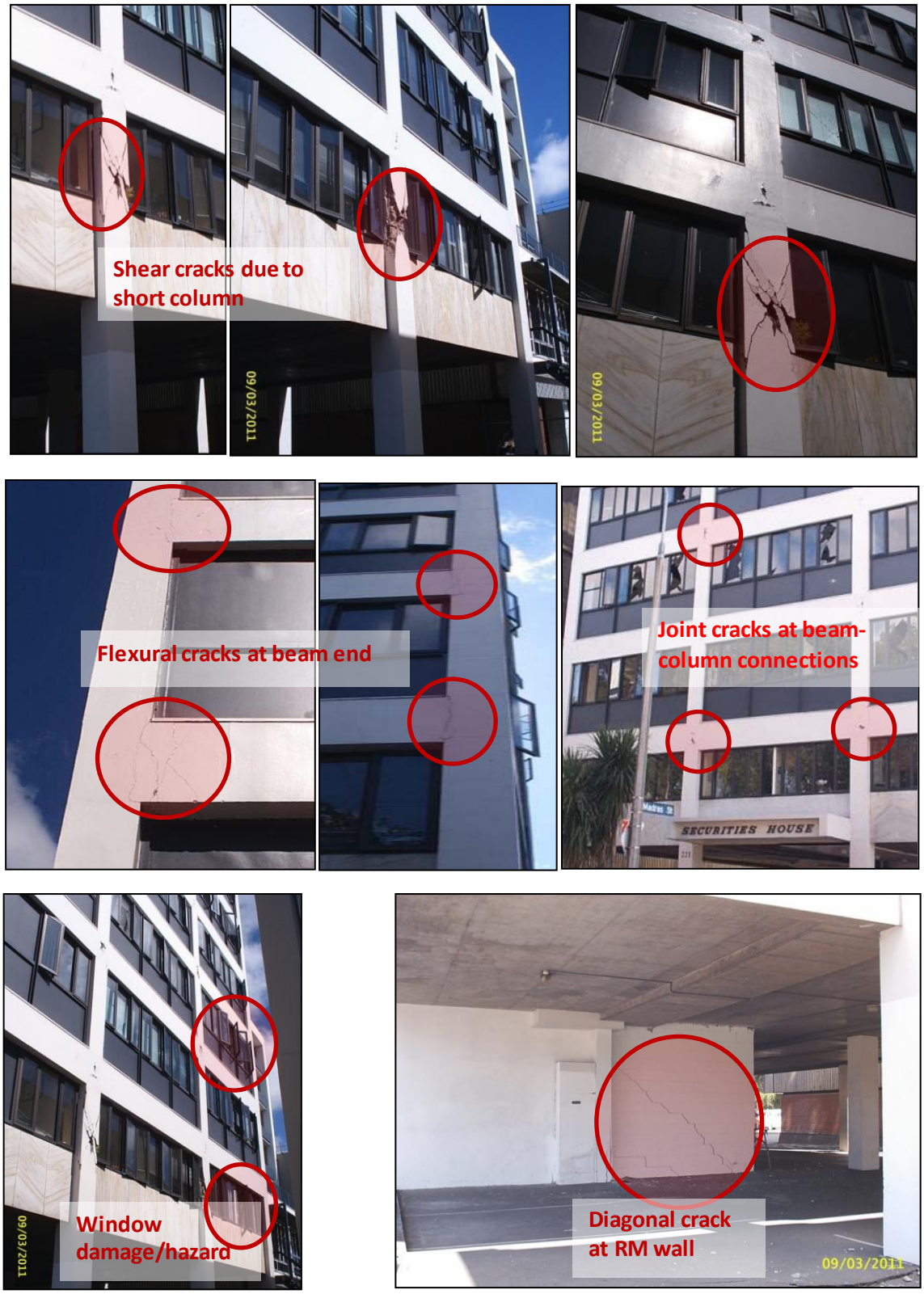

Figure 15: Photos showing the observed damage to the building (Pampanin et al. 2012).

2.6. **IEP results**

Initial Evaluation Procedure (IEP), suggested in NZSEE (NZSEE 2006) Guidelines (2014 Revision on Section 3) as the formal initial seismic evaluation procedure, was used to assess the building capacity in the aftermath of the Canterbury 2011 earthquake. IEP identifies potential structural weaknesses and identify the Earthquake Prone Buildings (EPB) based on the calculated %NBS values. An excel spreadsheet with detailed IEP steps and calculations is provided.

Table 9 shows the key assumptions made for the IEP assessment of the case study building while Figure 16 shows the specific IEP spreadsheet compiled for Securities House. The assessment indicates that the case study building can achieve 20%NBS in both the longitudinal and transverse direction, identified as Earthquake Prone Building (EPB), corresponding to a 'Grade D' building as defined by in the NZSEE building grading scheme. This is below the threshold for earthquake prone buildings (34%NBS) as recommended by the NZSEE. It has 10~25 times of risk relative to a new building, and considered to be "high risk" according to NZSEE grading system.

A Detailed Seismic Assessment (DSA) is required in order to confirm the results from IEP, also to investigate deeply in building potential weaknesses.

Table 9: Summary of IEP assumptions on the case study building (Chen 2015).

IEP ITEM	ASSUMPTION	JUSTIFICATION
DATE OF BUILDING DESIGN	1965-1976	Before Capacity Design Theory introduced in design and construction
SOIL TYPE	Type D	Soft soil
BUILDING IMPORTANCE LEVEL	2	Public building
DUCTILITY OF STRUCTURE	2	Reinforced concrete frames and RC structural walls
PLAN IRREGULARITY (FACTOR A)	0.7	Severe (core wall systems with stairs and service loading on the east side)
VERTICAL IRREGULARITY (FACTOR B)	0.7	Significant (rapid reinforcement details reduction)
SHORT COLUMNS (FACTOR C)	0.7	Significant
POUNDING (FACTOR D)	1	Insignificant
SITE CHARACTERISTIC (FACTOR E)	1	Insignificant
FACTOR F	0.8	Lower than 1 due to minimum transverse reinforcing and confinement details, and lack of capacity design

Table 10: Summary of IEP results (Chen 2015).

Building Name	***Securities House***				
Orthogonal Directions	**Potential Score**		**Potential Grade**	**Approximate Risk/New Building**	**Life-safety Risk Description**
Longitudinal	20%	EPB	D	10~25 times	high risk
Transverse	20%	EPB	D	10~25 times	high risk

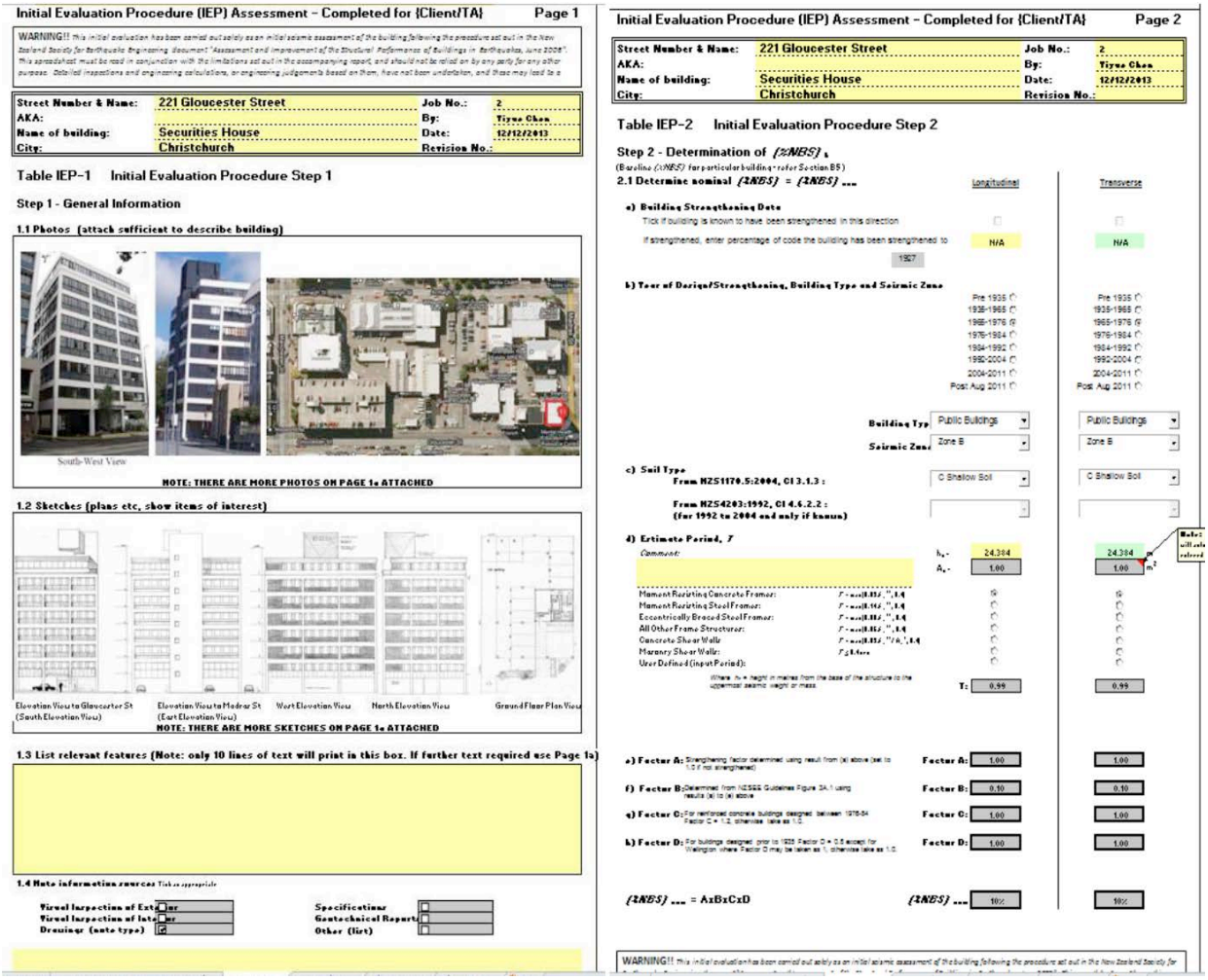

Figure 16: IEP spreadsheet for the case study building.

2.7. **Design assumptions**

The case study building has a complex structural system with RC moment resisting frames in both directions and a RC C-shaped wall on the east side which could strongly influence the structural response causing torsional irregularity.

The design example will focus on a SLaMA approach, using an ADRS format to evaluate the performance point, and more specifically the %NBS.

Several assumptions are needed in order to simplify the structural system and use the SLaMA approach, based on "by-hand" calculations.

As a first step, the lateral force-displacement capacity curves of all the lateral resisting systems (Frame 1, Frame A/D, coupled frame-wall system, wall flanges in x-direction) are independently

and analytically computed (SLaMa hand-based pushover), assuming a 2D response with no torsional effects. The relevant sections in the C5 are adopted to characterize the components, subassemblies and systems lateral response .

Notably, in the Y-direction, the wall web is connected to exterior columns by framing beams creating a symmetric dual system. The coupling effect is calculated following the section C5.8 relating to dual systems. Even though the two wall flanges in the x-directions have the role to supports the flat slab, their contribution to the lateral building stiffness cannot be neglected.

As a first simplification, the structural C-shaped RC shear wall is decoupled in a wall web (forming the dual system in the y-direction) and two wall flanges contributing to the building capacity in the X-direction.

Later, in Section 7 the SLaMA was repeated considering the coupled effect of flanges and web, and the influence on the global building behaviour is quantified.

The calculations performed to estimate the lateral capacity of the Frame 1 and the dual system (frame + wall), according to the SLaMA method, are reported in Section 4 and 5. The contribution of the other lateral resisting systems is accounted in determining the total building capacity in the two directions.

The global X and Y-direction Force-Displacement curves for the buildings are derived and the %NBS evaluated, in absence of any torsional effect.

Then, inelastic torsion effects due to the unbalanced stiffness/strength distribution in plan are accounted for following the simplified approach proposed by Paulay (2001) and Priestley et al. (2007) (reported in the Section C5.7.2 and C2F.4 of the guidelines).

In the section 8 the influence of joint stirrups, neglected as a first simplification, is evaluated.

Finally, Section 9 reports the comparison between analytical (SLaMA by hand) and numerical (software-based) pushover curves to assess the accuracy of the SLaMA and measure its level of confidence.

2.1. **Load analysis**

The gravity load analysis in case of a seismic event is carried out considering:

- the dead loads G generated from the weights of reinforced concrete structural systems;
- the superimposed dead load D_{SDL} accounting for the light-weight infill walls and other permanent interior finishing;
- the live loads Q due to occupancy and use;
- the combination factor for live loads Ψ_E.

The loads combination and related factor are taken according to NZS 1170.5 (2004) and reported in Table 11.

Table 11: Summary of gravity load analysis

$\rho_{concrete}$	(kN/m^3)	25
Ψ_E (Offices)	(-)	0.3
D_{SDL}	(kN/m^2)	0.50
Q	(kN/m^2)	3.00
Load combination	E_d	[G, E_u, Ψ_EQ]

The calculation resulted in a total mass about 226 tons per each floor (2213 kN).

The gravity loads acting on each column and the shear wall are calculated basing on tributary area. For RC walls, the self-weight of the wall is also considered.

The column axial loads for the Frame 1 and the shear walls are reported in Table 12.

Table 12: Frame 1 columns and walls gravity load

	Column		Wall	
	Exterior	Interior	Web	Flange
Floor	N_g	N_g	N_g	N_g
[-]	[kN]	[kN]	[kN]	[kN]
1	473	946	2624	3397
2	414	828	2296	2972
3	355	710	1968	2548
4	296	592	1640	2123
5	237	473	1312	1698
6	177	355	984	1274
7	118	237	656	849
8	59	118	328	425

3. COMPONENT CAPACITY

3.1. **Methodology and general assumptions**

The lateral capacity of beams, columns, beam-column joints and shear wall is calculated with reference to sections C5.5.2, C5.5.3, C5.5.4 and C5.5.5 of the NZSEE/MBIE guidelines (NZSEE/MBIE 2016c), respectively.

In particular:

- The beam flexural capacity is calculated and compared with degrading shear strength in order to detect premature brittle failures. For flexural-dominated beams, the ultimate limit state (ULS) drift capacity is computed accounting for longitudinal reinforcement buckling;
- The column flexural capacity is calculated considering the axial load and compared with the degrading shear strength. If a column flexural-shear failure was expected, the ULS drift corresponding to that mechanism is used. In the case of a flexural dominated column, the ultimate drift capacity is computed accounting for longitudinal reinforcement buckling;
- The beam-column joint capacity in terms of joint shear strength is evaluated considering the concrete compressive strength, joint geometry, longitudinal reinforcement type and anchorages of beam bars. The joint shear strength is later converted into the equivalent column moment to apply the hierarchy of strength principles at subassembly level. The joint deformability in terms of interstorey drift is assumed in compliance with available formulations C5.5.4.3 and Table C5.10 (NZSEE/MBIE 2016c);
- The C-wall system is decoupled into two rectangular walls resisting in X- and Y-directions. In the Y-direction, the coupling effects of the beams and exterior columns A4-D4 (Figure 3) are accounted for (Dual system). The wall capacity in terms of shear strength is calculated with available formulations which empirically account for all the possible failure mechanisms (C5.5.5.4, NZSEE/MBIE 2017). Drift limitations due to local bar buckling and interaction between shear and flexure were considered. The wall displacement capacity were computed according to the same mechanical approach used for RC columns, with formulations on the yielding curvature and plastic hinge length typical of shear walls.

3.2. **Beams**

The beam flexural capacity is computed using the basic principles of RC cross-sections subjected to bending moment as suggested in the section C5.5.2.2. Geometry and structural details are provided in Table 13. An increase of the 20% of the flexural strength in negative moment regions is considered to account for the potential "flange-effect" contribution from the slab reinforcement. By contrast, it is worth mentioning that NZSEE/MBIE guidelines (NZSEE/MBIE 2016c) suggest to increase the negative flexural strength of beams by the 50%, multiplying the negative flexural

capacity of the beams by 1.5. Due to the relatively adequate anchorage details of the beam longitudinal reinforcement, bent 90 degrees into the joint, no reduction of the flexural strength due to lack of bond is considered.

With reference to Level 1 exterior beams:

Table 13: Details of Level 1 exterior beam.

Beam width	b	[mm]	254
Beam height	h	[mm]	736.6
Longit. bar cover	clb	[mm]	38.1
Bay length	L_{bay}	[mm]	6800
Column height	h_c	[mm]	457.2
Shear span (L_{bay}-h_c)/2	l'_b	[mm]	3171.4
Stirrups diameter	d_{st}	[mm]	10
Stirrups spacing	s_{st}	[mm]	178
Number of legs	n_l	[-]	2
Longit. bar diameter	d_b	[mm]	24

Confined concrete ultimate strain

According to the criteria defined in the guidelines (C5.5.2.5), the beam concrete core can be assumed as fully confined (ϕ10 stirrups, 178mm spaced).

The confined concrete ultimate strain can be computed using the formulation C5.9:

$$\varepsilon_{cu} = 0.004 + \frac{1.4\rho_s f_{yh}\varepsilon_s}{f'_{cc}} = 0.004 + \frac{1.4 \cdot 0.00656 \cdot 300 \cdot 0.06}{31} = 0.0093$$

where:

- the volumetric ratio of transverse reinforcement can be computed using Eq. C5.10:

$$\rho_s = 1.5A_v/b_c s = 1.5 \cdot n_l \cdot \pi \cdot \left(\frac{d_{st}}{2}\right)^2 /(b - 2clb + d_b + d_{st})s = 0.00656;$$

- ε_s is assumed equal to 0.06 as suggested in the Table C5.8 of the NZSEE/MBIE guidelines;
- f'_{cc} is assumed equal to 1.2 f'_c= 1.2·25.8= 31MPa, in presence of good level of transverse reinforcement (i.e. s_{max}=178mm).

Once that the confined concrete ultimate strain in known, the flexural strength can be computed using the cross-section analysis. The results are reported in Table 14.

Table 14: Flexural capacity of Level 1 exterior beam.

Strain limit of transverse reinforcement	ε_s	[-]	0.06
Unconfined concrete ultimate strain	ε_c	[-]	0.004
Confined concrete ultimate strain	ε_{cu}	[-]	$0.004 + \frac{1.4\rho_s f_{yh}\varepsilon_s}{f'_{cc}} = 0.0093$
Positive yielding moment	M_{y+}	[kNm]	403
Negative yielding moment	M_{y-}	[kNm]	607
Positive ultimate moment	M_{u+}	[kNm]	477
Negative ultimate moment	M_{u-}	[kNm]	682
neutral axis depth at M_{u+}	c_+	[mm]	69.7
neutral axis depth at M_{u-}	c_-	[mm]	82.4

The deformation capacity of the RC members is evaluated in terms of yielding/ultimate curvature of the base cross-section subjected to the maximum bending moment in a cantilever scheme (see Figure 17a,b). The yielding and plastic curvature are evaluated assuming the curvature distributions depicted in Figure 17c,d respectively. Once the key points of the moment-curvature of a structural element have been evaluated, the corresponding lateral displacement can be calculated assuming a cantilever scheme and considering a proper plastic hinge length (see Figure 17). The corresponding moment-rotation curve can be derived by integrating the curvature profile (elastic and plastic) along the cantilever scheme and after defining a plastic hinge length.
It is worth noting that these rotations do not correspond to the 'member drift' or 'chord rotation' used in the following calculations.

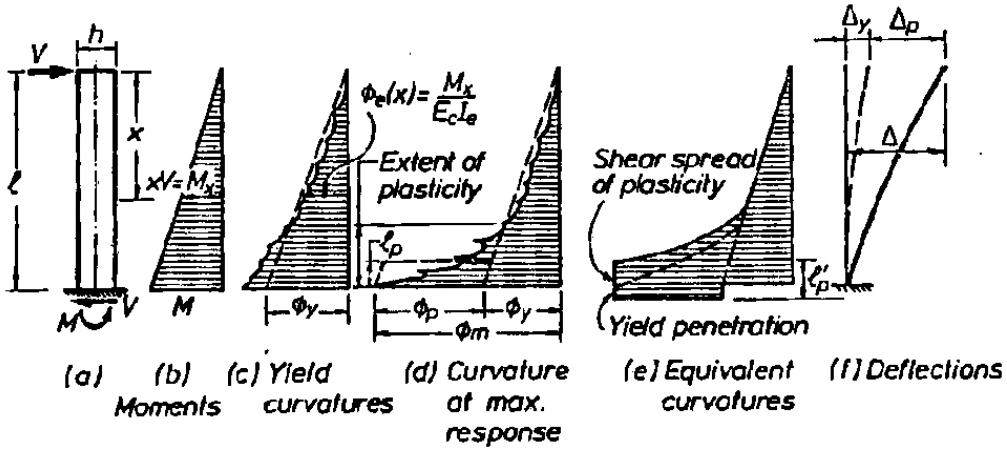

Figure 17: Schematic of component (a), moments (b), curvatures (c, d, e) and deflections (f) in a prismatic reinforced concrete cantilever subjected to lateral load (Paulay and Priestley 1992).

The ratio between the displacement at the top of the cantilever, Δ, and the member shear span, L_c, is named 'member drift' (or 'chord rotation' as defined in various international codes, i.e. Eurocode 8 (CEN 2005), ASCE/SEI 41 (2013), see Figure 18).

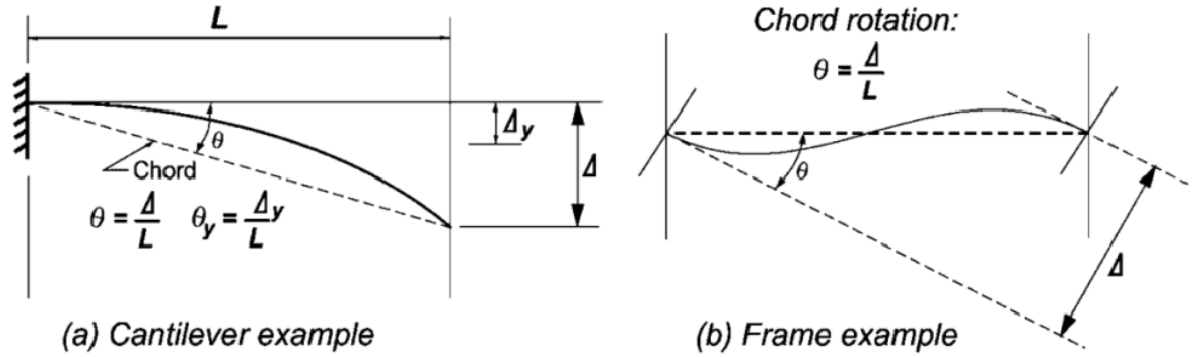

Figure 18: Definition of chord rotation (rotation angle or drift) (ASCE/SEI 41 2013).

Frame elements (i.e. beams and columns) behaves as depicted in Figure 18b, thus a conversion to cantilever scheme (Figure 18a) is needed. A double curvature frame member (Figure 18b) can be decoupled into two cantilevers (Figure 18a) having a member length L (the shear span named L_c in the following) about the half of the total member length (assumed point of contraflexure).

Yielding and ultimate curvature

For rectangular-section beams, formulation C5.5 (positive bending moment) results in:

$$\phi_y = \frac{2.0\varepsilon_y}{\mathrm{h}} = \frac{2.0 \cdot 0.0015}{0.7366} = 0.0041 \ \frac{\mathrm{rad}}{\mathrm{m}}$$

For flanged beams, formulation C5.6 (negative bending moment) results in:

$$\phi_y = \frac{1.7\varepsilon_y}{\mathrm{h}} = \frac{1.7 \cdot 0.0015}{0.7366} = 0.0035 \ \frac{\mathrm{rad}}{\mathrm{m}}$$

The ultimate curvature of the beam is given by C5.7:

$$\phi_u = \frac{\varepsilon_{cu}}{\mathrm{c}} = \frac{0.009}{0.0697(\mathrm{or}\ 0.0824)} = 0.134\ (or\ 0.113)\ \frac{\mathrm{rad}}{\mathrm{m}}$$

The ultimate curvature can be also assumed at the concrete cover spalling ($\varepsilon_{cu} = 0.004$). This leads to a more conservative estimation (see Figure 19). In the same figure, the simplified bilinear moment-curvature curves, derived with the previously described approach, are compared with more refined calculation (i.e. CUMBIA software, Kowalsky and Montejo 2007) both for rectangular and flanged beams. In the case of flanged beams, the 20% increase in the flexural capacity is simulated by increasing the longitudinal reinforcement by the 20% (2ϕ18, see Figure 19).

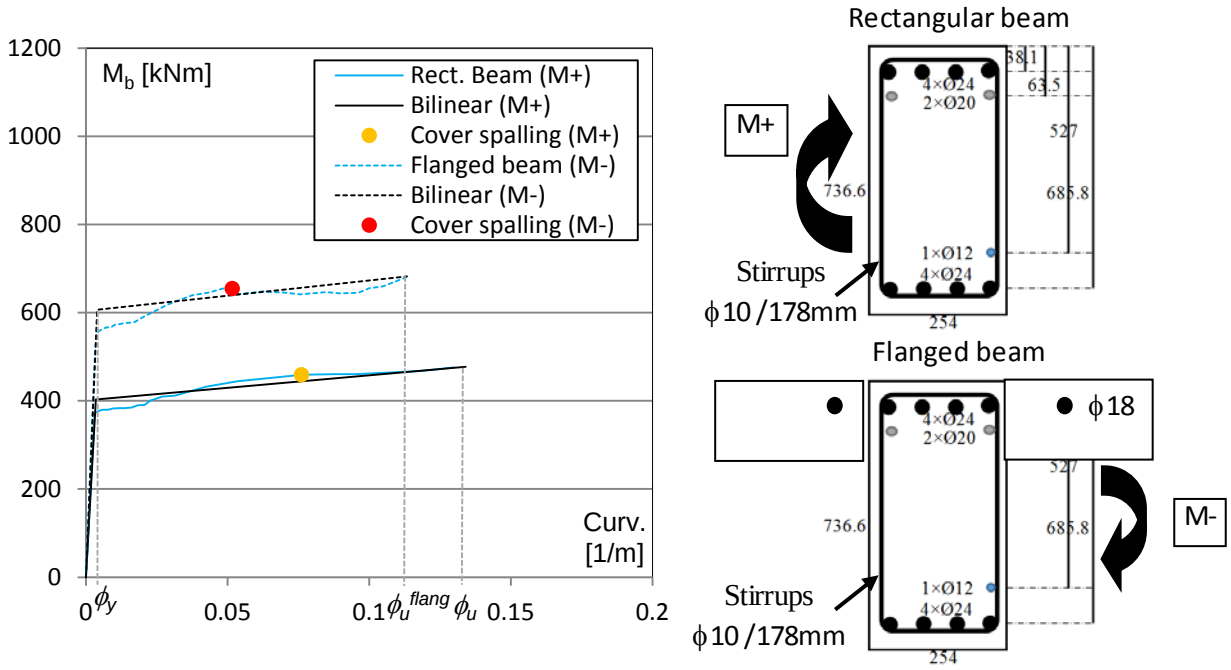

Figure 19: Moment-curvature curves of typical beams.

In this example, the ULS curvature is defined by the full development of the ultimate confined strain, ε_{cu}, in the concrete core. However, for special design/assessment purposes, the ultimate curvature can be limited at the concrete cover spalling to have a conservative prediction.

Component Drift

The beam displacement at the yielding measured at the contra-flexure point can be computed with Eq. C5.18 assuming $L_c = l'_b$. For the negative bending direction:

$$\Delta_y = \phi_y (H)^2/3 = \phi_y (L_c)^2/3 = 0.0035(3.1714)^2/3 = 0.0116\text{m}$$

To compute the ultimate beam displacement, the plastic hinge length is needed. It can be estimated using Eq. C5.20:

$$L_p = kL_c + L_{sp} = 0.05 \cdot 3171.4 + 158.4 = 0.317\text{m}$$

where:

$k = 0.2\,(f_u/f_{sy} - 1) \leq 0.08 = 0.2(375/300 - 1) = 0.05$

L_c=the distance of the critical section from the point of contra-flexure $= l'_b = 3171.4$ mm

L_{sp}=strain penetration $= 0.022 f_y d_b = 0.022 \cdot 300 \cdot 24 = 158.4$mm

As a general rule, the plastic hinge length calculated with the above expression, should be reduced to $L_p/5$ if plain round bars are used, if the reinforcement ratio is particularly low or if the beam-

column joint is inadequately constructed (for more information, see NZSEE, 2016c guidelines, Section C5.5.2.5). However, in this case, none of these conditions applies and, hence, no reduction of the bending moment capacity is considered.

The ultimate beam displacement can be computed using Eq. C5.17:

$$\Delta_u = \Delta_y + \Delta_p = 0.0116 + 0.110 = 0.122\text{m}$$

where:

$$\Delta_p = \phi_p L_p H = (\phi_u - \phi_y) L_p \cdot L_c = (0.113 - 0.0035) \cdot 0.317 \cdot 3.1714 = 0.110\text{m}$$

Once that the yielding and ultimate displacements are known, the member drift θ (or chord-rotation) can be computed dividing Δ/l'_b:

$$\theta_y = \Delta_y / l'_b = 0.0116/3.1714 = 0.0037 \text{ rad}$$

$$\theta_u = \Delta_u / l'_b = 0.122/3.1714 = 0.038 \text{ rad}$$

Note: at this stage the ultimate drift (evaluated assuming full developed flexural mechanism) should be checked against the bar buckling by using Eq. C5.33 (Berry and Eberhard 2005):

$$\theta_{bb} = \frac{3.25\left(1 + k_{e\_bb}\,\rho_{eff}\frac{d_b}{D}\right)\left(1 - \frac{P}{A_g f'_c}\right)\left(1 + \frac{L_c}{10D}\right)}{100} = \frac{3.25\left(1 + \frac{3.1714}{10 \cdot 0.736}\right)}{100} = 0.046rad$$

$k_{e\_bb} = 0$ because $s/d_b \geq 6$

P=0 (no axial load in the beam)

D = beam depth = h

Since $\theta_{bb} > \theta_u$, bar buckling does not limit the member drift.

Shear Strength in the plastic hinge regions

The shear strength model proposed by the NZSEE/MBIE guidelines (NZSEE/MBIE 2016c) accounts for shear strength degradation in the plastic hinge regions by means of the degradation factor, γ, see Figure 20, which only applies to concrete contribution.

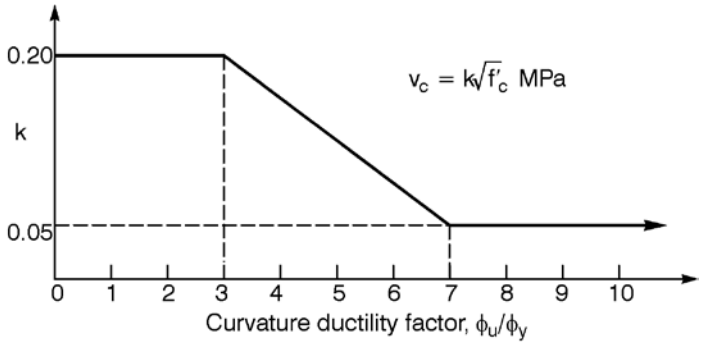

Figure 20: Shear strength degradation factor, γ, based on curvature ductility within the plastic hinge Priestley et al. (2007)

The probable shear strength, V_p, of beams, in the plastic hinge region, with rectangular stirrups or hoops is given by equation C5.1:

$$V_p = 0.85(V_C + V_s) = 0.85\,(\alpha\beta\gamma\sqrt{f_c'}\,b_w d + \frac{A_v f_{yt} d}{s})$$

where:

$$1 \le \alpha = 3 - \frac{M}{VD} \le 1.5 = 3 - \frac{L_c}{h/2} = 3 - \frac{3171.4}{736.6/2} = -5.6 < 1 \Rightarrow \alpha = 1$$

$\beta = 0.5 + 20\rho_l <= 1 = 0.5 + 20 * 0.013 = 0.76$

$\rho_l = A_l / A_g = 2432/(736.6 \cdot 254) = 0.013$

$b_w = 254$, width of beam web

d = effective depth of beam $= 0.8 \cdot h = 0.8 \cdot 736.6 = 589.3$mm

$A_v = n_l \cdot \pi \cdot (d_{st}/2)^2 = 157\text{mm}^2$

γ = shear strength degradation factor, 0.2 for $V_{p,max}$ and 0.05 for $V_{p,min}$

$$V_{p,max}(\gamma = 0.2) = 231\ kN$$

$$V_{p,min}(\gamma = 0.05) = 157\ kN$$

In this case, since $V_{p,min} \cdot l'_b = 157 \cdot 3.1714 = 498$ kNm$<M_u$-(682 kNm) , the shear failure limits the member drift at θ_s=0.01 rad (see Figure 21).

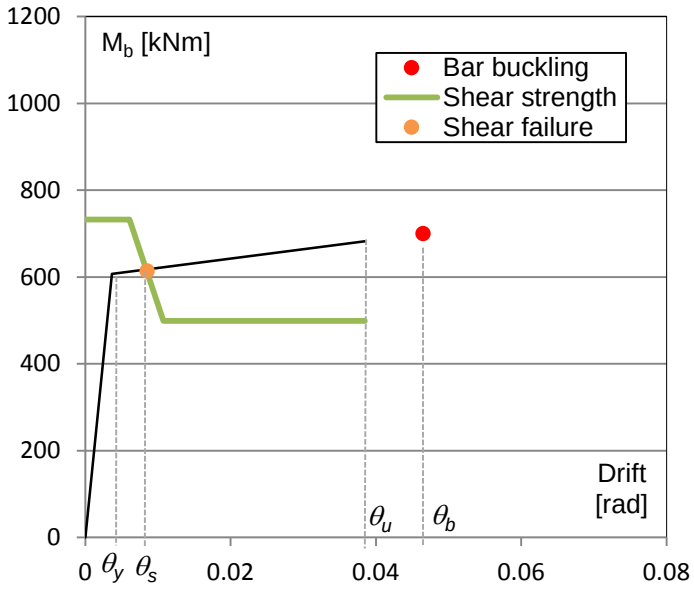

Figure 21: Typical Moment-Drift capacity of beams.

The plastic hinge properties for the beams of Frame 1 are reported in Table 15.

Table 15: Plastic hinge properties of Frame 1 beams

Bay	Level	Bending	M_y	θ_y	M_u	θ_u	θ_{bb}	$M(V_{p,min})$	Failure	θ_s
[-]	[-]	Direction	[kNm]	[rad]	[kNm]	[rad]	[rad]	[kNm]	[-]	[rad]
A/B (C/D)	1	+	403	0.0043	477	0.045	0.046	493	flex	-
		-	607	0.0037	682	0.038	0.046	498	shear	0.010
	2,3,4	+	349	0.0043	406	0.050	0.046	480	flex	-
		-	418	0.0037	487	0.050	0.046	480	shear	0.010
	5,6,7,R	+	192	0.0043	223	0.064	0.046	471	flex	-
		-	230	0.0037	268	0.063	0.046	471	flex	-
B/C	1	+	403	0.0043	477	0.045	0.046	493	flex	-
		-	607	0.0037	682	0.038	0.046	498	shear	0.010
	2,3,4	+	255	0.0043	296	0.054	0.046	475	flex	-
		-	306	0.0037	355	0.053	0.046	475	flex	-
	5,6,7,R	+	192	0.0043	223	0.064	0.046	471	flex	-
		-	230	0.0037	268	0.063	0.046	471	flex	-

3.3. **Columns**

For the columns, the same approach adopted to evaluate the capacity of the beam plastic hinges is assumed.

In this case study, given the use of deformed bars and the adequate lap splice length, no reduction of the flexural strength due to bond slip (deformed bars) is considered.

For example, the geometry and details of Level 1 exterior column A1 are reported in Table 16.

Table 16: Details of Level 1 exterior column A1.

Column width	b	[mm]	457.2
Column height	h	[mm]	457.2
Longit. bar cover	clb	[mm]	38.1
Storey height	H	[mm]	3050
Beam height	h_b	[mm]	736.6
Shear span (H-h_b)/2	L_c	[mm]	1156.7
Stirrups diameter	ϕ_{stirr}	[mm]	10
Stirrups spacing	s_{stirr}	[mm]	76
Number of legs	n_{lx}=n_{ly}	[-]	3
Longit. bar diameter	d_b	[mm]	28

In Eq. C5.9 the volumetric ratio of transverse reinforcement ρ_s, Eq. C5.10, should be replaced by a first principles approach (C5.5.3.5). According to Mander et al. (1988):

Confined concrete ultimate strain

The confined concrete ultimate strain can be computed using the formulation C5.9:

$$\varepsilon_{cu} = 0.004 + \frac{1.4\rho_s f_{yh}\varepsilon_s}{f'_{cc}} = 0.004 + \frac{1.4 \cdot 0.015 \cdot 300 \cdot 0.06}{31} = 0.0163$$

where:

the volumetric ratio of transverse reinforcement can be computed as:

$$\rho_s = \rho_{sx} + \rho_{sy} = (A_{vx}/d_c s) + (A_{vy}/b_c s) \Rightarrow$$

$$\rho_s = n_{lx} \cdot \pi \cdot \frac{\left(\frac{d_{st}}{2}\right)^2}{(d - 2clb + d_b + d_{st})s} + n_{ly} \cdot \pi \cdot \frac{\left(\frac{d_{st}}{2}\right)^2}{(b - 2clb + d_b + d_{st})s} = 0.015$$

Once that the confined concrete ultimate strain in derived, the flexural strength can be computed using the section analysis and accounting for the contribution of axial load N. At this stage, only

gravity loads (see Table 12) are considered. A summary of the column flexural capacity is reported in Table 17.

Table 17: Flexural capacity of Level 1 column (A1).

Strain limit of transverse reinforcement	ε_s	[-]	0.06
Unconfined concrete ultimate strain	ε_c	[-]	0.004
Confined concrete ultimate strain	ε_{cu}	[-]	$0.004 + \frac{1.4\rho_s f_{yh}\varepsilon_s}{f'_{cc}} = 0.0163$
Axial load	N_g	[kN]	473
Yielding moment	M_y	[kNm]	496
Ultimate moment	M_u	[kNm]	530
neutral axis depth at M_u	c	[mm]	123.8

Yielding and ultimate curvature

For rectangular-section columns, the yield curvature can be calculated (Priestley et al. 2007):

$$\phi_y = \frac{2.12\varepsilon_y}{\mathrm{h}} = \frac{2.12 \cdot 0.0015}{0.4572} = 0.007 \ \frac{\mathrm{rad}}{\mathrm{m}}$$

The available ultimate curvature for a column is given by C5.7:

$$\phi_u = \frac{\varepsilon_{cu}}{\mathrm{c}} = \frac{0.0163}{0.1238} = 0.132 \ \frac{\mathrm{rad}}{\mathrm{m}}$$

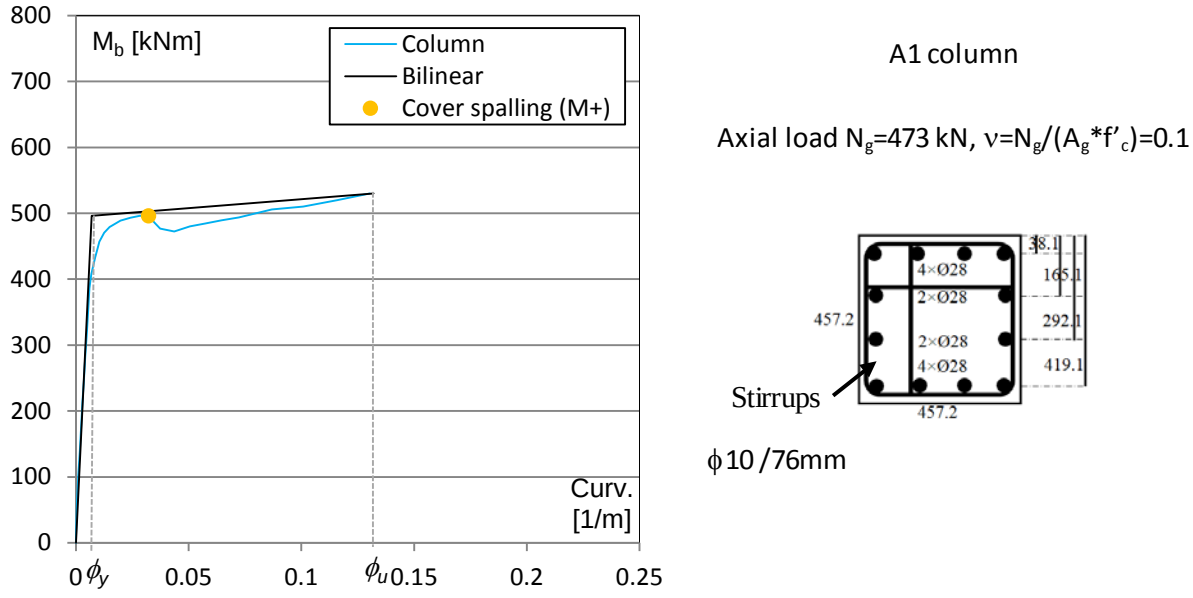

Figure 22: Moment-curvature behaviour of A1 column.

Component Drift

The column displacement at the yielding, measured at the contra-flexure point, can be computed with Eq. C5.18.

$$\Delta_y = \phi_y (H)^2/3 = \phi_y (L_c)^2/3 = 0.007(1.1567)^2/3 = 0.003\text{m}$$

To compute the ultimate column displacement, the plastic hinge length is needed. It can be computed using Eq. C5.20:

$$L_p = kL_c + L_{sp} = 0.05 \cdot 1156.7 + 184.8 = 0.243\text{m}$$

where:

$k = 0.2\,(f_u/f_{sy} - 1) \leq 0.08 = 0.2(375/300 - 1) = 0.05$

L_c=the distance of the critical section from the point of contra-flexure = 1156.7 mm

L_{sp}=*strain penetration* = $0.022 f_y d_b = 0.022 \cdot 300 \cdot 28 = 184.8$mm

The ultimate column displacement can be computed using Eq. C5.17:

$$\Delta_u = \Delta_y + \Delta_p = 0.003 + 0.035 = 0.038\text{m}$$

where:

$$\Delta_p = \phi_p L_p H = (\phi_u - \phi_y) L_p \cdot L_c = (0.132 - 0.007) \cdot 0.24 \cdot 1.1567 = 0.035\text{m}$$

Once that the yield and ultimate displacements are known the corresponding member drifts θ can be computed dividing the displacement by L_c:

$$\theta_y = \Delta_y / L_c = 0.003/1.1567 = 0.0027 \text{ rad}$$

$$\theta_u = \Delta_u / L_c = 0.038/1.1567 = 0.033 \text{ rad.}$$

Note: at this stage the ultimate drift should be checked against the bar buckling by using Eq. C5.33 (Berry and Eberhard 2005):

$$\theta_{bb} = 3.25 \left(1 + k_{e\_bb} \rho_{eff} \frac{d_b}{D}\right) \left(1 - \frac{P}{A_g f_c'}\right) \left(1 + \frac{L_c}{10D}\right) / 100 = 0.053 \text{ rad}$$

$k_{e\_bb} = 40$ because $s/d_b < 6$

$\rho_{eff} = \rho_s f_{ys} / f'_c$

D = column depth = h

A_g = column gross section area

Since $\theta_{bb} > \theta_u$, the bar buckling does not limit the member drift.

Shear Strength in the plastic regions

The shear strength model suggested in the NZSEE/MBIE guidelines (NZSEE/MBIE 2016c) for RC columns accounts for the contribution provided by the concrete mechanism, steel shear reinforcement and the axial compressive load N (shown in Figure 23a as P), respectively. The coefficient, γ, accounts for the strength degradation of the concrete contribution with the curvature ductility, see Figure 23b.

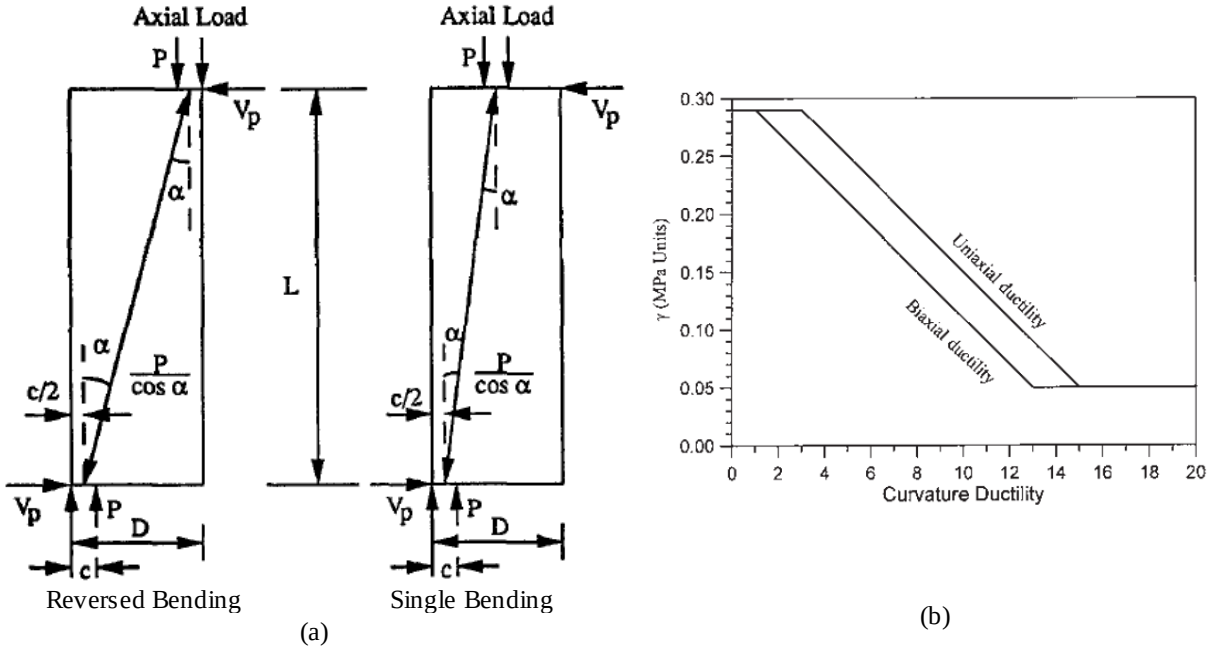

Figure 23: Column shear strength assessment model: (a) contribution of the axial load (Priestley et al. 1994); (b) shear strength degradation factor (Kowalsky and Priestley 2000).

The probable shear strength, V_p, of columns in the plastic hinge region, is given by equation C5.27:

$$V_p = 0.85\,(V_c + V_s + V_n)$$

where:

a) The shear contribution from the concrete, V_c, can be evaluated using Eq. C5.28:

$$V_c = \alpha\beta k\sqrt{f'_c}(0.8A_g)$$

where:

$$1 \le \alpha = 3 - \frac{M}{VD} \le 1.5 = 3 - \frac{L_c}{h/2} = 0.94 < 1 \Rightarrow \alpha = 1$$

$\beta = 0.5 + 20\rho_l <= 1 = 0.5 + 20 * 0.035 = 1.2 > 1$; $\beta = 1$

$\rho_l = A_l / A_g = 7390/457.2^2 = 0.035$

$$V_{c,max}(k = 0.29) = 246\ kN$$

$$V_{c,min}(k = 0.05) = 42.5\ kN$$

b) The shear contribution from the steel shear reinforcement, V_s, is computed using Eq. C.5.29.

$$V_s = \frac{A_v f_{yt} d''}{s}\cot 30^\circ = \frac{235.6 \cdot 300 \cdot 295.3}{76}1.73 = 475kN$$

where:

$A_v = n_{lx} \cdot \pi \cdot (d_{st}/2)2 = 235.6\ mm^2$

$d'' = h\text{-}c\text{-}clb = 457.2\text{-}123.8\text{-}38.1 = 295.3\ mm$

c) The shear contribution from the axial compressive load N on the column is given by Eq. 5.31

$$V_n = N \cdot \tan\alpha = 473 \cdot 0.144 = 68.1\ kN$$

where: $\tan\alpha = (h\text{-}c)/H = (457.2\text{-}123.8)/2313.4 = 0.144$

Using Eq. C5.27, the shear strength at the minimum and maximum ductility demand can be computed:

$$V_{p,max} = 0.85\ (V_{c,max} + V_s + V_n) = 671\ kN$$

$$V_{p,min} = 0.85\ (V_{c,min} + V_s + V_n) = 498\ kN$$

In this case, since, $V_{p,min} \cdot L_c = 498 \cdot 1.1567 = 576$ kNm$> M_u$, the shear failure does not limit the member drift (see Figure 25). When a column flexural-shear mode is expected, a more accurate estimation of the ULS drift can be obtained with Eq. C5.32 (Elwood and Moehle 2005b):

$$\Delta_s = L_c \left(0.03 + 4\rho_s - 0.024 \frac{\nu}{\sqrt{f_c'}} - 0.025 \frac{P}{A_g f_c'} \right) \geq 0.01 L_c$$

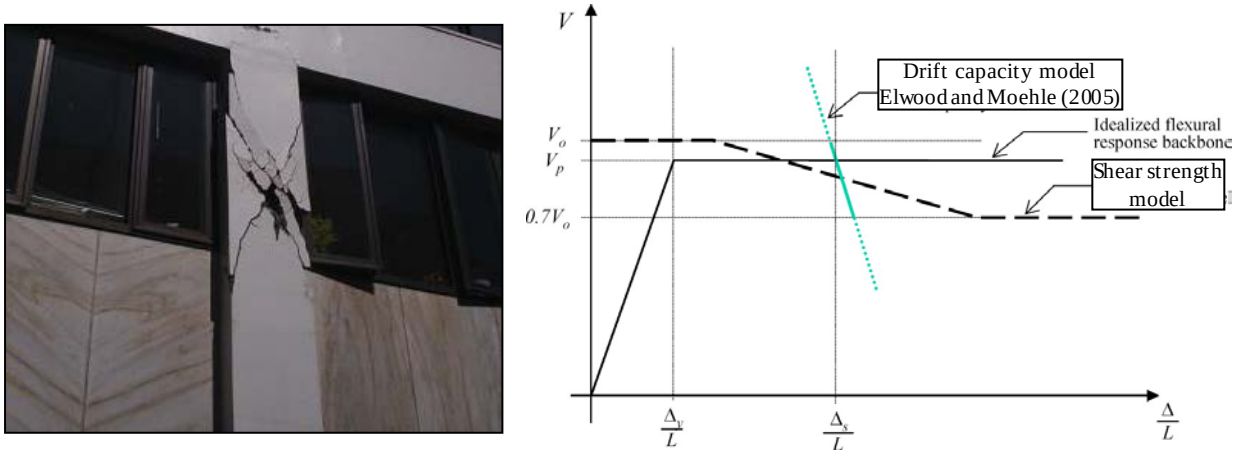

Figure 24: Drift capacity model at the column shear failure.

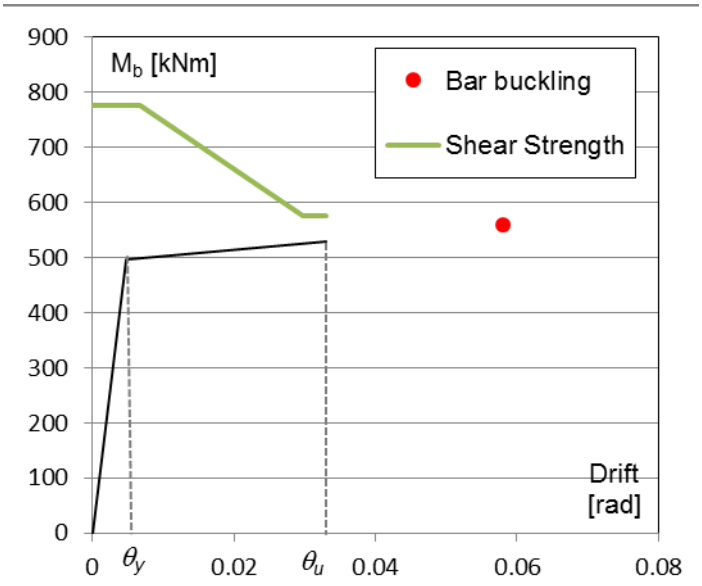

Figure 25: Moment-Drift capacity of a typical column.

The plastic hinge properties for the columns of Frame 1 are reported in Table 18.

Table 18: Plastic hinge properties of Frame 1 columns.

Bay [-]	Level [-]	M_y [kNm]	θ_y [rad]	M_u [kNm]	θ_u [rad]	θ_{bb} [rad]	$M(V_{p,min})$ [kNm]	Failure [-]	θ_s [rad]
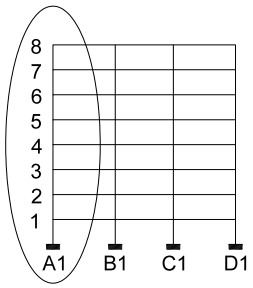 Exterior (A1,D1)	1	496	0.0027	530	0.033	0.053	576	flex	-
	2	490	0.0027	528	0.067	0.054	572	flex	-
	3	485	0.0027	526	0.073	0.054	571	flex	-
	4	477	0.0027	514	0.074	0.055	573	flex	-
	5	207	0.0027	223	0.097	0.050	449	flex	-
	6	195	0.0027	212	0.100	0.051	442	flex	-
	7	183	0.0027	203	0.092	0.051	432	flex	-
	8	169	0.0027	191	0.093	0.052	428	flex	-
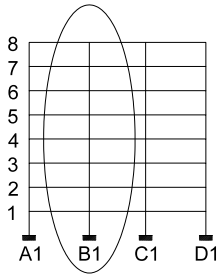 Interior (B1,C1)	1	616	0.0027	681	0.104	0.053	841	flex	-
	2	604	0.0027	669	0.109	0.054	848	flex	-
	3	590	0.0027	653	0.105	0.056	855	flex	-
	4	422	0.0027	460	0.103	0.057	852	flex	-
	5	400	0.0027	442	0.108	0.059	846	flex	-
	6	230	0.0027	243	0.101	0.049	463	flex	-
	7	207	0.0027	227	0.100	0.050	449	flex	-
	8	183	0.0027	203	0.094	0.051	437	flex	-

3.4. **Beam-column joints**

The geometric details of the exterior joint subassembly of Frame 1 at Level 1 (A1) are reported in Table 19.

Table 19: Details of Level 1 exterior joint subassembly (A1).

Column width	b_c	[mm]	457.2
Column height	h_c	[mm]	457.2
Longit. bar cover	clb	[mm]	38.1
Column lenght	l_c	[mm]	3050
Beam height	h_b	[mm]	736.6
Bay length	L_{bay}	[mm]	7600
Half beam length	l_b	[mm]	3800
Gravity axial load	N_g	[kN]	473

The joint core is well detailed (5 ϕ10 stirrups, 100 mm spaced, A_{st} = 2x5x3.14x10^2/4 = 785mm^2). However, it was not designed to achieve capacity design criteria. This may result in the joint cracking, joint shear failure and, in turn, in a reduced capacity of the subassembly limiting the seismic performance of the whole frame. It is worth mentioning that, initially, the presence of joint stirrups was neglected in order to be more conservative. Nevertheless, in Section 7, the capacity of the building is re-assessed considering the joint stirrups to evaluate the influence on the hierarchy of strength and building capacity.

For interior and exterior beam-column joints without shear reinforcement, the probable horizontal joint shear force that can be resisted is given by Eq. C5.35. This equation is based on the Mohr's circle theory applied to the joint panel subjected to external actions transmitted by framing members (Priestley 1997). Details are given in Figure 26. The same approach is adopted in international standards (CEN 2005; MI 2008).

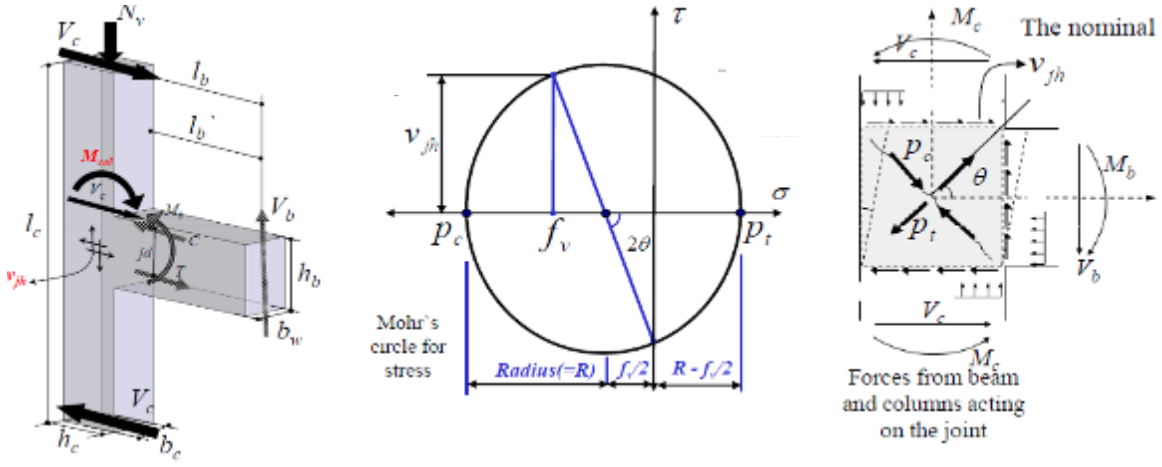

Figure 26: (a) Free-body diagram of a beam-column joint subassembly; (b) Mohr's circle theory applied to calculate the joint shear and principal tensile/compression stresses; (c) Moment, shear and stresses at joint region (modified after Pampanin et al. 2003; Akguzel and Pampanin 2010; Tasligedik et al. 2016).

It is worth mentioning that f_v is the axial stress on the joint panel, coming from the gravity axial load, while f_h is the horizontal confinement stress due to the joint stirrups, if present.

$$V_{pjh} = 0.85\, b_j h \sqrt{(k\sqrt{f_c'})^2 + k\sqrt{f_c'}(f_v + f_h) + f_v f_h} \leq 1.92\sqrt{f_c'}\, b_j h$$

$$= 0.85 \cdot 457.2 \cdot 457.2 \sqrt{(k\sqrt{25.8})^2 + k\sqrt{25.8}(2.26 + 0) + 2.26 \cdot 0}$$

$$\leq 1.92\sqrt{f_c} \cdot 457.2 \cdot 457.2$$

where:

$b_j = b_c$ =457.2 mm (as per NZS3101:2006)

$h = h_c = 457.2$ mm

$f_v = N/(b_c\ h_c) = 473000/(457.2 \times 457.2) = 2.26$ N/mm^2

$f_h = A_{st} f_{sy}/(b_j h_b) = 785 \times 300/(457.2 \times 736.6) = 0.70$ N/mm^2 (neglected, $f_h = 0$)

The following values of the coefficient k, suggested by the NZSEE/MBIE guidelines (NZSEE/MBIE 2016c) as function of the reinforcement detailing, are used:

- for interior joints, k = 0.8 (note that compression failure rather than tensile failure would govern in an interior beam-column joint)
- for exterior joints with beam longitudinal (deformed) bars anchored by bending the hooks into the joint core, k = 0.4 (at the failure), 0.3 (at first cracking)

Joint first cracking (k=0.3) $V_{pjh,fc}$ =427 kN ≤ 2022 kN
Joint failure (k=0.4) $V_{pjh,max}$ =525 kN ≤ 2022 kN

The joint shear strength is then converted into equivalent column moments (calculated at the interface with the beam) to be used in the strength hierarchy. More details on the physical meaning of the equivalent column moment are given in Section 4.1. . This results in:

$$M_{col} = \frac{V_{jh}}{\left[\frac{l_c}{l_b jd}\left(l_b - \frac{h_c}{2}\right) - 1\right]}\left(\frac{l_c - h_b}{2}\right)$$

$$= \frac{V_{jh}}{\left[\frac{3050}{3800 \cdot 0.9 \cdot (736.6 - 38.1)}\left(3800 - \frac{457.2}{2}\right) - 1\right]}\left(\frac{3050 - 736.6}{2}\right)$$

Joint first cracking (k=0.3) $M_c(V_{pjh,fc})$=140 kNm
Joint failure (k=0.4) $M_c(V_{pjh,max})$ =172 kNm

Figure 27 shows the capacity curve of the joint A1.

The step by step process to convert the joint shear strength into equivalent column moment here applied is also indicated in the NZSEE guidelines (Eq. C5.45 in Table C5.11). The original procedure is recalled in Table 20, for convenience.

Horizontal shear force acting on the joint core	$V_{jh} = T - V_c$	C5.38

$\frac{\quad)}{\phi}\ kNm$	C5.53

Table 20: Step by step procedure to convert the joint shear strength in equivalent column moment (NZSEE 2016, adapted from Akguzel and Pampanin, (2012).

Furthermore, the equivalent column moment calculated in the centroid of the joint panel is computed. It is obtained multiplying the column shear for half of the column clear height (in this case 1156.7mm). The latter is needed to include the joint panel non-linear behaviour in a numerical model (Pampanin et al. 2003). More details on this approach are given in Section 9.

The plastic hinge properties for the joints panels in Frame 1 are reported in Table 21.

Table 21: Joint hinge properties.

Bay [-]	Level [-]	$V_{pjh,fc}$ [kN]	$M_c(V_{pjh,fc})$ [kNm]	$M_{c,j}(V_{pjh,fc})$ [kNm]	θ_{crack} [rad]	$V_{pjh,max}$ [kN]	$M_c(V_{pjh,max})$ [kNm]	$M_{c,j}(V_{pjh,max})$ [kNm]	θ_{peak} [rad]	θ_u [rad]
Exterior (A1,D1)	1	427	140	185	0.0002	525	172	227	0.005	0.010
	2	388	127	168	0.0002	479	157	207	0.005	0.010
	3	372	122	161	0.0002	462	152	200	0.005	0.010
	4	355	117	154	0.0002	444	146	192	0.005	0.010
	5	338	111	146	0.0002	425	140	184	0.005	0.010
	6	319	105	138	0.0002	406	133	176	0.005	0.010
	7	299	98	130	0.0002	386	126	167	0.005	0.010
	8	278	183	241	0.0002	364	239	315	0.005	0.010
Interior (B1,C1)	1	540	177	233	0.0003	1050	344	454	0.0075	0.015
	2	485	159	210	0.0003	958	314	415	0.0075	0.015
	3	459	151	199	0.0003	924	303	400	0.0075	0.015
	4	432	142	187	0.0003	888	291	384	0.0075	0.015
	5	403	132	174	0.0003	851	279	368	0.0075	0.015
	6	372	122	161	0.0003	812	266	351	0.0075	0.015
	7	338	111	146	0.0003	771	253	334	0.0075	0.015
	8	299	196	259	0.0003	728	478	630	0.0075	0.015

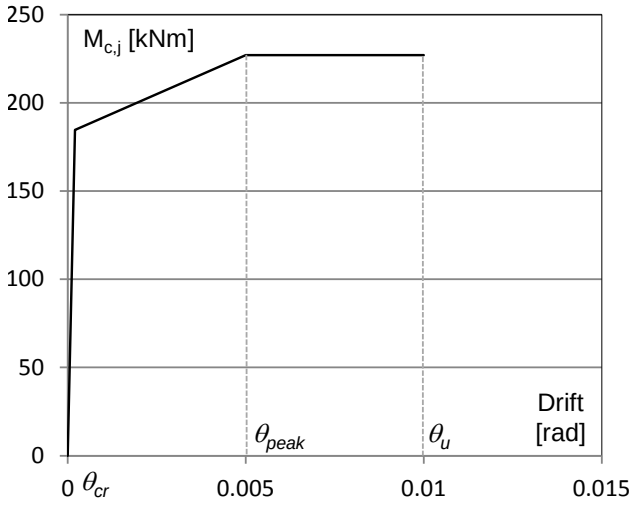

Figure 27: Moment-Drift capacity of joint A1.

4. FRAME 1 LATERAL CAPACITY

In this section, the capacity curve of frame 1 is calculated following the step-by-step SLaMA approach. For the sake of synthesis, the same level of detail of Frame 1 is not given for Frame A. The capacity curve of the Frame A can be calculated by analogy, following the calculations shown in this section.

4.1. **Strength hierarchy**

In order to compare the capacity of the beam-column joint with those of the framing members a unique parameter is needed. In the procedure proposed in (Calvi et al. 2002), the equivalent column moment is used. The procedure consists in calculating the moment needed on the column corresponding to the achievement of a specified capacity on the other framing members (i.e. development of the plastic hinge on the beam, joint shear failure, etc.). The mechanism associated with the lowest column moment it is likely to happen first and characterize the strength hierarchy. Once the capacity of the framing member is evaluated, it can be represented in an Equivalent Column Moment-Axial Load interaction diagram, or performance domain (see Figure 29). In order to assess the failure sequence using a performance domain, the demand is needed. It is defined as bending moment expressed as a function of the variation of the axial load due to the lateral sway of the frame (static equivalence). Hence, the seismic demand can be represented in the performance domain. The intersections of the demand and the lateral capacity of each component provides the sequence of the failure mechanism in a joint sub-assembly.

The member flexural and shear strengths are calculated with the previous formulations varying the axial load. The equivalent column moment associated to a specific joint shear can be computed with the procedure proposed in Table C5.11 and already discussed in the previous section.

Based on basic equilibrium relations of the joint subassembly, the column moment associated with the column shear can be computed as:

$$M_c = V_c * L_c$$

Similarly, the column moment associated to the beam moment is:

$$M_c = M_b(l_b L_c / l'_b l_c / 2)$$

where: L_c and l'_b are the column and beam shear span, respectively.

Note that the column moment associated with the beam shear strength can be derived with the previous equation and considering that $M_b = V_b * l'_b$.

For interior beam-column subassemblies, the column moment associated to the beam moment can be calculated summing the contribution of the two framing beams.

The seismic demand represented by the axial load variation as a function of the lateral force, F, on the frame, can be expressed (following Eq. C5.74 in the NZSEE 2017 guidelines; see), as:

$$N_{seismic} = N_g \pm \alpha F = N_g \pm \alpha F \frac{F_c}{V_c} = N_g \pm \alpha V_c \frac{F}{V_c}$$

where:

- N_g is the gravity axial load (see Table 11 for details);
- α depends on the global geometry of the building (height and total bay length, see Figure C5.41 in the NZSEE (NZSEE/MBIE 2016c) guidelines).

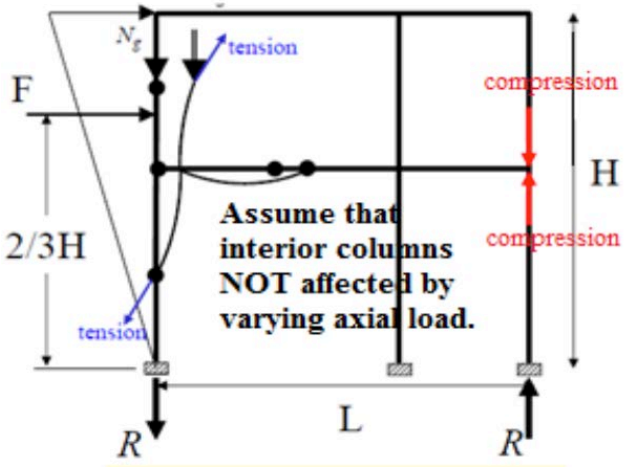

Figure 28: Example of axial load variation in a frame (NZSEE/MBIE 2016c).

It is worth noting that the expression above for simplicity, and on the conservative side, here neglects the contribution of the base column moment to the overall Overturning Moment (OTM), which can be in the range of 20-30% depending on the frame geometry.

With reference to the joint A1, the axial load variation at the ground floor columns is computed using the approach suggested at C5.6.2. Given a total building height, H=24.4m, and total length of Frame 1, L=20.4m, α = 2H/3L= (2*24.4/3*20.4)=0.80.

In order to estimate the axial load increase as function of the column shear V_c and, in turn, of the column moment, M_c, the ratio F/V_c needs to be computed. It is suggested to use a value of 4, for regular frames (more information can be found in Kam, 2011).

Once that all the strength are converted into equivalent moment in the column, the performance domain can be drawn. Figure 29 shows the performance domain of the external joint at the first floor (joint A1).

Figure 29 outlines a failure sequence typical of existing beam-column subassemblies designed with seismic details not conforming to current seismic codes (i.e. lack of adequate amount of joint stirrups). The joint cracking and joint shear failure anticipate the development of the beam hinge both in the push and pull direction. Note that in the pull direction the beam shear failure for large ductility demand anticipates the joint failure. However, it is worth mentioning that this mechanism cannot appear before the beam yielding.

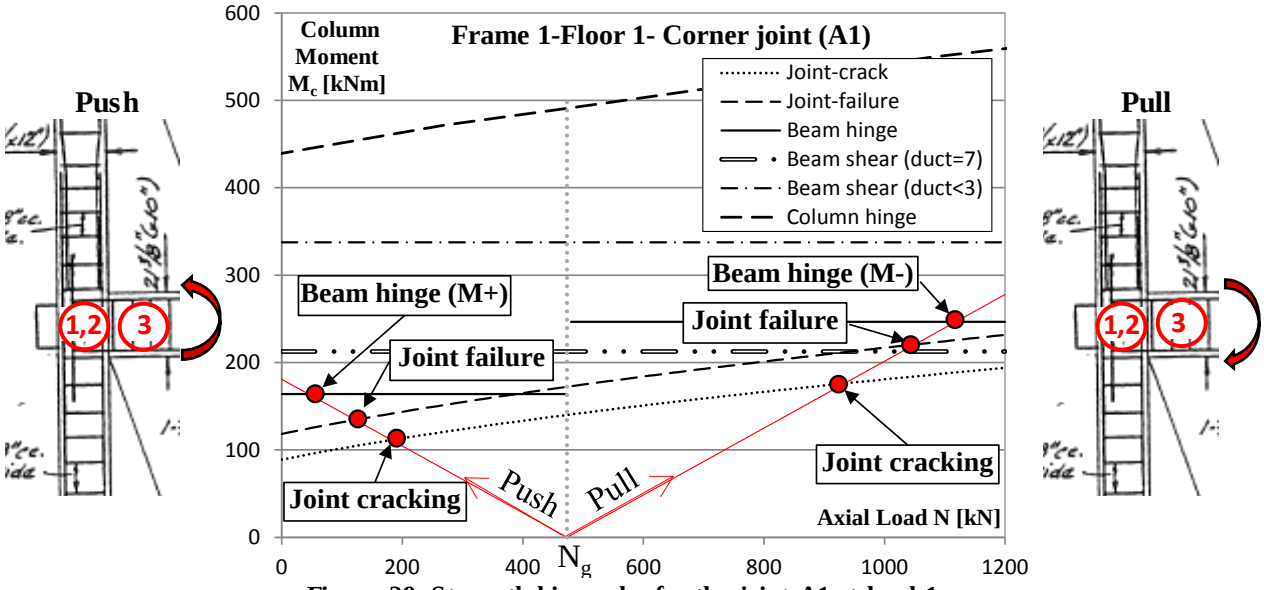

Figure 29: Strength hierarchy for the joint A1 at level 1.

4.1.1. *Effects of material properties variation on the sequence of events/hierarchy of strength*

At this stage, in order to evaluate the effects of the material properties on the strength hierarchy (as suggested in the section C5.4.1 of NZSEE 2017 guidelines), the probable concrete compressive strength is reasonably modified by a variation of $\pm 20\%$ (f'_c=25.8+20% = 30MPa and f'_c=25.8 - 20% = 20MPa).

For the strength hierarchy depicted in Figure 29, this variations does not produce significant effects; the sequence of events is always governed by the joint shear strength.

A summary of the effects of the variation of concrete compressive strength on the strength hierarchy for the joint subassemblies of Frame 1 is reported in Table 22.

Table 22: Strength hierarchy summary

Joint [-]	Level [-]	Hierarchy [-]	Hierarchy (f_c+20%)	Hierarchy (f_c-20%)	M_c [kNm]	V_c [kN]
Exterior A	1	**JF**	JF	JF	140	121
	2	**JF**	JF	JF	128	111
	3	**JF**	JF	JF	126	109
	4	**JF**	JF	JF	124	107
	5	**BH**	BH	BH	77	67
	6	**BH**	BH	BH	77	67
	7	**BH**	BH	BH	77	67
	8	**BH**	BH	BH	154	133
Exterior D	1	**JF**	JF	JF	219	189
	2	**JC-BH**	JC-BH	JC-BH	169	146
	3	JC-BH	JC-BH	**JF**	163	141
	4	JC-BH	JC-BH	**JF**	153	132
	5	**BH**	BH	BH	93	80
	6	**BH**	BH	BH	93	80
	7	**BH**	BH	BH	93	80
	8	**BH**	BH	BH	186	161
Interior B, C	1	**JF**	JF	JF	348	301
	2	**JC-BH**	JC-BH	JC-BH	226	195
	3	**JC-BH**	JC-BH	JC-BH	226	195
	4	**JC-BH**	JC-BH	JC-BH	226	195
	5	**JC-BH**	JC-BH	JC-BH	170	147
	6	**JC-BH**	JC-BH	JC-BH	170	147
	7	**JC-BH**	JC-BH	JC-BH	170	147
	8	**CH**	CH	CH	183	158

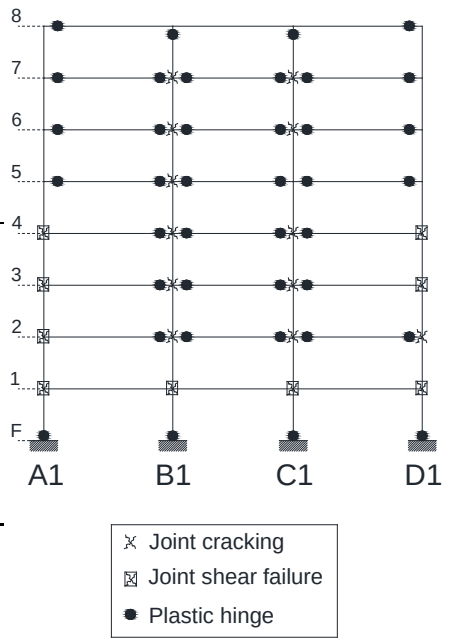

where: JC is the joint first cracking; JF is the joint shear failure; BH is the activation of beam plastic hinge.

It should be also noted that **in few cases the concrete strength variation affects the strength hierarchy**. Indeed, for the exterior joint subassembly D1, a variation of the concrete compressive strength of -20% (20MPa) would activate a joint panel shear failure instead of a beam hinging at level 3 and 4.

Given the fact that such a variation can be reasonably expected in cast-in-situ RC buildings, it might be appropriate to consider the joint shear failure as the governing mechanism and, thus, evaluate both strength and deformation capacity of the frame accordingly.

Alternatively, on-site core sampling at the same level/floor and closer to that joint (but outside the Plastic hinge region) would be recommended to gain further yet targeted information on the material properties. The FRP strengthening of the joint panel can significantly improve the subassembly performances avoiding the joint panel shear failure and promoting the more ductile beam hinging (see Akguzel and Pampanin 2012; Del Vecchio et al. 2015 for details on the design procedure).

4.2. **Capacity curves**

Once the nonlinear behaviour of all the structural components is evaluated, the lateral capacity of seismic resisting systems can be assessed.

In this example the lateral capacity of the Frame 1 is calculated considering three different failure mechanism (upper bound, lower bound and in-between/actual, see Figure 30) suggested in Section C5.6.3.

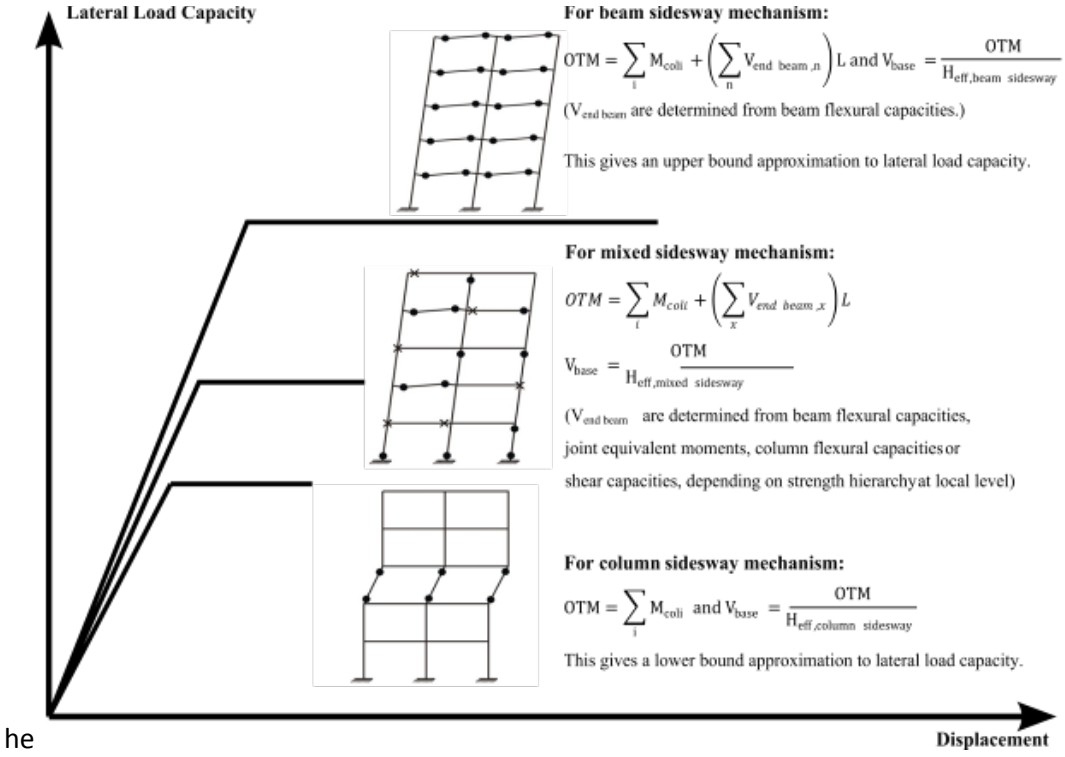

Figure 30: Lateral load capacity versus displacement for different global mechanisms (NZSEE/MBIE 2016c).

4.2.1. *Beam sidesway mechanism – upper bound*

This mechanism represents an upper bound of the lateral load capacity and it assumes that all the beams plastic hinges have formed (yielded) at all floors and at the base columns (see Figure 32). The base shear, $V_{b,1}$, can be computed dividing the overturning moment, $OTM_{,1}$ (Eq. C.5.76), by the frame effective height, H_{eff} (see Figure 23).

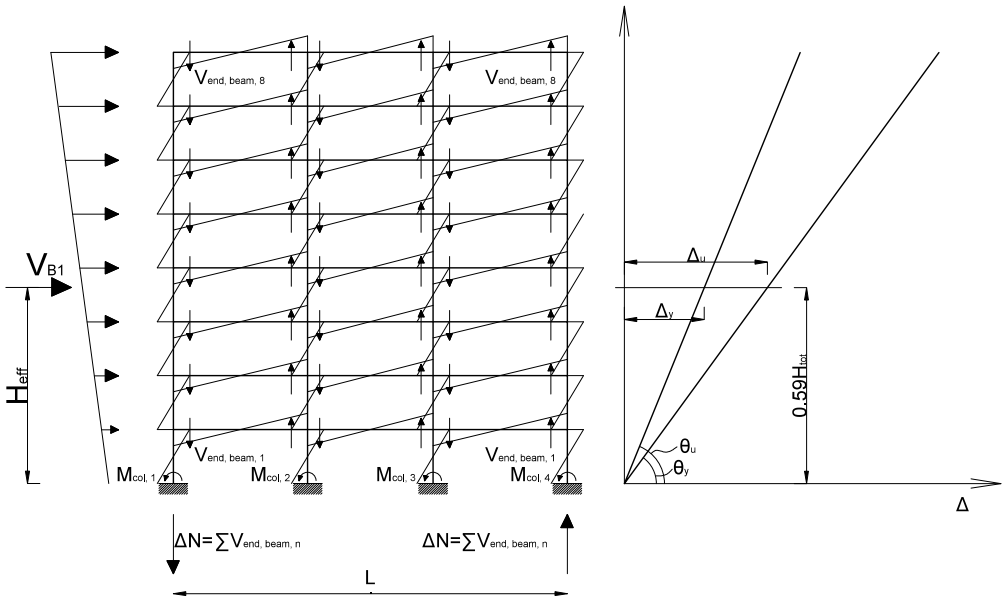

Figure 31: Overturning moment calculation.

$$OTM,1 = \mathrm{V_{b,1}} * \mathrm{H_{eff}} = \sum_{\mathrm{i}} M_{\mathrm{col,i}} + \left(\sum_{\mathrm{n}} V_{\mathrm{end\ beam,n}}\right) L$$

where:

$V_{end\ beam}$ is the end beam shear resulting in column axial load (evaluated in correspondence of the maximum flexural capacity, see Table 15).

$M_{col,i}$ is the column flexural capacity at the base (see Table 18). The exterior column flexural capacity (A1, D1) is computed considering the axial load variation due to the beam shear (ΔN positive or negative, depending on the load direction).

H_{eff} is herein computed using the displacement profiles suggested by NZSEE 2006 (2012) section 7.2.4d for $4< n\leq 20$:

$$\mathrm{H_{eff}} = [0.64 - 0.0125(n-4)]\ \mathrm{H} = 0.59 \cdot 24.4 = 14.4\mathrm{m}$$

With reference to the yielding moment of exterior beams reported in Figure 32, the maximum allowable shear on the exterior beams (axial load variation, $\Delta N_{s,n}$ on columns) at the last floor $V_{end\ beam,8}$ can be estimated as:

$$V_{\text{end beam,8}} = \frac{(M_{b,left} + M_{b,right})}{L_{bay}} = \frac{(192 + 230)}{6.3} = 66.6 \text{ kN}$$

Once that the beam seismic shear is computed at each floor, the $OTM_{,1}$ can be computed:

$$OTM,1 = (384 + 616 + 616 + 564) + [(4 * 66.6) + (3 * 120.9) + 159.2)20.4 = 18261\ kNm$$

and the base shear $V_{b,1}=OTM_{,1}/H_{eff}=18261/14.4=1268$ kN.

The frame top displacement at the significant points of the beam nonlinear behaviour can be computed using the component drift reported in Table 15.

- Yielding displacement $\Delta_y=\min(\theta_{y,beams})\cdot H_{eff}=0.0037\cdot 14.4= 53$ mm
- Ultimate displacement (beam shear failure) $\Delta_u=\min(\theta_s)\cdot H_{eff}=0.01\cdot 14.4= 144$ mm
- Ultimate displacement (beam bar buckling) $\Delta_u=\min(\theta_{bb})\cdot H_{eff}=0.038\cdot 14.4= 547$ mm

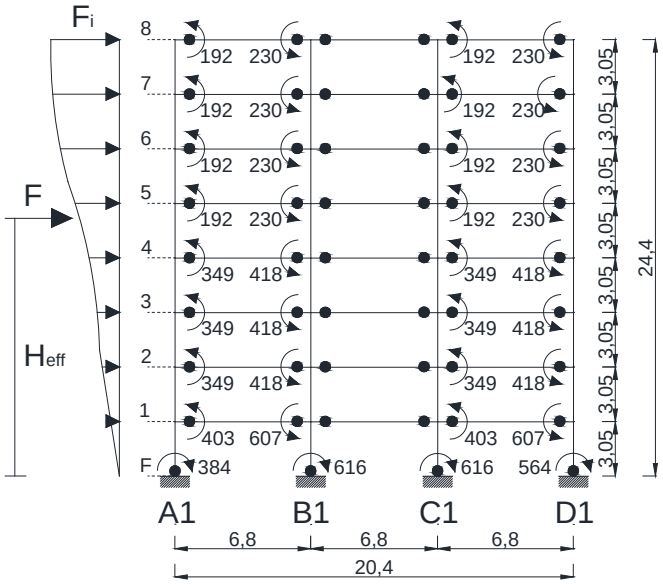

Figure 32: Distribution of moments for the beam sidesway mechanism.

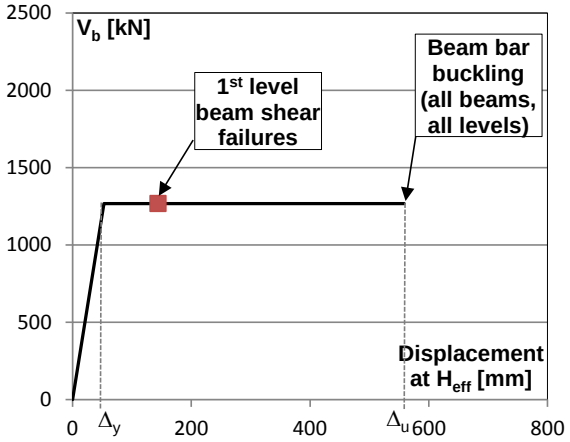

Figure 33: Pushover curve of Frame 1 due to beam sidesway mechanism.

4.2.2. *Column sidesway mechanism – lower bound*

The frame lateral capacity referring to the column sidesway mechanism should be computed assuming a soft-storey mechanism at each of the building level. Then it can be assumed that the mechanism with the lowest base shear is the most probable or, as suggested in the Chapter 2, to use the Sway Index (see C2A.2) to determine the weakest floor.

Here, for sake of simplicity, it is assumed that the mechanism involves the ground floor columns.

This mechanism represent a lower bound of the lateral load capacity and it assumes that all the columns at the same level are yielded forming a soft-storey mechanism (see Figure 34).

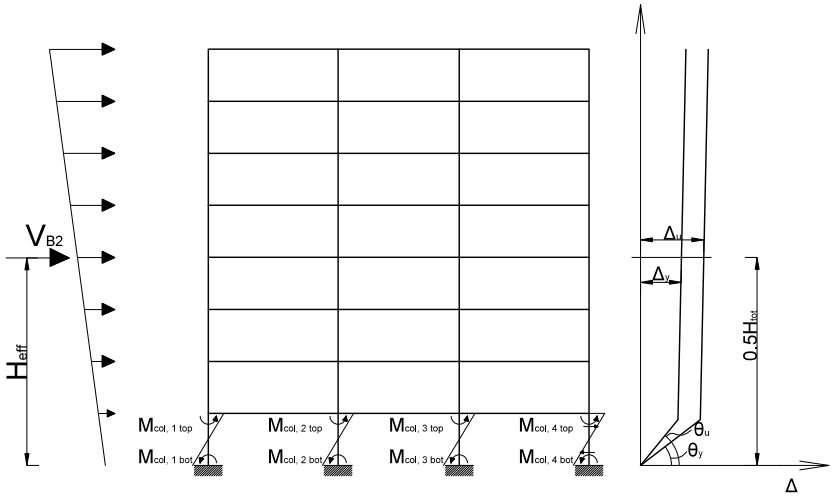

Figure 34: Column-sidesway mechanism overturning moment and assumed displacement shape.

The base shear, $V_{b,2}$, can be computed with Eq. C.5.77:

$$V_{b,2} = \sum_i M_{col,base,i} / (0.5\ h)$$

where:

$M_{col,base,i}$ is the column flexural capacity at the base (ground level, see Table 18). For sake of simplicity, the column moments associated with the gravity load is used for the calculations. In the case that the column sidesway mechanism governs the building lateral response, more refined estimation of the base shear can be obtained considering the influence of axial load variation due to seismic shaking on the column flexural capacity.

h is the clear interstorey height of the ground floor.

$$V_{b,2} = \frac{496 + 496 + 616 + 616}{0.5 \cdot 2.3} = 1933\ \text{kN}$$

This is higher than the base shear corresponding to the beam sidesway mechanism. This means that a column sidesway mechanism would not be expected at the ground level, but more likely at a higher level, more likely the 4th floor, where tapering in the columns is happening.

The frame top displacement at the significant points of the nonlinear behaviour of base columns can be computed using the component drift reported in Table 18.

- Yielding displacement $\Delta_y = \min(\theta_{y,columns}) \cdot H_{eff} = 0.0027 \cdot 12200 = 33$ mm

- Ultimate displacement (Concrete core crushing) $\Delta_u = \min(\theta_u) \cdot H_{eff} = 0.033 \cdot 12200 = 403$ mm

where H_{eff} can be taken as 0.5H=12.2m for column sidesway mechanism (Priestley 1997).

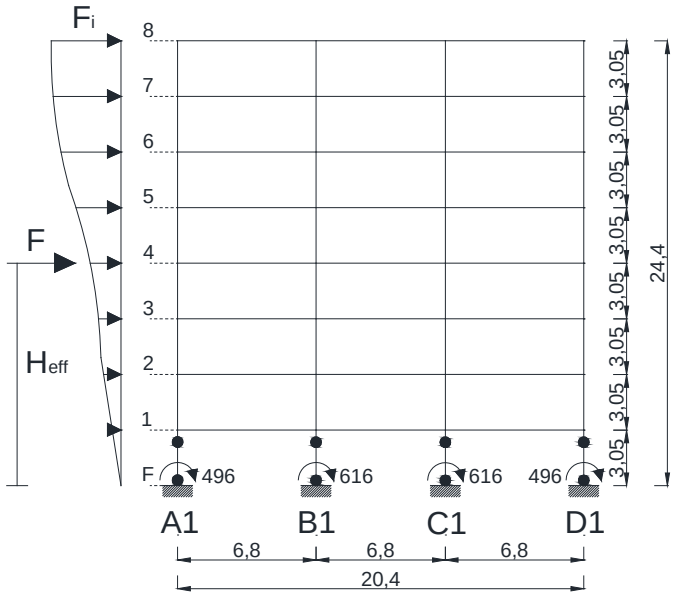

Figure 35: Moment distribution for column sidesway mechanism.

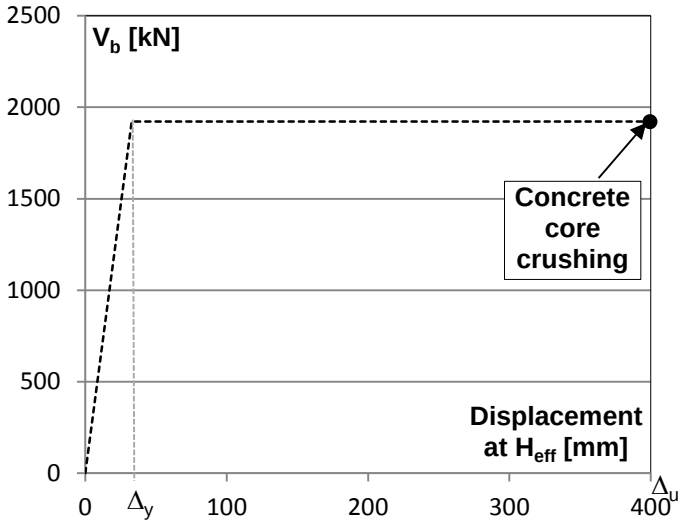

Figure 36: Pushover curve of Frame 1 due to column sidesway mechanism.

4.2.3. *Mixed sidesway mechanism - actual*

This mechanism represents the most refined estimation of the Frame 1 lateral behaviour. In fact, the strength hierarchy accounts for all the possible failure mechanisms that may significantly reduce the structural capacity, including the joint shear failure (Figure 37). The results of the strength hierarchy, considering the variation of the axial load on the joint subassemblies and are reported in Table 22.

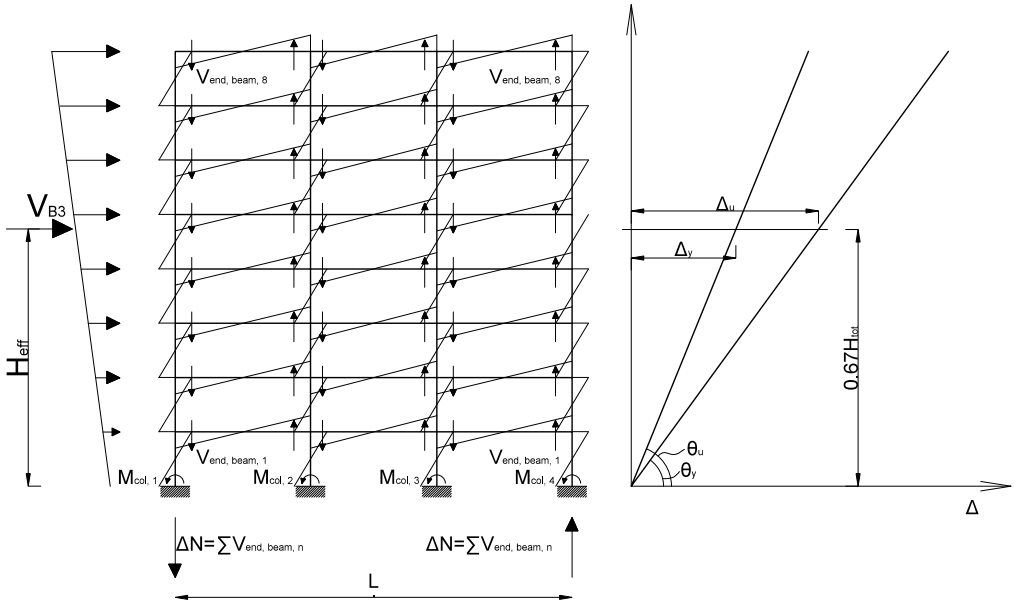

Figure 37: Mixed-sidesway overturning moment and assumed displacement profile.

The base shear, $V_{b,1}$, can be computed dividing the overturning moment, $OTM_{,3}$ (Eq. C.5.78), by the frame effective height, H_{eff}.

$$OTM,3 = V_{b,1} * H_{eff} = \sum_{i} M_{coli} + \left(\sum_{n} V_{end\ beam,n}\right) L$$

where:

$V_{end\ beam}$ is the beam end shear resulting in additional column axial load (computed in correspondence of the maximum flexural capacity).

$M_{col,i}$ is the column flexural capacity (evaluated with the strength hierarchy to account for axial load variation)

H_{eff} is computed in first approximation as:

$$H_{eff} = 0.67\ H = 0.67 \cdot 24.4 = 16.3m$$

A summary of the component failure mode at each floor is reported in Figure 38 along with the related column and beam moments. In this example, the beam moment is calculated as the sum of the moments of the columns framing in the joint, divided by the number of beams (1 for exterior joints, 2 for interior) $M_b = \sum Mc / n_b$. The actual beam moment should be calculated inverting formulations used in section 4.1 to calculate the column moment. The adopted approximation leads, in this case, to slight underestimate the base shear.

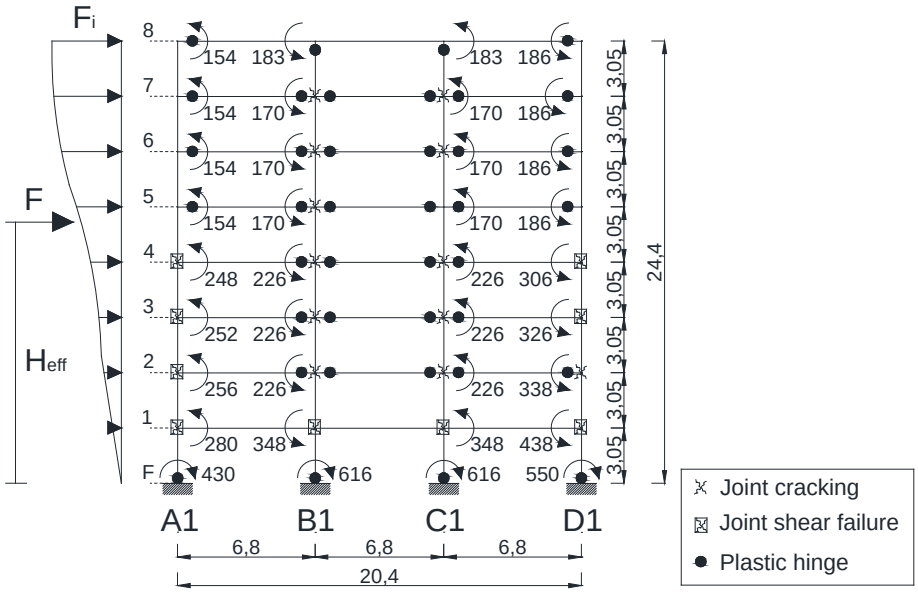

Figure 38: Moment distribution on the Frame 1 for mixed sidesway mechanism.

With reference to the bending moment at the exterior beams reported in Figure 38, the maximum allowable shear on the exterior beams (axial load variation, $\Delta N_{s,n}$ on columns) at the last floor $V_{end\ beam,8}$ can be estimated as:

$$V_{\text{end beam,8}} = \frac{\left(M_{b,left} + M_{b,right}\right)}{L_{bay}} = \frac{(154 + 183)}{6.3} = 53.5 \text{ kN}$$

Once that the beam shear is known at each floor, the OTM,3 can be computed

$$OTM,3 = (430 + 616 + 616 + 550) + (571)20.4 = 13860\ kNm$$

Corresponding to a base shear $V_{b,3}=OTM_{,3}/H_{eff}=13860/16.3=852$ kN

The frame top displacement at the significant points of the joint nonlinear behaviour can be computed using the component drift reported in Table 21. In this case, the joint drift at the peak strength is used to compute the frame displacement at the yielding because the hierarchy of strength outlined that the joint cracking has significant influence on the frame response.

- Peak displacement $\Delta_y=\min(\theta_{peak})\cdot H_{eff}=0.005\cdot16.3=81$mm
- Ultimate displacement (joint shear failure) $\Delta_u=\theta_u\cdot H_{eff}=0.01\cdot16.3=162.7$ mm

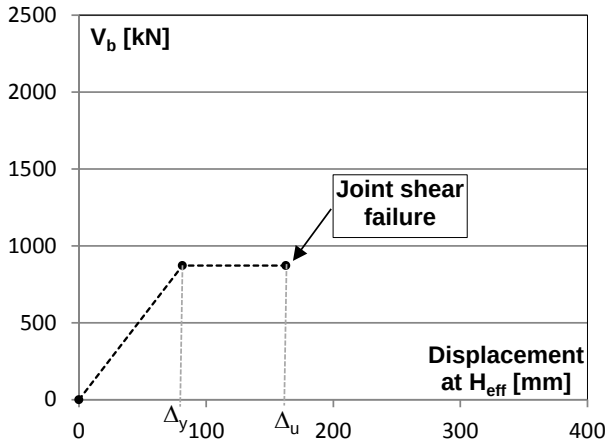

Figure 39: Pushover curve of Frame 1 due to mixed sidesway mechanism.

As outlined in Figure 40, the lateral capacity of the mixed sidesway mechanism, limited by the joint shear failure, is significantly lower than that associated to the beam sidesway mechanism. Thus, in this example the pushover curve of the mixed sidesway mechanism is assumed as representative of the Frame 1 lateral capacity.

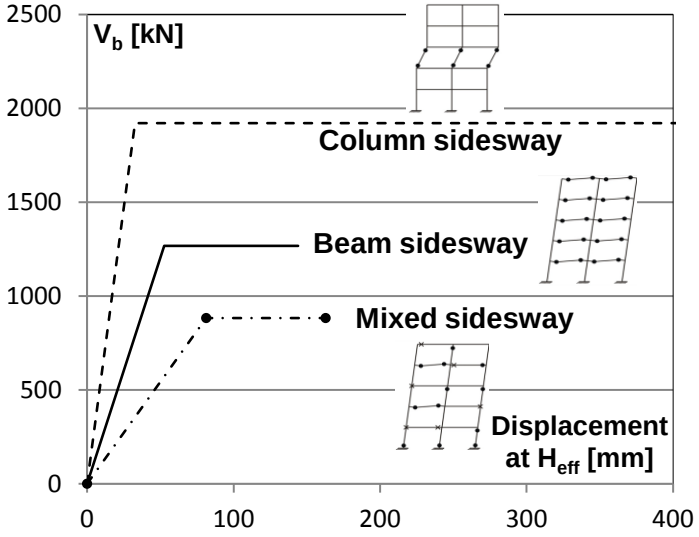

Figure 40: Comparison of Frame 1 pushover curves.

5. LATERAL CAPACITY OF THE OTHER RESISTING SYSTEMS

The lateral capacity of the C-wall and its interaction with the surrounding frame in Y-direction (dual system) is assessed decoupling the C-wall in the two X- and Y- directions.

In particular, the wall web is considered as part of a dual system (i.e. wall + frame) in the Y-direction. It is assumed that the wall flanges contributing to the building capacity in the X direction along with Frame A and Frame D whose capacity is independently determined according to a similar step-by-step procedure as described in the previous sections for the Frame 1.

5.1. **Wall lateral capacity**

In order to characterize the lateral capacity of the dual system and the contribution of the wall flanges in the X direction, the formulations provided in C5.5.5 for cantilever wall are considered. The moment-curvature capacity of the wall cross-sections at each level accounting for the axial load variation and the different longitudinal reinforcements need to be derived. The wall flexural strength is checked against the shear strength to detect shear failures along the wall height. Indeed, flexure-shear interaction as well as shear failure prior to yielding are likely to govern the behaviour of walls.

The probable flexural strength of a shear wall at the critical sections can be computed following the procedure previously described for the columns.

For example, the geometry and reinforcement details of wall web at level 1 (Y directions) are reported in Table 23. The schematic of the cantilever walls studied in this example is shown in Figure 41, resuming the assumptions adopted for the calculations.

Table 23*:* Details of wall web at Level 1 (Y direction)

Wall width	b	[mm]	203.2
Wall length	l_w	[mm]	6100
Longit. bar cover	clb	[mm]	38.1
Total height	H	[mm]	24400
Stirrups diameter	ϕ_{stirr}	[mm]	10
Stirrups spacing	s_{stirr}	[mm]	254
Number of legs	$n_{lx}=n_{ly}$	[-]	2
Longit. bar diameter	d_b	[mm]	20

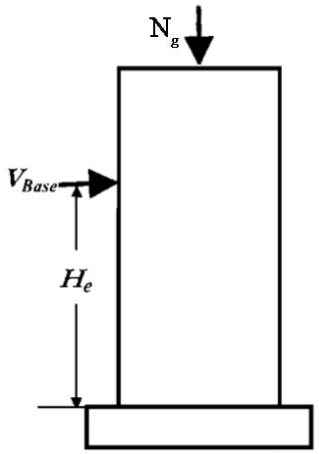

Figure 41: Schematic of the wall models.

As already reported in the characterization of the column nonlinear behaviour, the confined concrete ultimate strain can be computed using the formulation C5.9. In this case it results in ε_{cu}=0.0093 using ρ_s=0.0043.

However, the buckling of longitudinal reinforcements should be also considered. In this case, because s/d_b=12.7 >7, according to the buckling limitation included in the section C5.5.5.5, the steel in compression cannot yield. This limitation can be severe leading to ultimate curvatures slightly higher than yielding curvature. For this reason in this example the unconfined concrete ultimate strain ε_{cu} =0.004 is assumed as ultimate limit state for the wall curvature.

Once the confined concrete ultimate strain is known, the flexural strength can be computed using the cross-section analysis and accounting for axial load. At this stage, only gravity loads (see Table 12) are considered. A summary of the wall flexural capacity is reported Table 24.

Table 24: Flexural strength of wall web at Level 1 (Y direction).

Axial load	N_g	[kN]	2624
Yielding moment	M_y	[kNm]	20900
Ultimate moment	M_u	[kNm]	18800
neutral axis depth at M_u	c	[mm]	1350

Yielding and ultimate curvature

For rectangular-section walls C5.67:

$$\phi_y = \frac{2\varepsilon_y}{l_w} = \frac{2 \cdot 0.0015}{6.1} = 0.00049 \ \frac{\text{rad}}{\text{m}}$$

The ultimate curvature for the wall web is given by C5.7:

$$\phi_u = \frac{\varepsilon_{cu}}{\text{c}} = \frac{0.0093}{1.35} = 0.0069 \ \frac{\text{rad}}{\text{m}}$$

Wall Drift

The wall displacement at yielding can be computed by Eq. C5.18:

$$\Delta_y = \phi_y (H)^2/3 = 0.00049(24.4)^2/3 = 0.097\text{m}$$

To compute the wall displacement at the ultimate limit state (ULS), the plastic hinge length is computed using Eq. C5.69:

$$L_p = kL_c + 0.1\, l_w + L_{sp} = 0.05 \cdot 24400 + 0.1 \cdot 6100 + 132 = 1.96\text{m}$$

where:

$k = 0.2\,(f_u/f_{sy} - 1) \leq 0.08 = 0.2(375/300 - 1) = 0.05$

L_c = total wall height = 24400 mm

L_{sp} = *strain penetration* = $0.022 f_y d_b = 0.022 \cdot 300 \cdot 20 = 132$mm

The wall ULS displacement can be computed using Eq. C5.17:

$$\Delta_u = \Delta_y + \Delta_p = 0.097 + 0.305 = 0.4\text{m}$$

where:

$$\Delta_p = \phi_p L_p H = (\phi_u - \phi_y) L_p \cdot L_c = (0.0069 - 0.00049) \cdot 1.96 \cdot 24.4 = 0.305\text{m}$$

Once the yielding and ultimate displacements are known the member drift θ (or chord-rotation) can be computed as Δ/L_c:

$$\theta_y = \Delta_y / L_c = 0.097/24.4 = 0.004 \text{ rad}$$

$$\theta_u = \Delta_u / L_c = 0.4/24.4 = 0.016 \text{ rad}$$

At this stage, the buckling of longitudinal reinforcements should be also considered. In this case, the unconfined concrete ultimate strain ε_{cu} =0.004 is assumed as ultimate limit state for the wall curvature. With this limitation, the ultimate wall displacement (derived from sectional analysis) is:

$$\theta_{bb}=\Delta_{bb}/L_c=0.197/24.4=0.008 \text{ rad}$$

Shear Strength of wall

The probable shear strength of walls is based on the model from Krolicki et al., 2011. This is conceptually similar to the model for columns. However, some coefficients are specifically calibrated for structural walls. In particular, the coefficient γ_p, governing the concrete contribution was subjected to changes (see Figure 42).

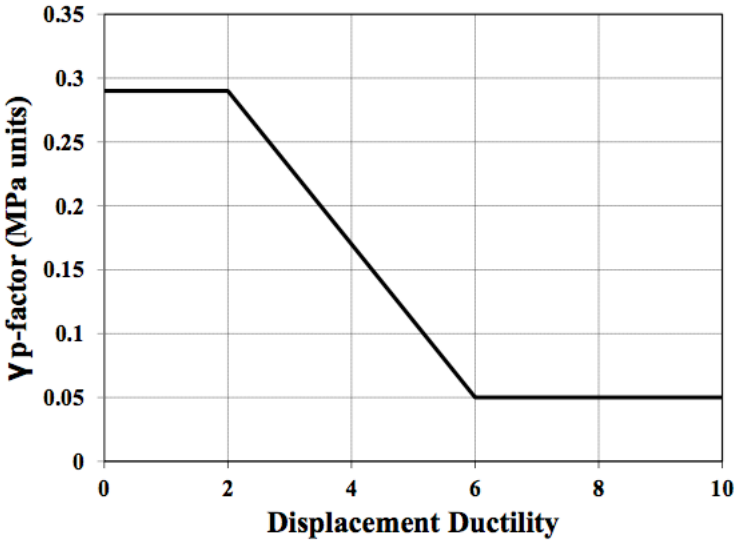

Figure 42: γ_p coefficient in the model by Krolicki et al., 2011.

The wall shear strength, V_p, is given by equation C5.57:

$$V_p = 0.85(V_c + V_s + V_n)$$

where:

a) the shear contribution from the concrete, V_c, can be evaluated by Eq. C5.58:

$$V_c = \alpha_p \beta \gamma_p \sqrt{f'_c}(0.8A_g)$$

$$1 \le \alpha_p = 3 - \frac{M}{Vl_w} = 3 - \frac{L_s}{l_w} = -1 < 1 \Rightarrow \alpha = 1$$

with:

- $\beta = 0.5 + 20\rho_g <= 1 = 0.5 + 20 * 0.0152 = 0.80$
- $\rho_g = A_l / A_g = 18850/(6100 \cdot 203.2) = 0.0152$ (ratio of total longitudinal reinforcement over the gross cross- sectional area of the member)
- $V_{c,max}(\gamma_p = 0.29) = 1 * 0.8 * 0.29 * \sqrt{25.8} * (0.8 * 6100 * 203.2) = 1168\ kN$
- $V_{c,min}(\gamma_p = 0.05) = 1 * 0.8 * 0.05 * \sqrt{25.8} * (0.8 * 6100 * 203.2) = 201\ kN$

b) The shear contribution from the steel shear reinforcement, V_s, is evaluated with Eq. C.5.61:

$$V_s = \frac{A_v f_{yt} h_{cr}}{s} = \frac{157 \cdot 300 \cdot 8161}{254} = 1513 kN$$

where:

$A_v = n_{lx} \cdot \pi \cdot (d_{st}/2)2 = 157\ mm^2$

$h_{cr} = (l_w\text{-}c\text{-}clb)\ /\tan\theta_{cr} \le h_w = (6100\text{-}1350\text{-}38.1)/\tan 30° = 8161\ mm$

$\theta_{cr} = 45\text{-}7.5(M/Vl_w) \ge 30° = 45\text{-}7.5(24.4/6.1) = 15° < 30° \Rightarrow \theta_{cr} = 30°$

c) The shear strength contribution from the axial compressive load N on the column is given by Eq. 5.65:

$$V_n = N \cdot (l_w\text{-}c)/2h_w = 2624 \cdot (6100\text{-}1350)/(2 \cdot 24400) = 255\ kN$$

Using C5.57:

$$V_{p,max} = 0.85(V_{c,max} + V_s + V_n) = 0.85(1168+1513+255) = 2496\ kN$$

$$V_{p,min} = 0.85(V_{c,min} + V_s + V_n) = 0.85(201+1513+255) = 1673\ kN$$

In this case, because $V_{p,min} \cdot L_c = 1673 \cdot 24.4 = 40821\ kNm > M_u$, the shear failure does not limit the member drift (see Figure 43).

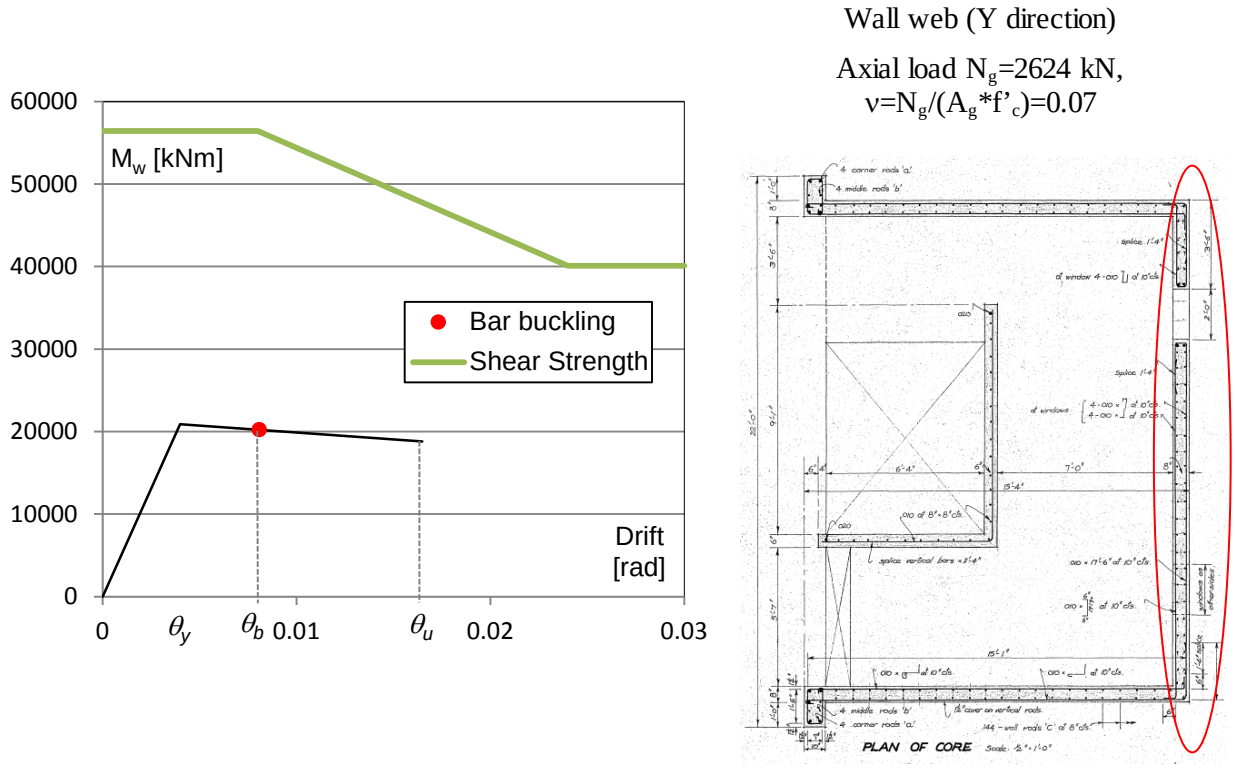

Figure 43: Moment-curvature capacity of wall web at the ground floor.

5.2. **Structural wall lateral capacity**

The lateral capacity of a structural wall as part of a structural system can be identified according to C5.7 and C5.8. When assessing the flexural capacity of a structural wall, it is reasonable to assume a first mode behaviour (Priestley et al. 2007).

Note that at a later stage the interaction with the floor system, potentially changing the response, might need to be checked.

The wall capacity can be assessed with the following steps:

- Plot the distribution of resisting moment along the wall height;
- Assuming a reverse triangular force distribution along the wall height, the moment distribution demand can be computed using basic principles of static;
- Shift the moment profile over the wall region affected by tension diagonal cracking (tension shift). This height can be estimated as half length of the wall (l_w);

- Compare demand and capacity to detect the position of the plastic hinge along column height;

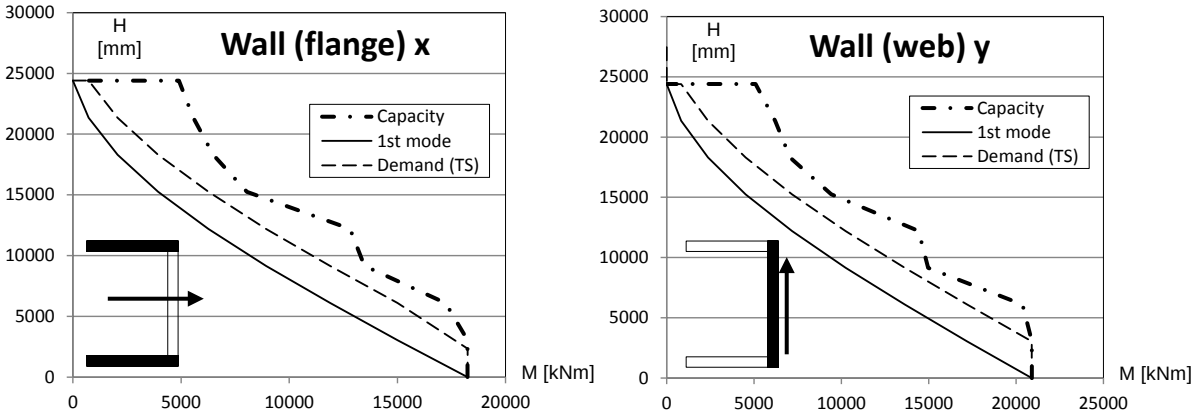

Figure 44: Moment distribution along the wall height.

In this case the moment capacity is always higher than demand except at the column base, thus a plastic hinge is expected to develop at the wall base.

The displacement profile of a cantilever wall can be reasonably assumed. The pushover curve for the wall web and flanges are reported in Figure 45.

Note that in order to assess the wall capacity as part of a more complex structural system an effective height, H_{eff}, about 0.67 of the total height is assumed. This assumption allows to calculate the base shear (the flexural capacity divided by H_{eff}) and the displacement capacity, the wall drift (previously calculated) multiplied by H_{eff}.

For the wall web in the Y direction, the base shear can be computed as:

$$V_b = M_b / H_{eff} = 20900/(0.67 \cdot 24.4) = 1278 \text{ kN}.$$

The yielding displacement is:

$$\Delta_y = \theta_y \cdot 0.67 \cdot 24.4 = 0.004 \cdot 0.67 \cdot 24.4 = 65 \text{mm}.$$

The ultimate displacement in correspondence of the bar buckling can be assumed as:

$$\Delta_u = \theta_{bb} \cdot 0.67 \cdot 24.4 = 0.008 \cdot 0.67 \cdot 24.4 = 130 \text{ mm}$$

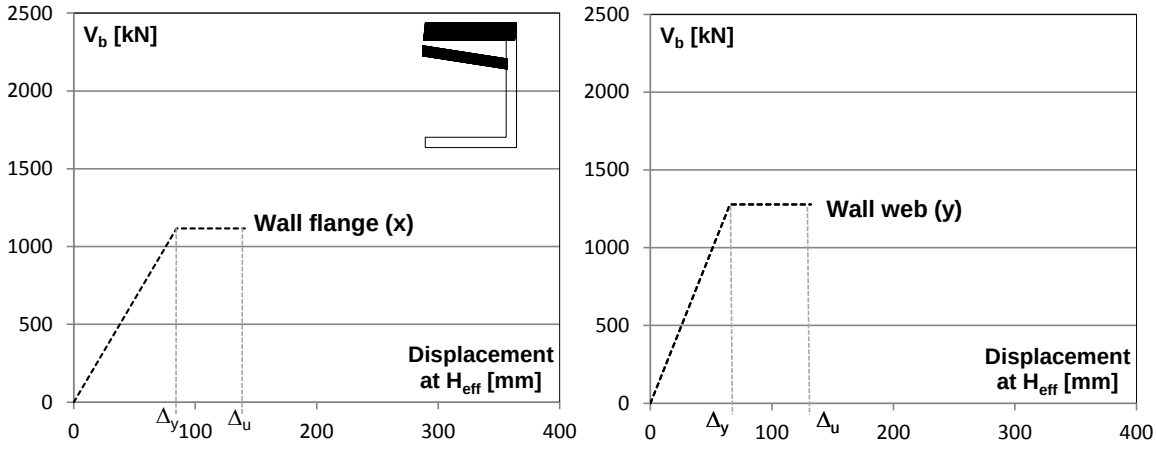

Figure 45: Pushover curves of cantilever walls.

5.3. **Dual system lateral capacity**

According to Section C5.8, the probable strength of beams, column and joints of the frames surrounding the RC shear wall need to be assessed following the procedure covered in the frame section.

In this example, the nonlinear behaviour of framing members is assumed as those reported in the previous paragraphs for Frame 1.

Their contribution at each floor can be computed imposing to the weaker frame member the drift at the significant points of the wall nonlinear behaviour, i.e. yielding and ultimate drift, as illustrated in Figure 46a. This allows to compute the distribution of bending moment, shear and axial load on the frames and the corresponding actions transmitted to the wall.

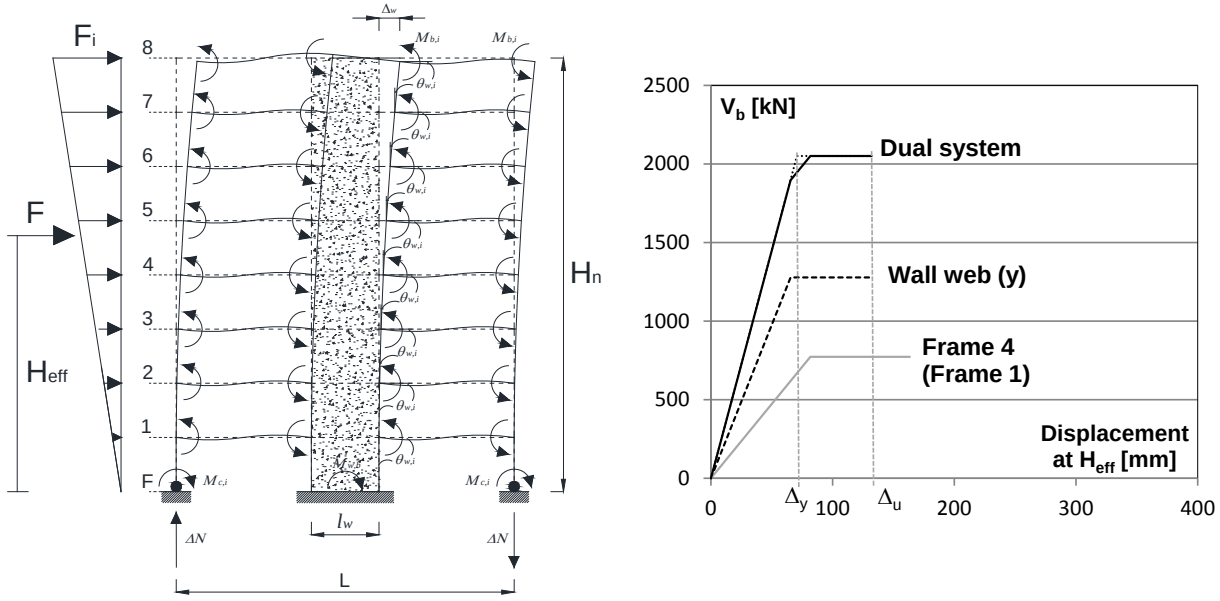

(a) **(b)**

Figure 46: Lateral capacity of the dual system: plastic mechanism assumed for the calculations (a); pushover curve (b).

The pushover curve of the dual system and the contribution of the cantilever wall and the surrounding frame are depicted in Figure 46b. It is worth noting that, in this case study, the frame provides a substantial contribution to the total base shear. To obtain a more refined assessment of the lateral response of the dual system, the shear and flexural strength previously calculated can be now compared with a more refined estimation of the shear and bending moment demand determined accounting for the contribution of the frames at each floor.

5.4. **Frame A/D lateral capacity**

The lateral capacity of the Frame A/D is calculated with the same procedure adopted for the Frame 1 and illustrated in detail in the previous sections. The lateral capacity and the most probable mixed sidesway mechanism accounting for the strength hierarchy of the joint subassemblies are reported in Figure 47.

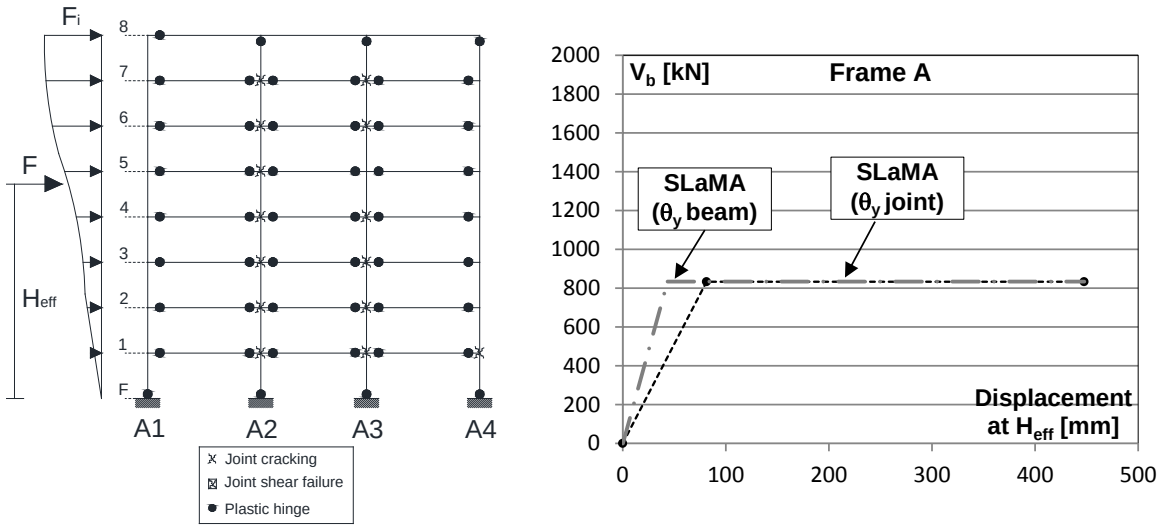

(a) **(b)**

Figure 47: Frame A/D: (a) mixed sidesway mechanism; (b) lateral capacity.

In the case of Frame A/D, the strength hierarchy outlines that for most of the joint subassemblies the joint cracking anticipates the beam hinging (see Figure 47a). This may significantly affect the lateral deformability of the resisting frame, because after the cracking, the joints exhibit large shear deformation leading to a significant reduction of the frame lateral stiffness. To account for this phenomenon, the joint contribution to the total drift should be computed and added to the beam deformation. However, for sake of simplicity in this example the Frame A/D lateral capacity is computed twice. First considering the beam deformability at the yielding (θ_y=0.0027 rad) and then considering the joint deformability at the peak strength (θ_y=0.005 rad) to estimate the frame initial stiffness. The capacity curve referring to the joint deformability is used for the following calculations, because it leads to a more conservative assessment of the seismic capacity.

6. SEISMIC PERFORMANCE ASSESSMENT

6.1. **Building lateral capacity**

Once that the force-displacement capacity curves (pushover) of the lateral resisting systems in the two independent directions (X- and Y) were assessed (see Figure 33), they need to be properly combined to obtain the building global response. In particular, two different situations are simulated:

a) 2D response of the overall systems assuming (no torsional effects)

b) 3D response including torsion between the centre of mass and centre of strength, e_{actual}.

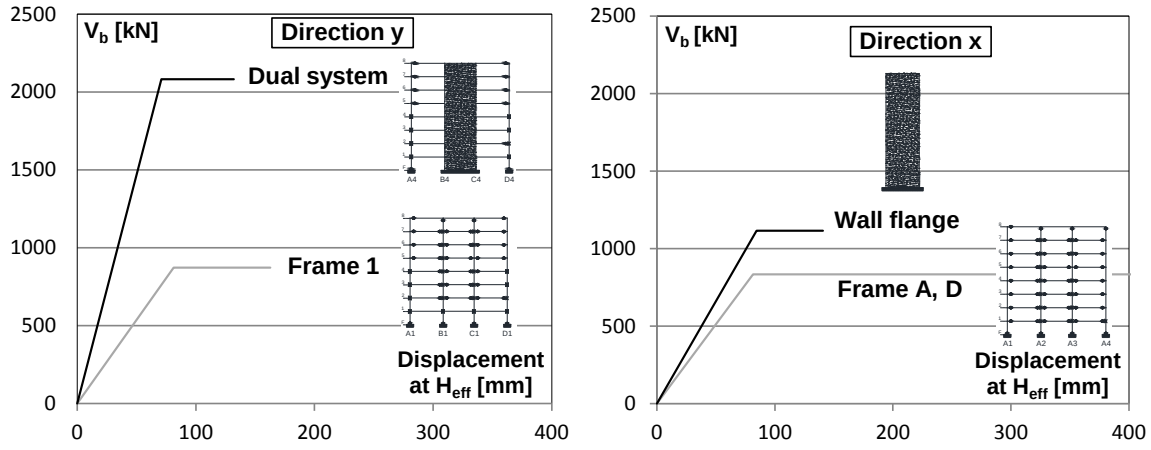

Figure 48: Lateral capacity of resisting systems.

The effect of torsion can be accounted for with the Method C reported in section C2F.4: Absence of strength eccentricity (Paulay 2001), see Figure 49. This method can be applied if the strength eccentricity exceeds 2.5% of the relevant lateral dimension of the plan. It consists in reducing the lateral strength of members trying to eliminate the strength eccentricity.

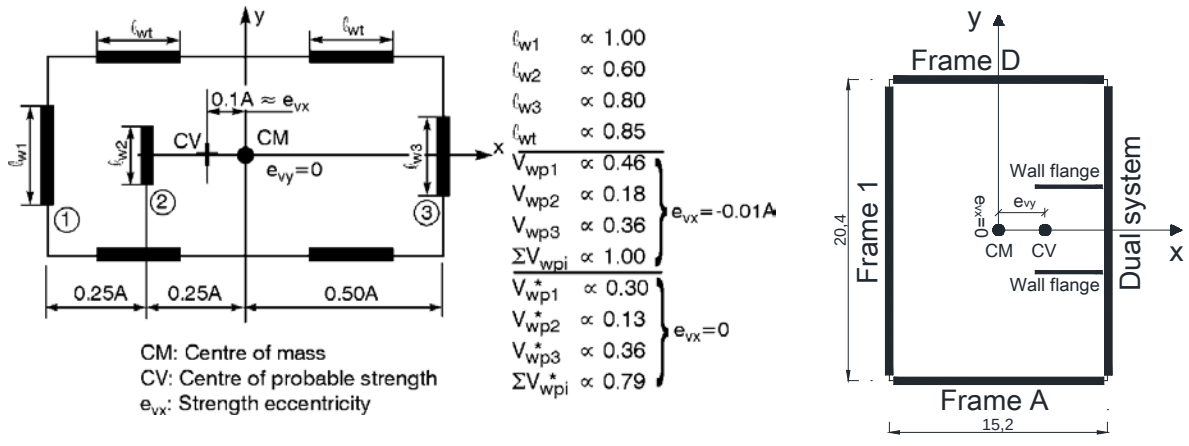

(a) **(b)**

Figure 49: Torsional effects in walled buildings: absence of strength eccentricity method (Paulay 2001); (b) application to the case study building.

In this case, for the X direction the strength eccentricity, e_{vx}, is zero and the building lateral capacity can be obtained summing the contribution of the two frames A and D and the two wall flanges (see Figure 49b). For the Y direction, the strength eccentricity can be computed as:

$$e_{vy} = \frac{\sum V_b \cdot d_m}{\sum V_b} = \frac{(2082 \cdot 7.62) + (852 \cdot (-7.62))}{2082 + 852} = 3.20m$$

which is higher than $0.025L_x = 0.025 \cdot 15.24 = 0.38m$.

In the Y direction there are only two lateral resisting systems: Frame 1 and the Dual System and the strength of the dual system is higher than that of Frame 1; in order to eliminate the eccentricity, the strength of the dual systems should be taken equal to the strength of the Frame 1. For this reason, the total building strength in the Y direction is taken as two times the strength of Frame1. The lateral capacity of the building in the two directions is reported in Figure 50, along with the lateral capacity in the Y direction neglecting 3D torsional effects (2D capacity).

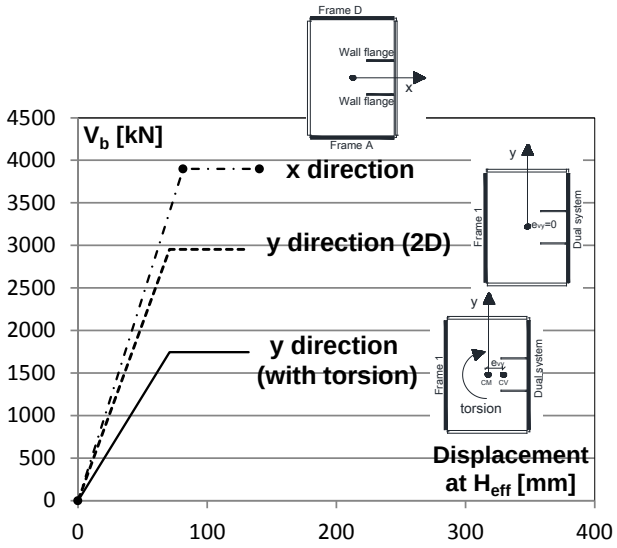

Figure 50: Lateral capacity of resisting systems in the two directions.

6.2. **Seismic demand**

According to Chapter 3 of the NZSEE/MBIE guidelines (NZSEE/MBIE 2016c), the seismic demand is represented by the response spectrum in the ADRS format. The horizontal acceleration design response spectrum is derived in accordance with NZS 1170.5:2004 (NZS 1170.5 2004). A return period of 500 years and soil site D (consistent with the building site) without considering near fault effects are considered. The return period factor R is taken equal to 1 (distance to nearest fault, D > 20 km) and the hazard factor Z is taken equal to 0.3 as suggested in (Department of Building and Housing 2011). The calculated acceleration response spectrum is reported in Figure 52 along with the spectra of the signals recorded in the CBD (at the stations reported in Figure 51) during the 2011 Christchurch earthquake.

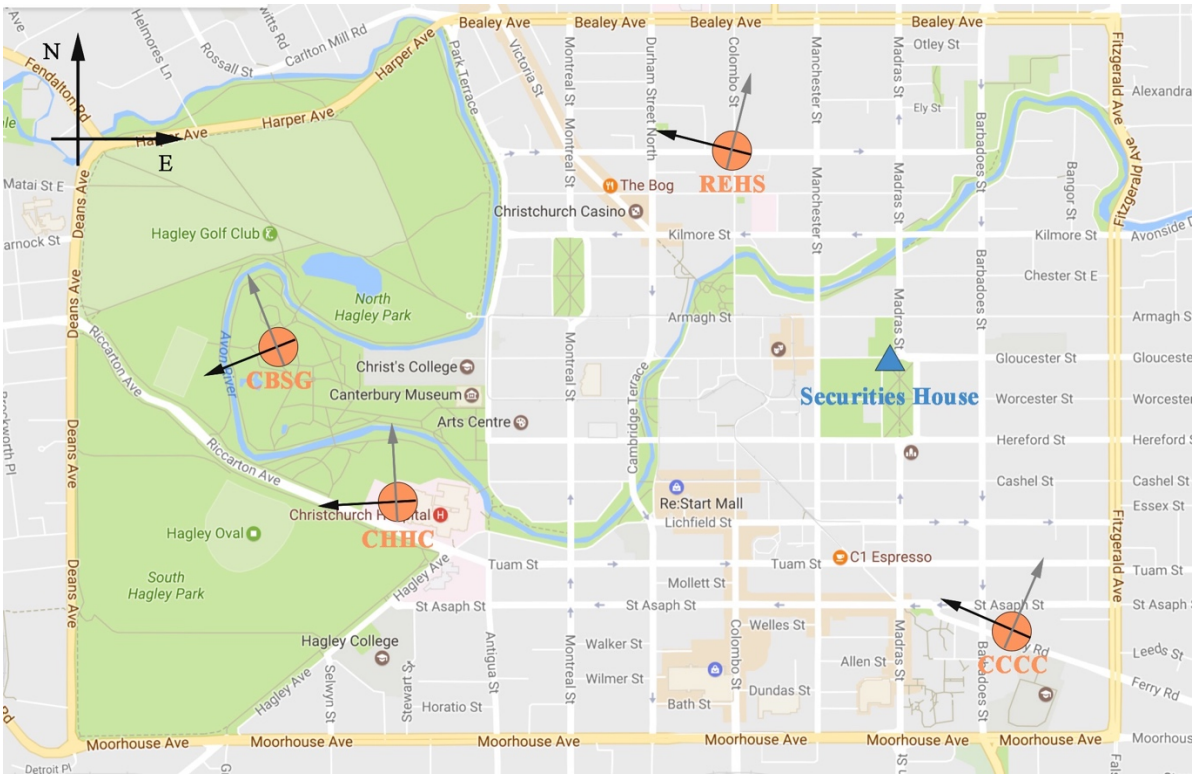

Figure 51: CDB ground motion recording stations and building location.

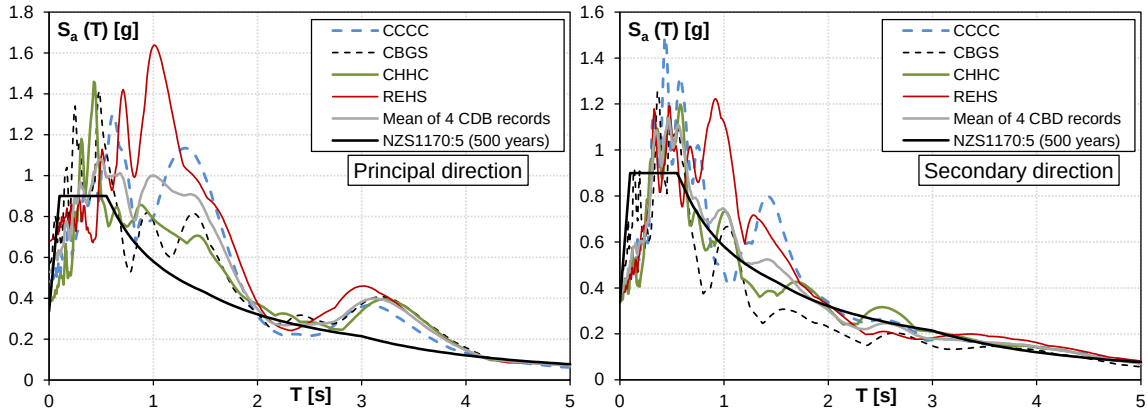

Figure 52: Spectra of the signals recorded in the CBD during the 2011 Christchurch earthquake.

6.3. **Seismic score: %NBS**

The seismic demand is represented by the response spectrum in the ADRS format considering both the code spectrum (500 years return period) and the mean spectrum of the four CDB records (see Figure 50). The acceleration-displacement response spectrum is derived from the acceleration response spectrum assigning at each of the spectral acceleration S_a the related spectral

displacement S_d. The spectral displacement can be derived inverting Eq. C3.2 of the NZSEE/MBIE guidelines (NZSEE/MBIE 2016c):

$$S_d[mm] = S_a \cdot K_\delta(T) = S_a \cdot 9810 \cdot \frac{T^2}{4 \cdot \pi^2}$$

The ADRS spectra derived from the four CBD records are reported in Figure 53 for both the principal and secondary horizontal direction. The comparison of the mean response spectrum of the four records with the NZS 1170:5 (NZS 1170.5 2004) spectra (500 years return period) outlines the significant differences in the principal direction both in terms of spectral acceleration and displacement.

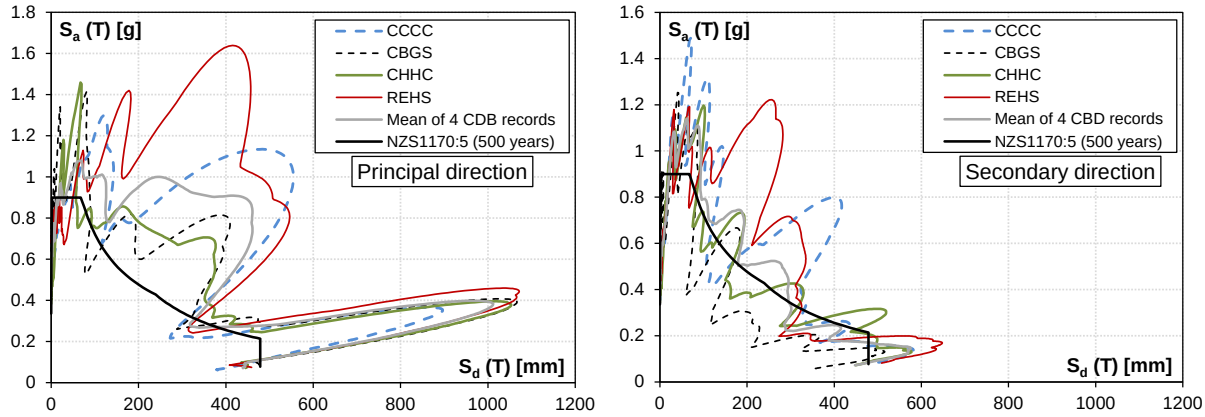

Figure 53: ADRS spectra of the signals recorded in the CBD during the 2011 Christchurch earthquake.

According to Chapter 2 of the NZSEE guidelines (NZSEE/MBIE 2016c), the building capacity is represented by Force-displacement (pushover) curves properly converted to be represented in the ADRS format. The frame capacity in terms of acceleration can be derived dividing the base shear for the effective mass. Since the case study building has more than five floors, the mass participating to the higher modes could be relevant (as observed in C2.4.2). In this case, the effective mass is assumed equal to the 80% of the tributary mass of the building. This assumption is based on the results of dynamic numerical simulations using a linear elastic model of the Frame 1, Frame A, Dual system and Wall flanges which outlined that the masses participating to the first mode is 78%, 79%, 65%, 63%, respectively. The total floor mass, calculated from the seismic load analysis (see Section 2.1), is about 226 tons for each level. To be conservative, the 80% of the total mass is assumed to participate to the building first mode. The effective mass can be estimated as m_{eff}=0.8*8*226=1446 tons.

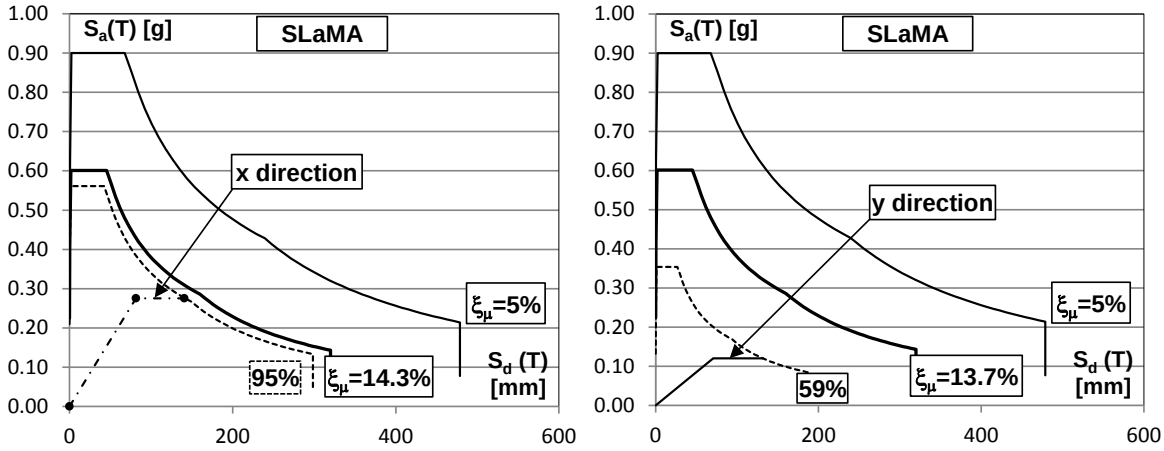

Figure 54: Demand vs. Capacity in the ADRS format for both directions with torsion.

The %NBS can be computed as the ratio of the seismic intensity leading to the ULS capacity of the building and the seismic intensity corresponding to a 500 years design.

The ductility capacity of the frame can be estimated as $\mu_C=\Delta_u/\Delta_y$ and is approximately 2.0 and 1.8 for the X and Y direction, respectively. The demand at the performance point can be derived reducing the elastic response spectrum for the damping reduction factor K_ξ (both $S_a(T)$ and $S_d(T)$ are multiplied for K_ξ) function of the ductility demand (see Section C2D). As depicted in Figure 54 the displacement demand is about 148 mm and 224 mm for the X and Y directions, respectively. This resulted in a %NBS:

- X direction: %NBS= (141/148)*100=95% (seismic rating A)
- Y direction: %NBS= (132/224)*100=59% (seismic rating C)

Percentage of New Building Standard (%NBS)	Letter grade	Relative risk (approx)
>100	A+	< 1 time
80–100	A	1–2 times
67–80	B	2–5 times
33–67	C	5–10 times
20–33	D	10–25 times
<20	E	> 25 times

Figure 55: Grading system for earthquake risk (NZSEE 2006)

Taking the minimum %NBS of the two directions, and calculating the seismic rating as per Table A3.1 in the guidelines (summarized in Figure 55), leads to a class C building. If the torsional effects and the actual eccentricity in the X direction are neglected and the building lateral capacity

in the Y direction is taken as the 2D curve in Figure 50. The % NBS in that direction results about the 77% which significantly differs from the 59% determined accounting for torsional effects.

Note: as the strength eccentricity plays a key role in the assessment of the overall building performance and %NBS, more refined analysis, including the contribution of the wall to the lateral stiffness and the torsional behaviour of the building, are needed.

The step-by-step procedure described herein allows to identify the structural systems/members which limit the building seismic capacity.

In this example, the seismic performance is limited by the lateral capacity of Frame 1 in the Y direction. In particular, the joint panel extensive cracking is detrimental for the building seismic performances. This may allow to design efficient retrofit solutions targeting the improvement of the seismic capacity of weak members.

In order to have a more reliable estimation of the building response to the 2011 Christchurch earthquake the building capacity is compared with the mean ADRS spectra derived from the four CBD records. It can be reasonably assumed with that the principal earthquake direction approximately corresponds to the E-W direction (X direction of the building) and the secondary earthquake direction to the N-S direction (Y direction of the building). The comparison between earthquake demand and building capacity is reported in Figure 56.

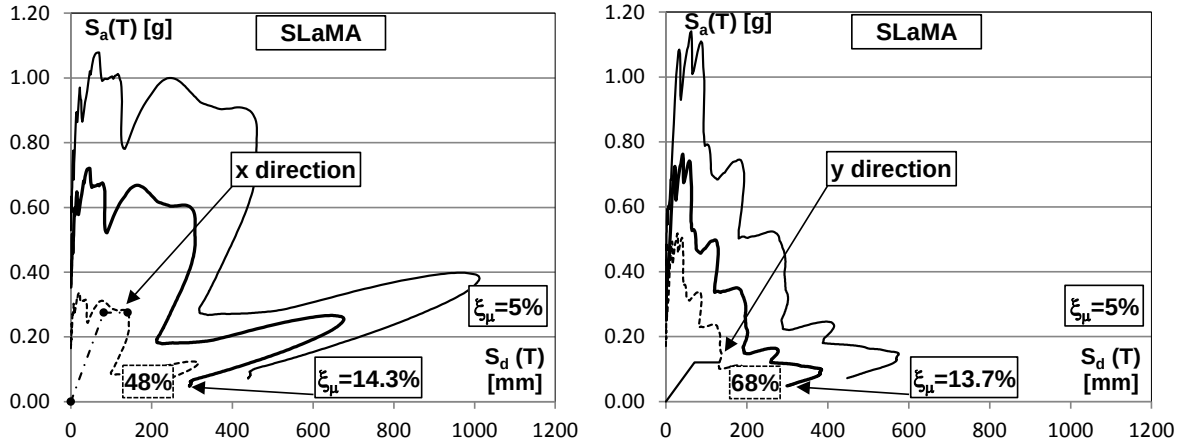

Figure 56: Demand vs. Capacity in the ADRS format for both directions considering the mean spectra of the four CBD records.

The comparison outlines that the %NBS in the building X direction (48%) is significantly lower than that estimated using the NZS1170:5 code spectrum (95%). Slight differences can be observed in the Y direction (68% instead of 59% estimated with the code spectrum). This is due to the significant differences between the code spectrum and the mean spectrum of the four CDB records (see Figure 53) and probably related to the high directivity effects of the 2011 Christchurch earthquake (Bradley and Cubrinovski 2011).

6.4. **Displacement capacity of gravity columns and short columns**

The later capacity of short (captive) columns need to be properly assessed in order to account for the detrimental effects that column shear failures (see may have on the seismic capacity of capacity of the building in the two directions (see Table C5.1 of the NZSEE/MBIE guidelines 2016c). This is because, typically, gravity columns were designed to sustain gravity load and not lateral actions. This can be done by either assessing the strength hierarchy of the relevant joint subassemblies or at global level limiting the displacement capacity of the building.

In this example, the latter approach is adopted. With reference to column reinforcement details reported in Figure 13, the ultimate lateral displacement of columns at the loss of gravity load can be assessed using the following formulation proposed by Elwood and Moehle (2005a):

$$\theta_u = 0.04\left(\frac{1+\tan^2 65°}{\tan 65° + P\left(\frac{s}{A_{st} f_{yt} d_c \tan 65°}\right)}\right)$$

The lateral capacity of columns B2 and C2 is assessed (see Figure 13 for reinforcement details). The gravity columns drift capacity is reported in Table 25.

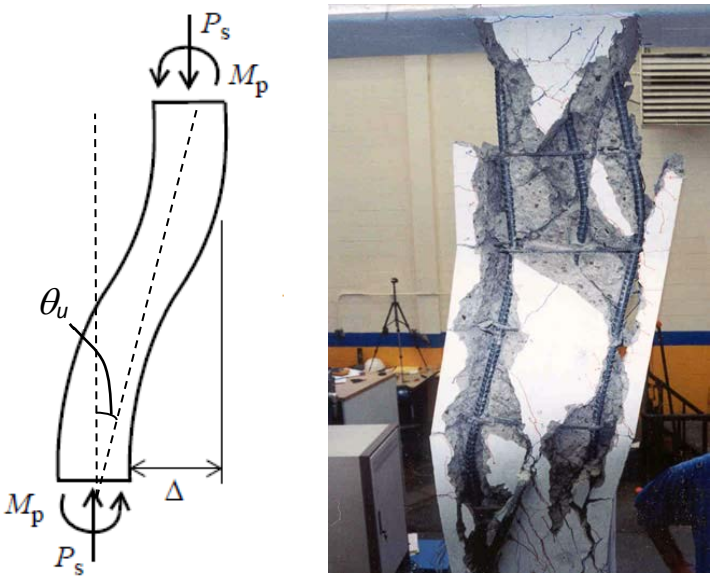

Figure 57: Deformed shape at loss of axial load capacity for gravity columns (Elwood and Moehle 2005a).

Table 25: Drift capacity of gravity columns.

Level [-]	N_g [kN]	d_{st} [mm]	n_l [-]	s [mm]	d_c [mm]	θ_u [-]
1	1893.0	10	2	228.6	409	0.018
2	1656.4	10	2	228.6	409	0.020
3	1419.7	10	2	228.6	409	0.022
4	1183.1	10	2	228.6	409	0.026
5	946.5	10	2	228.6	409	0.030
6	709.9	10	2	228.6	409	0.037
7	473.2	10	2	228.6	409	0.047
8	236.6	10	2	228.6	409	0.065

The results point out that the drift capacity of gravity columns is always higher than the maximum drift demand of the building in the two directions (Δ_{max}/H_{eff} =141/16340=0.009 rad).
Thus, in this case, the gravity load failure of non-ductile columns is not likely to affect the building lateral capacity.

Note: this is in agreement with the observed damage showing short column shear failures only in the Frames A and D in the transverse or x-direction (see Figure 15).

The installation of sprandel beam at the first floor make the columns A1-to-A4 (equal to D1-to-D4) of the Frame A/D and A1-to-D1 of the Frame 1 susceptible to shear failure (see Figure 58a).

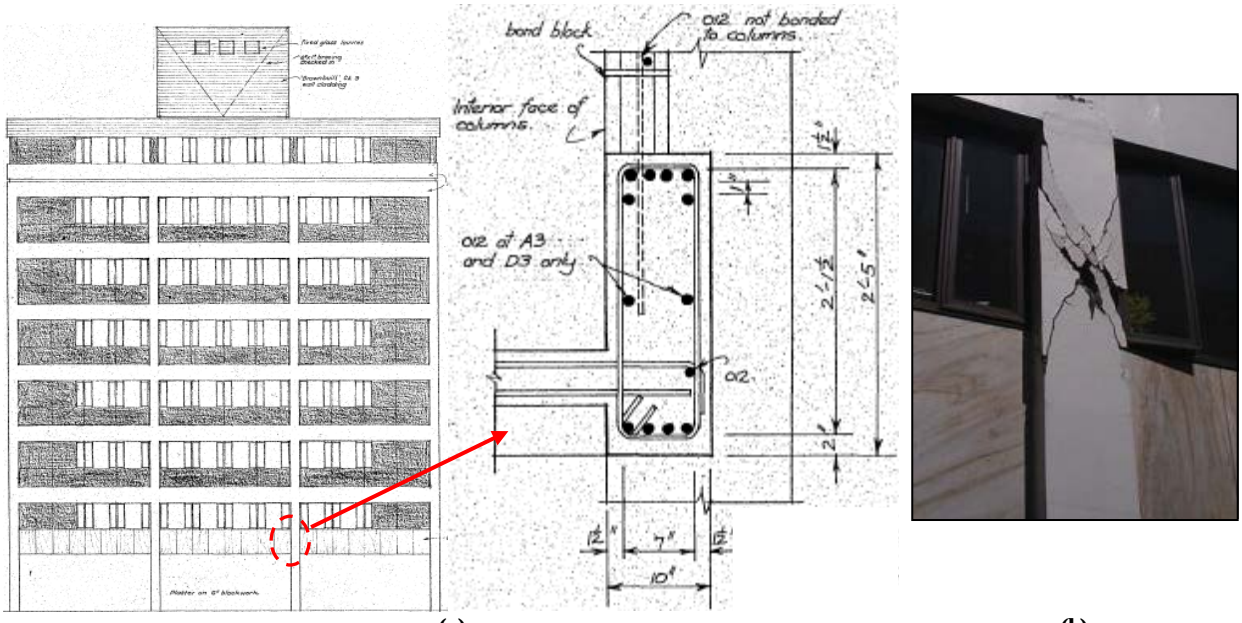

(a) **(b)**

Figure 58: (a) Details of the sprandel beam at the building first floor; (b) severe shear cracks to first floor short column.

To consider the influence of shear failure of short columns, the capacity of the columns at the first floor was re-assessed considering a reduced column shear span (L_c=763mm instead of 1156.7). The characterization of the lateral capacity of short columns is performed according to the procedure showed in section 3.3. The characterization outlines that the short column may exhibits a flexure-shear failure (in agreement with observed damage, see Figure 58b). However, the ultimate displacement capacity at the loss of gravity load is about 20.6 mm (about 0.03 rad drift) which is significantly greater than the maximum drift demand of the building. Thus, a gravity load collapse due to shear failure is not expected.

7. INFLUENCE OF WALL FLANGES

In Section 5, a first conservative assumption was to consider the beahaviour of the web and the flanges of the C-shaped wall completely decoupled. However, it should be recognised that a certain level of coupling may exist and, in general, it should be verified by in situ inspections. At this stage, given the absence of detailed information, this effect was investigated considering a full coupling between flanges and web. Hence, the SLaMA was repeated considering the Moment-Curvature capacity of a C-shaped cross-section.

The moment-curvature analysis of the C-section at each floor allow to draw the moment capacity profile along the height of the wall. Safety checks on the shear capacity confirmed that they do not limit the flexural capacity. In Figure 60 the capacity profile in both directions was compared to moment demand due to a linear force profile. It is clear that the critical section of the wall is located at the base. It is also evident that, parallel to the flanges, the moment capacity depends on the sign of the action. In fact, if the web is in tension the moment capacity of the C-shaped section is higher. This is schematized in Figure 59.

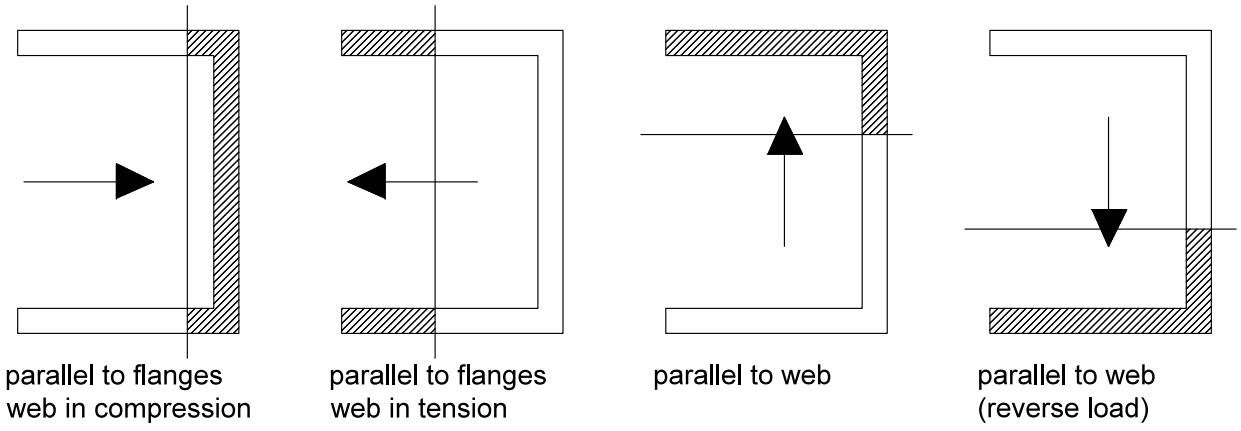

Figure 59: Compressed zone of the C-wall depending on the load direction.

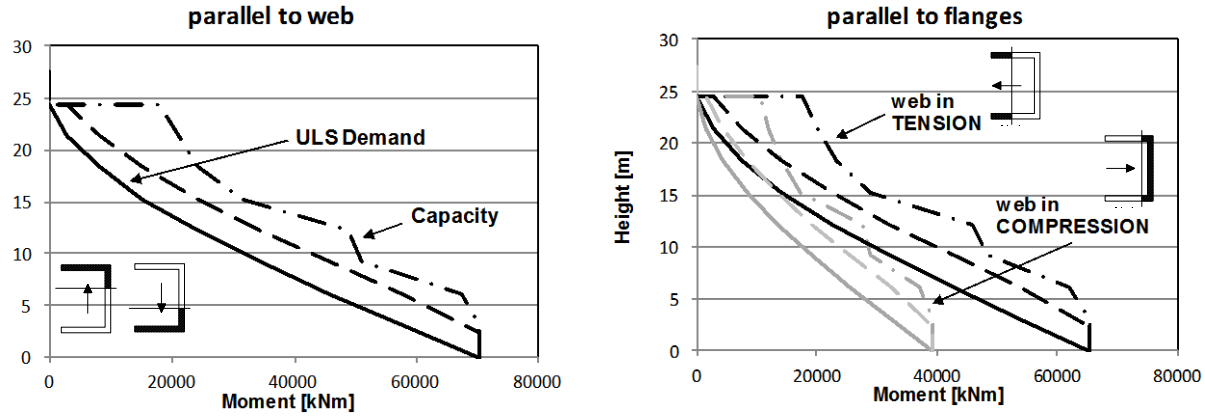

(a) (b)

Figure 60: Moment capacity profile of the C-wall: parallel to web (a); parallel to flanges (b).

Due to change in the sign of the seismic action, the most conservative configuration (web in compression) is considered. In this case, the lateral capacity of the C wall in the X direction corresponds to 7% increase in base shear and approximately the same ultimate displacement, if compared to the capacity of the decupled flanges (see Figure 61). This leads to a 5% increase in the seismic score (%NBS) of the building in the X direction.

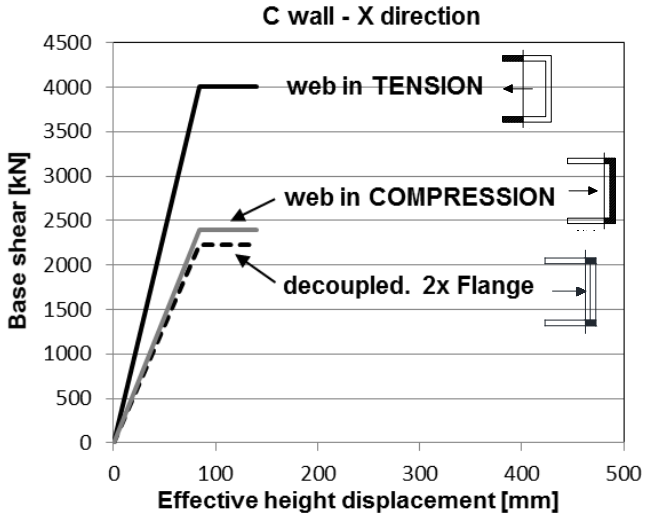

Figure 61: Capacity of the C wall in the direction parallel to the flanges.

In the direction parallel to the web, the C-wall moment capacity is particularly high due to the tension/compression action of the flanges (see Figure 60a). This leads to a peak base shear of the dual system about 5100 kN. This is more than the double the strength of dual system capacity in which only the wall web is considered (2080 kN). In terms of global behaviour in the Y-direction, the increased capacity of the dual system leads to an increase in strength eccentricity, given that the capacity of Frame 1 did not changed. Considering that the eccentricity should be eliminated in

order to account for the inelastic torsional effects, the capacity of the building in the Y-direction is twice the capacity of Frame 1. This leads to the same global capacity curve derived in Section 6.1. Hence, the seismic performance of the structure (%NBS) does not change.

8. INFLUENCE OF JOINT STIRRUPS

As stated in Section 3.4, the presence of joint stirrups was neglected in the calculation reported in the previous paragraphs (f_h=0). However, the beam-column joints of the case study building have 5ϕ10 stirrups with 2 legs, as reported in the structural drawings (see Figure 62). In this section, their influence is considered and the building capacity with joint stirrups is computed and compared with the previous calculations in terms of hierarchy of strength, global capacity and building seismic score.

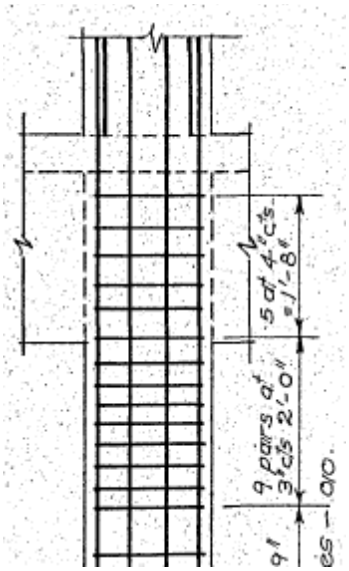

Figure 62: Detail of the joint stirrups.

To show the influence of joint stirrups, the external joint at the third floor in frame 1 (joint A3) is considered. For interior and exterior beam-column joints without shear reinforcement, the probable horizontal joint shear force that can be resisted is given by Eq. C5.36:

$$V_{pjh} = 0.85\, b_j h \sqrt{(k\sqrt{f'_c})^2 + k\sqrt{f'_c}(f_v + f_h) + f_v f_h}$$

$$= 0.85 \cdot 431.8 \cdot 457.2 \sqrt{\left(k\sqrt{25.8}\right)^2 + k\sqrt{25.8}(1.70 + 0.74) + 1.70 \cdot 0.74}$$

where:

$b_j = b_b + h_c/2 = 431.8$mm (as per NZS3101:2006)

$h = h_c = 457.2$ mm

$f_v = N/(b_c\ h_c) = 354900/(457.2 \cdot 431.8) = 1.70$ N/mm^2

$f_h = A_{st} f_{sy}/(b_j h_b) = 785 \times 300/(431.8 \cdot 736.6) = 0.74$N/mm^2

Hence, considering the appropriate values for the coefficient k the capacity of the joint can be calculated.

Joint first cracking (k=0.3) $V_{pjh,fc} = 453.2$kN≤ 2022 kN
Joint failure (k=0.4) $V_{pjh,max} = 539.6$kN≤ 2022 kN

Finally, the joint shear strength is converted into equivalent column moments calculated at the interface with the beam:

$$M_{col} = \frac{V_{jh}}{\left[\frac{l_c}{l_b jd}\left(l_b - \frac{h_c}{2}\right) - 1\right]}\left(\frac{l_c - h_b}{2}\right)$$

$$= \frac{V_{jh}}{\left[\frac{3050}{3800 \cdot 0.9 \cdot (736.6 - 38.1)}\left(3800 - \frac{457.2}{2}\right) - 1\right]}\left(\frac{3050 - 736.6}{2}\right)$$

Joint first cracking (k=0.3) $M_c(V_{pjh,fc}) = 148.7$ kNm
Joint failure (k=0.4) $M_c(V_{pjh,max}) = 177$ kNm

Due to the presence of the joint stirrups, the capacity of the joint was increased by 22% and 17% at the first cracking and at the peak strength, respectively.

For example, Figure 63 shows the performance domain calculated for the joint A3 of frame 1 with and without considering the stirrups in the calculation of the joint shear strength.

If the joint stirrups are neglected (Figure 63a) the strength hierarchy outlines a joint shear failure in the push direction and a joint shear failure in the pull direction after the joint cracking and beam yielding.

Including the joint stirrups (Figure 63b), in the push direction the beam yielding is expected before the joint shear failure. In the pull direction, the joint shear failure is anticipated by the beam flexure-shear failure.

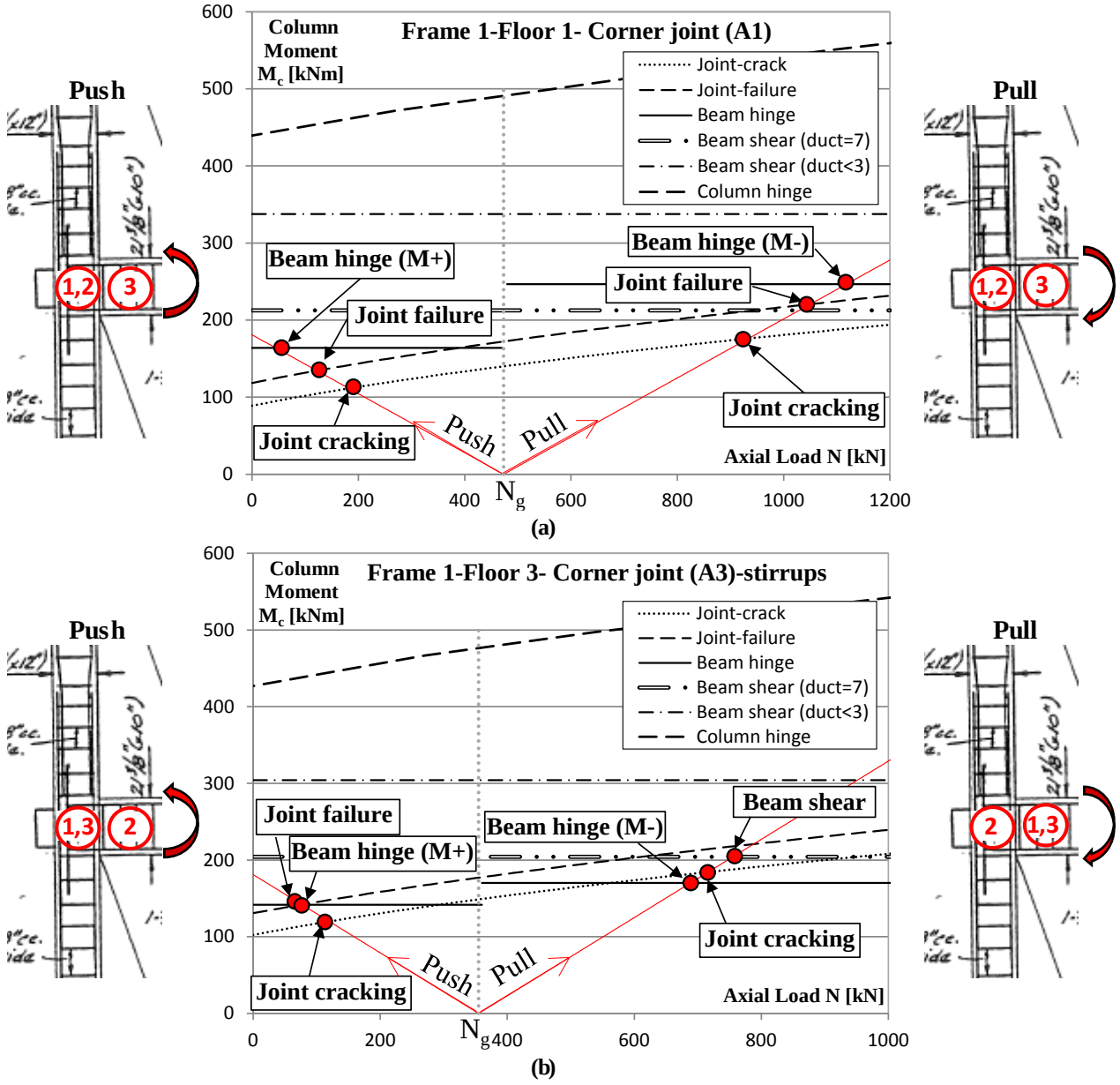

Figure 63: Joint A3 performance domain: without joint stirrups (a); with joint stirrups (b).

The results of the application of strength hierarchy for the joint subassemblies of the Frame 1 considering the joint stirrups are reported in Table 26. In this particular case, the hierarchy of strength is slightly modified by the joint stirrups. In fact, multiple joint shear failures are still expected. This means that the probable inelastic mechanism is still a mixed-sidesway. Finally,

although a slight increase in the base shear of Frame 1 is expected (approximately 40 kN), its ultimate displacement is governed by the shear failure of corner joints (θ_u=0.01 rad).

Table 26: Influence of joint stirrups on strength hierarchy

Joint [-]	Level [-]	Hierarchy w/o stirrups	Hierarchy with stirrups
Exterior A	1	JF	JF
	2	JF	JF
	3	JF	**JC-BH**
	4	JF	JF
	5	BH	BH
	6	BH	BH
	7	BH	BH
	8	BH	BH
Exterior D	1	JF	JF
	2	JC-BH	JC-BH
	3	JC-BH	**BH**
	4	JC-BH	**BH**
	5	BH	BH
	6	BH	BH
	7	BH	BH
	8	BH	BH
Interior B, C	1	JF	JF
	2	JC-BH	JC-BH
	3	JC-BH	JC-BH
	4	JC-BH	JC-BH
	5	JC-BH	JC-BH
	6	JC-BH	JC-BH
	7	JC-BH	JC-BH
	8	CH	CH

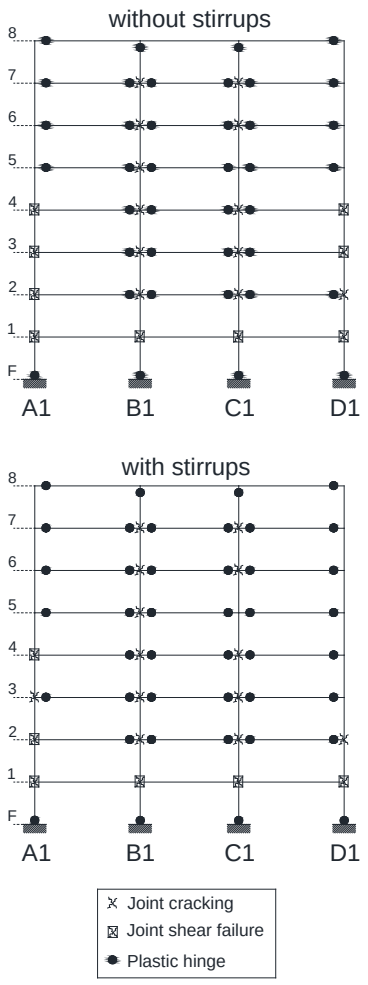

where: JC is the joint first cracking; JF is the joint shear failure; BH is the activation of beam plastic hinge.

Similar considerations hold for frame A and the dual system, for which the strength is slightly increased while the ultimate displacement does not change. The building capacity curves, in both X and Y directions, are shown in Figure 64 and compared with those obtained neglecting joint stirrups. The slight difference between the curves leads to a negligible variation in the %NBS (about the 1% in both directions).

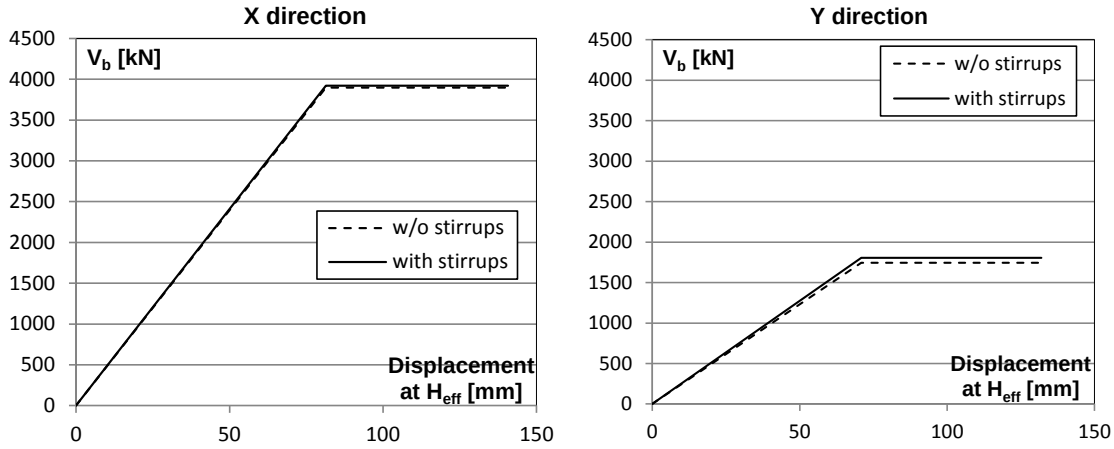

Figure 64: Global capacity curves with or withour the joint stirrups.

9. NUMERICAL PUSHOVER ANALYSES

SLaMA can be an useful tool to drive the development of a reliable numerical model and to check the results of software-based analysis against significant modelling errors. First of all, the results of the application of the hierarchy of strength can be used to assess the capability of the numerical model to reproduce the non-linear behaviour of the members and to capture all the expected local failure mechanisms. In this study, a refined numerical model is also used to assess the accuracy of the SLaMA to predict the capacity curve of the lateral resisting systems.

9.1. **Modelling assumptions**

A two dimensional non-linear numerical model developed within the finite element method (FEM) software Ruaumoko (Carr 2009) was adopted to assess the capacity of lateral resisting systems. A lumped plasticity approach, concentrating RC member nonlinearities in critical members such as the sections at the end of the beams and columns and beam-column joints, was adopted (see Figure 65). The influence of joint response on rotational capacity of framing members (with not negligible effects on the interstorey drift and frame deformability, see also Calvi et al. 2002; Pampanin et al. 2002; Del Vecchio et al. 2014; Del Vecchio et al. 2016) was considered including joint rotational springs that connect the beam and column members that converge in one node of the structure. In this way, the relative rotation between beam and column is governed by the above mentioned lumped spring. Beams and columns were modelled by means of mono-dimensional elastic elements with inelastic behaviour concentrated at the edges in plastic hinge regions (Giberson model, see the Ruaumoko manual, Carr 2009). The proposed numerical models were extensively validated at both subassembly and frame level under static and dynamic loading (Magenes and Pampanin 2004; Galli 2005).

The nonlinear behaviour of the beam hinges was schematised using a bilinear Moment-Curvature relationship and the equivalent plastic hinge length (both described in Section 3.2) which allow to define a "one-component Beam member" in Ruaumoko. In order to reproduce the change in strength and stiffness due to the axial load variation in the columns, their non-linear behaviour was schematized in Ruaumoko by means of the model "general quadratic beam-column member" which allows to characterize the Moment-curvature based on the axial load-moment interaction diagram (details in Section 3.3). In order to have a meaningful comparison with the results of SLaMA, no hardening was considered for beam and column members. Special attention was reserved to the beam-column joints. In fact, the rotational springs were governed by a column moment-drift relationship (calculated in Section 3.4) following the modelling method proposed by Pampanin et al. (2003). In this example, the joint shear strength was characterised considering the gravity load transmitted by the columns. Hence, the effect of the variation of axial load on the joint capacity was neglected. Where the axial load variation significantly modifies the strength hierarchy (see Figure 29), the designer may characterize the joint non-linear behaviour by means of an Equivalent column moment – Axial load interaction diagram, which allows to consider the axial load variation due to the seismic shaking. The influence of the axial load variation was considered in the strength hierarchy, see Section 4.1.

The Pushover analyses were conducted in displacement-control applying a linear force profile and neglecting P-Delta effects, in order to be consistent with the assumptions in the SLaMA assessment procedure. The floor slab was assumed rigid in the horizontal plane. The columns are assumed fully restrained at the base.

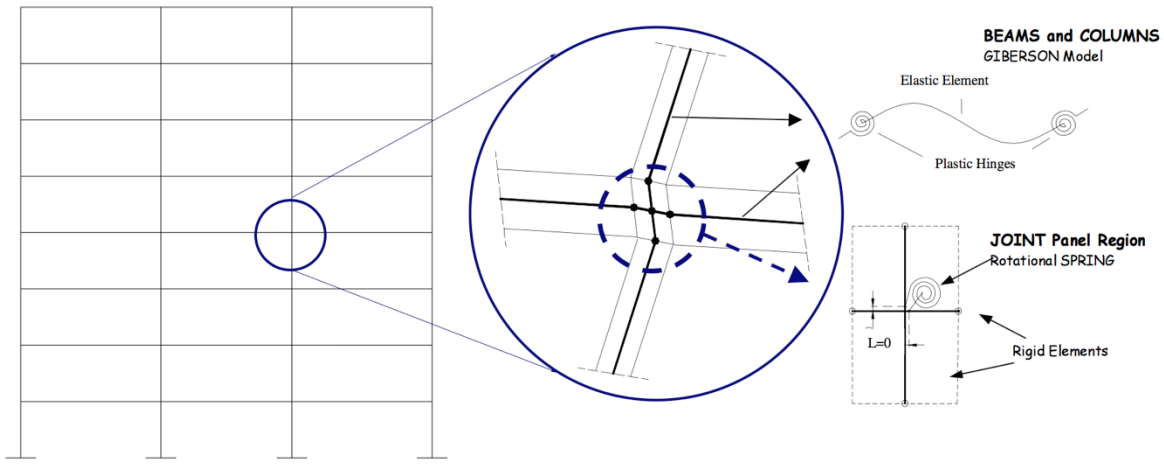

Figure 65: Modelling strategy (after Pampanin et al. 2002).

9.2. **Results and comparison with SLaMA curves**

The top displacement, conventionally used to represent pushover curves, is converted to the displacement at the effective height resulting in the lateral capacity of the equivalent SDOF system (Priestley et al. 2007). The pushover curves obtained from numerical analysis are compared in Figure 67 with those derived by using the SLaMA.

SLaMA allows to create, with simple calculations, a fuse of pushover curves including the actual capacity curve. Thus, a fast check on the reliability of the analytical/numerical capacity curves could be performed comparing the numerical curve with the SLaMA curves. An example on the use of the SLaMA to assess the reliability of the numerical curve is reported in Figure 66.

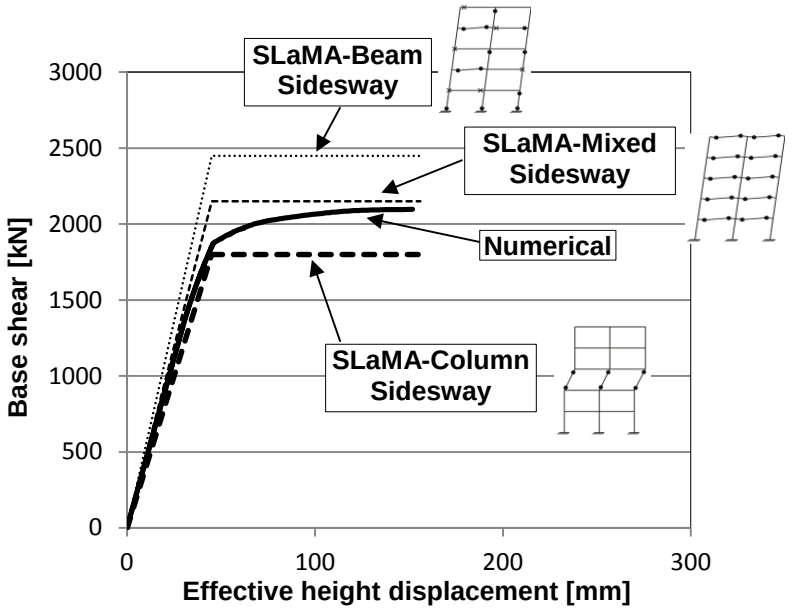

Figure 66: Example of a comparison between SLaMA and Numerical capacity curves.

Commonly, the lower bound capacity is represented by the pushover curve of a column sidesway mechanism. While, the upper bound is the capacity curve of the global beam sidesway mechanism. The mixed sidesway mechanism accounting for the strength hierarchy between the joint and the framing members is the most-probable mechanism generating the capacity curve with the best approximation of the numerical curve.

In this case, as anticipated in Section 4.2.2, the lower bound capacity curve (due to a local column sidesway mechanism) is higher than the upper bound. This means that this mechanism is not likely

to characterize the lateral response of the case study building and it is omitted in the following figures.

Figure 67a, b shows the comparison between the SLaMA and the numerical model in terms of lateral capacity curve of Frame 1 and Frame A, respectively. The SLaMA curves well approximate the actual capacity curve obtained using the refined numerical model. It is deemed that the most important parameters affecting the seismic response of the structural system are the initial stiffness, the ultimate displacement and the maximum base shear. All these parameters are estimated with a satisfactory agreement. The main gap between the curves can be observed after the first yielding (first change of stiffness in the numerical curve). This is due the assumption of the SLaMA that all the structural members reach the yielding at the same global displacement demand, which is a clear approximation. A satisfactory agreement can be observed also comparing the assumed plastic mechanism with that outlined by the numerical analyses (see Figure 68 and Figure 69). This remarks the effectiveness of the SLaMA approach predicting the lateral capacity curve and failure mechanism of RC frames.

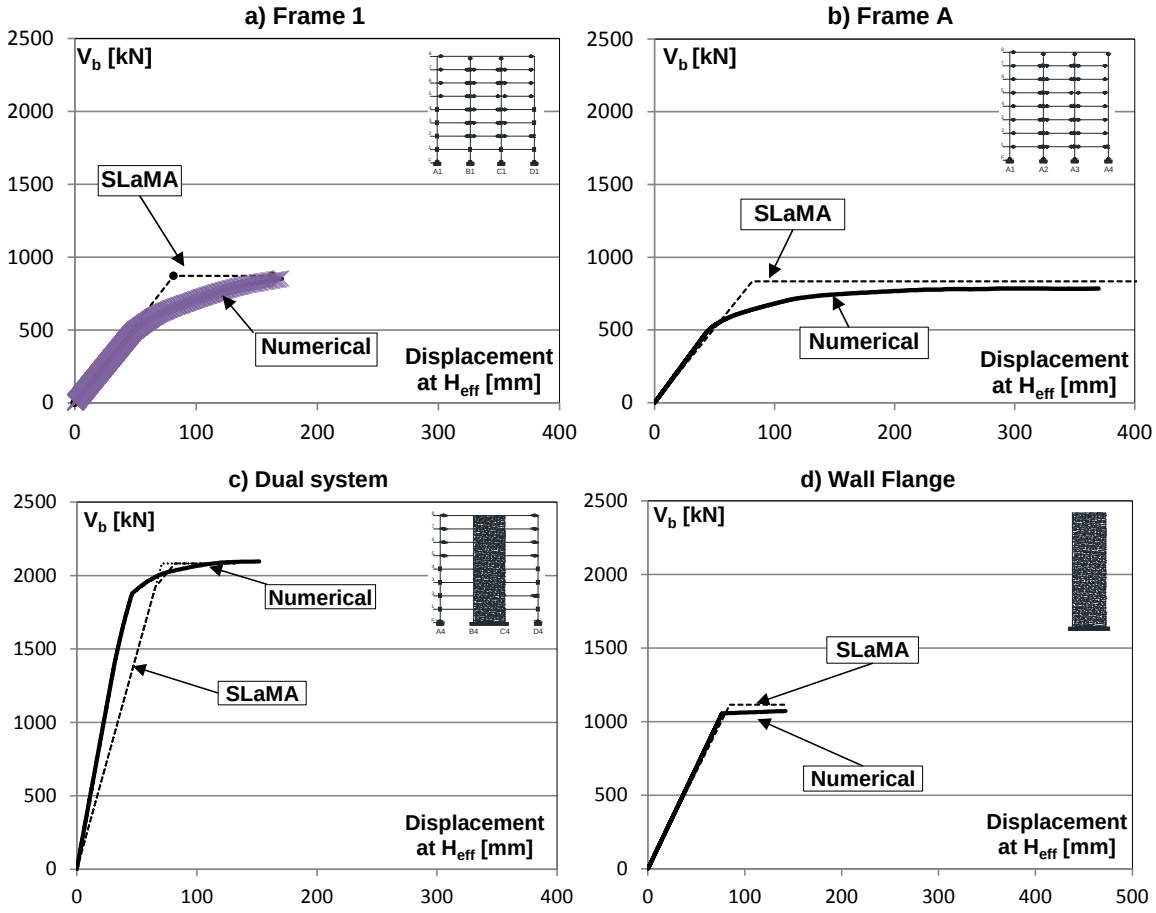

Figure 67: SLaMA vs Numerical capacity curve comparison for Frame 1, Frame A, dual system and wall flange.

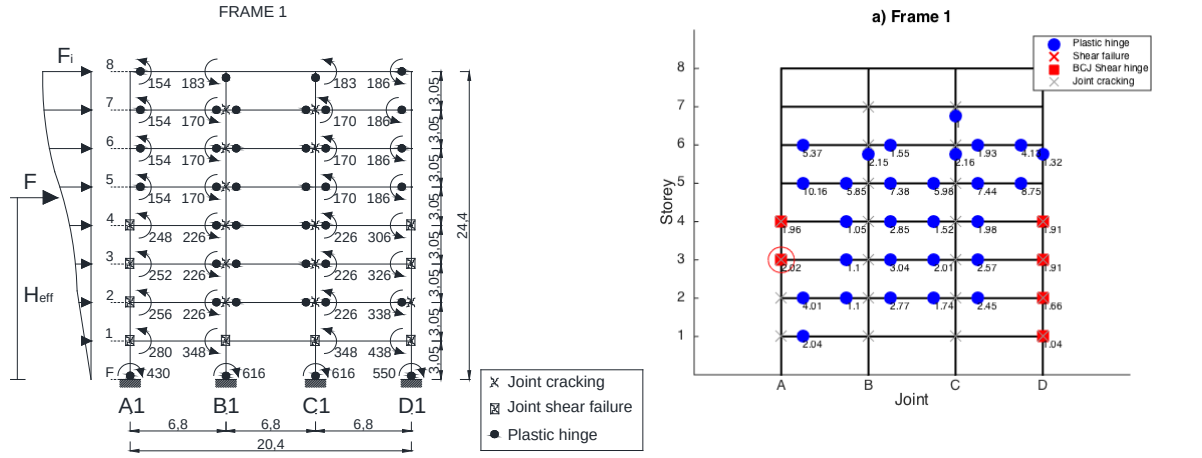

(a) (b)

Figure 68: Frame 1 plastic mechanism: SLaMA (a) and numerical pushover (b).

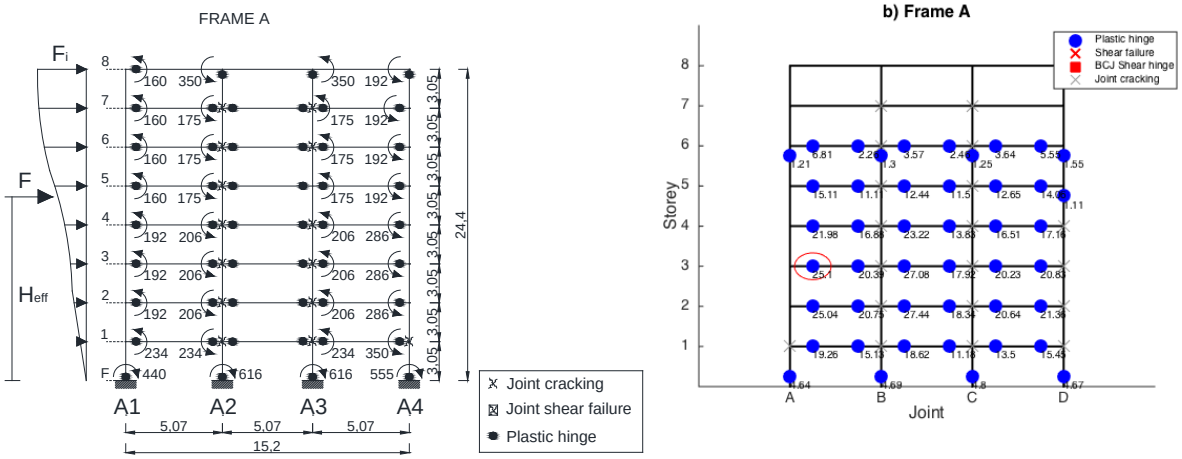

(a) (b)

Figure 69: Frame A plastic mechanism: SLaMA (a) and numerical pushover (b).

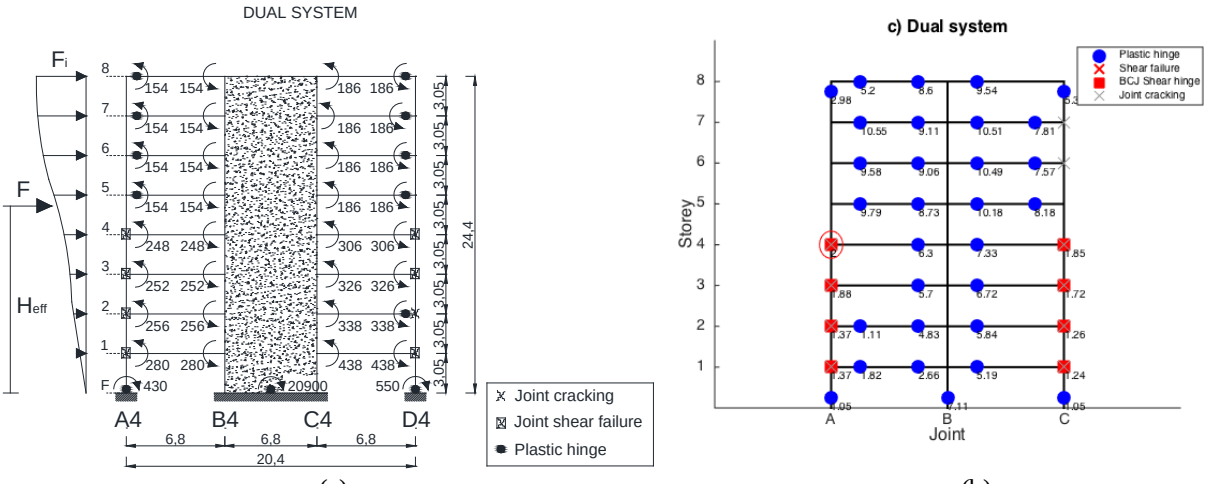

(a) (b)

Figure 70: Dual system plastic mechanism: SLaMA (a) and numerical pushover (b).

Although a good agreement can be observed for the Frame 1 and Frame A/D, significant differences can be observed for the Dual system. Although the maximum base shear and the ultimate displacement are accurately estimated, the comparison with the numerical curve reported in Figure 67c outlines a significant gap in the initial stiffness. In order to investigate on the source of such an approximation, the plastic mechanism predicted using the strength hierarchy in the SLaMA approach is compared in Figure 70 with that obtained from numerical analysis. The plastic mechanism predicted using the SLaMA well matches the one derived from refined numerical analysis. For this reason a good agreement in terms of maximum base shear and ultimate displacement is observed. The gap in the initial stiffness is due the assumption of the SLaMA on the lateral response of the wall. Indeed, according to C5.8.2.2 of the NZSEE/MBIE guidelines (NZSEE/MBIE 2016c), it is assumed that the wall behaves as a cantilever system. By contrast, the stiffness of the frames participating to the lateral response of the dual system changes the deformed shape of the wall and a contraflexure point at about $0.7H_{eff}$ is observed in the numerical analysis. This leads SLaMA to underestimate the lateral stiffness of the dual system.

To obtain a more refined assessment of the wall behaviour and failure mode, the shear and flexural strength previously calculated in Step 1 can be now compared with a more refined estimation of the shear and bending moment demand determined accounting for the contribution of the frames at each floor. This may help to identify the height at the point of contraflexure, which can be used to have reliable estimation on the initial stiffness of the dual system.

The global capacity curve of the building in the two directions is calculated summing the numerical capacity curves of each of lateral resisting systems, following the same approach explained in Section 6.1.

Figure 71 shows the seismic score of the building (%NBS) estimated using the numerical pushover curves and the comparison with the %NBS calculated with SLaMA.

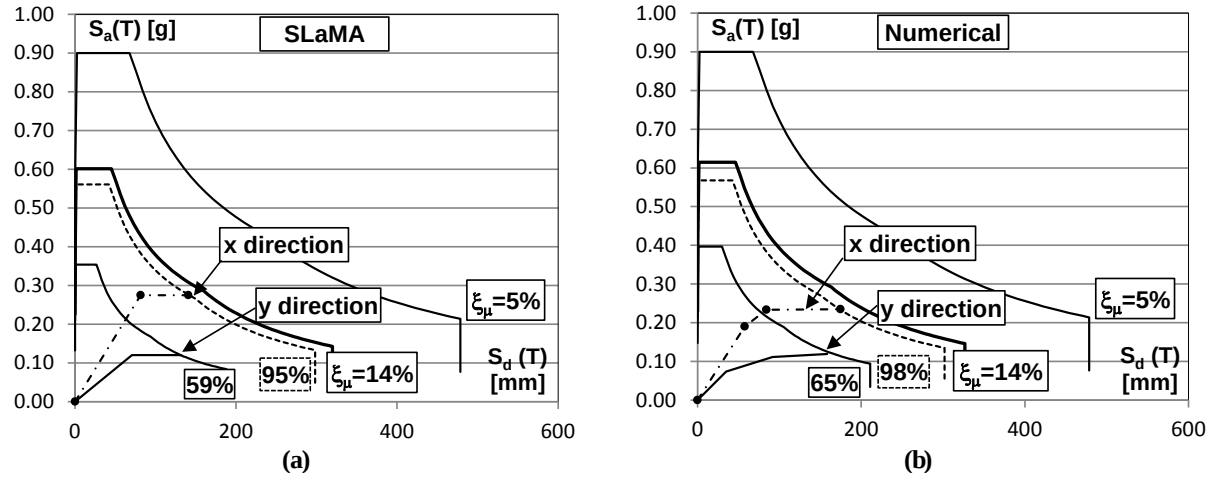

Figure 71: SLaMA vs Numerical seismic score comparison.

Although the use of numerical analyses leads to a better refinement in terms of capacity curve, the final result in terms of %NBS is very similar (see Figure 71). The numerical analyses lead to a seismic score of 98%NBS in the X direction and 65% in the Y (see Figure 71b). On the other side, the SLaMA leads to more conservative predictions 95% and 59% in the X and Y direction, respectively (see Figure 71a). Overall, considering the ability to capture the inelastic mechanism and assessing the seismic score within reasonable error compared to numerical pushover analyses, it is deemed that SLaMA is an effective assessment method for existing buildings.

9.3. **Influence of the modelling assumptions**

In this case, the joint panel springs were modelled by means of Equivalent Column Moment-Rotation curves in which the capacity was based on the gravity axial load. This was done to be consistent with the capabilities of the commonly used commercial software. However, such an approach neglects the influence of the variation of axial load on the joint strength. This, in turn may affect the predicted spread of inelastic demand in the numerical analysis that, in this way, may not follow the actual hierarchy of strength predicted with SLaMA. This modelling assumption is equivalent to neglecting the seismic axial load in the computation of the hierarchy of strength. It is deemed that this effect should be carefully taken into account when conducting numerical analyses.

In order to account for the axial laod variation during the seismic shaking, the numerical analyses were repeated using Equivalent Column Moment-Axial Load interaction diagrams. In the case of the Frame 1, Figure 72 shows the comparison the plastic mechanism at the ULS for both the models with Moment-Rotation springs (joints M-R characterization) and the one with Moment-Axial Load springs (joints M-N characterization).

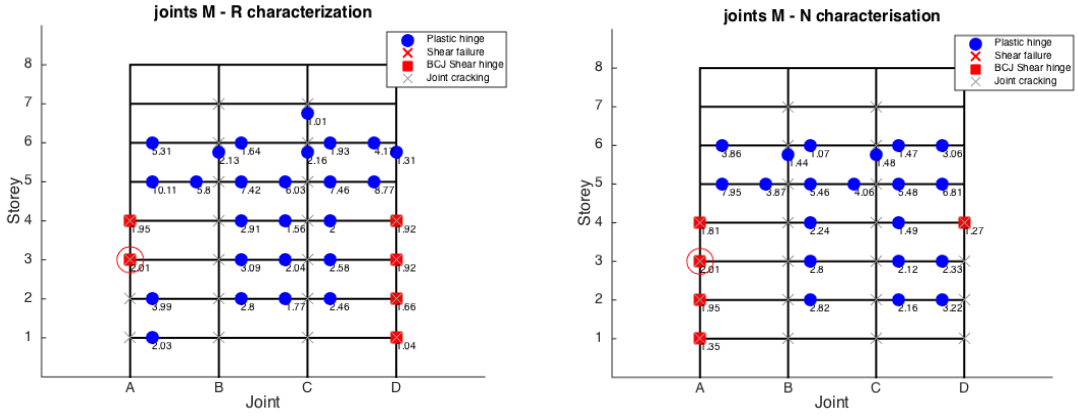

Figure 72: Influence of the axial load variation on the plastic mechanism of Frame 1.

Focusing on joints A1, A2, D2, and D3 it is worth noting that the strength hierarchy changes moving from the MR to the MN model. In fact, for these joints the hierarchy of strength changes if the seismic axial load is considered or not. In particular, for the joint A1 (see Figure 29), after the joint cracking, the hierarchy of strength changes from beam hinge to joint failure if the seismic axial load is neglected or not, respectively. It is noteworthy that this effect does not interest internal columns where the axial load variation due to seismic shaking is negligible.

10. GEOTECHNICAL ASPECTS

Once that the seismic capacity of the superstructure was assessed, the actions transmitted to the foundation during a seismic event can be estimated.

In particular, the shear force transmitted by the beams becomes axial load for the columns that can be estimated as illustrated in the previous sections. Thus at each level of the superstructures there is an axial load variation in the columns due to the seismic shaking. This variation leads to significant changes of the actions transmitted to the foundation, especially at the exterior columns (A1 and D1 in Figure 73). In particular, considering the to push the structural system in the N-S direction (see Figure 73), the axial load in column A1 decreases and axial load in column D1 increases.

A summary of the axial load variation due to the most probable mixed sidesway mechanisms on the lateral resisting systems is reported in Table 27 for both the X and Y load direction along with the yielding moment of the columns at the ground floor. Figure 73 and Figure 74 reports the axial load variation in the X and Y direction, respectively.

Table 27: Summary of axial load transmitted to the foundation

		Seimic action direction X (W-E)		Seimic action direction Y (N-S)	
Column	$N_{gravity}$	$N_{gravity+}N_{seismic}$	$M_{yielding,base}$	$N_{gravity+}N_{seismic}$	$M_{yielding,base}$
[-]	[kN]	[kN]	[kNm]	[kN]	[kNm]
A1	473.2	-214.0	440	-83.0	430
A4	473.2	1274.3	555	-83.0	430
D1	473.2	-214.0	440	1108.3	550
D4	473.2	1274.3	555	1108.3	550
B1 (C1)	946.5	259.2	440	946.5	616
B4 (C4)	946.5	1747.5	n.a.	946.5	n.a.
A2 (A3)	946.5	946.5	616	390.3	430
D2 (D3)	946.5	946.5	616	1581.5	550
B2 (C2, B3, C3)	1893.0	1893.0	616	1893.0	616
Wall web	2623.6	2623.6	n.a.	2623.6	20900
Wall flanges	3396.7	3396.7	18240	3396.7	n.a.
		+ compression - tension		+ compression - tension	

It should be also considered that bending moment and shear are also transmitted by the columns to the foundation. The maximum bending moment transmitted by each column is the yielding moment computed accounting for the axial load variation (see Table 27). Furthermore, a total base shear, about 1760 kN and 3898 kN in the X and Y direction, respectively, is transmitted by the lateral resisting systems.

The actions transmitted by the superstructure can be used to perform the safety checks on the existing foundation system from a structural and geotechnical standpoint, which are out of the scope of this report.

Details of the foundation system are reported in Figure 75.

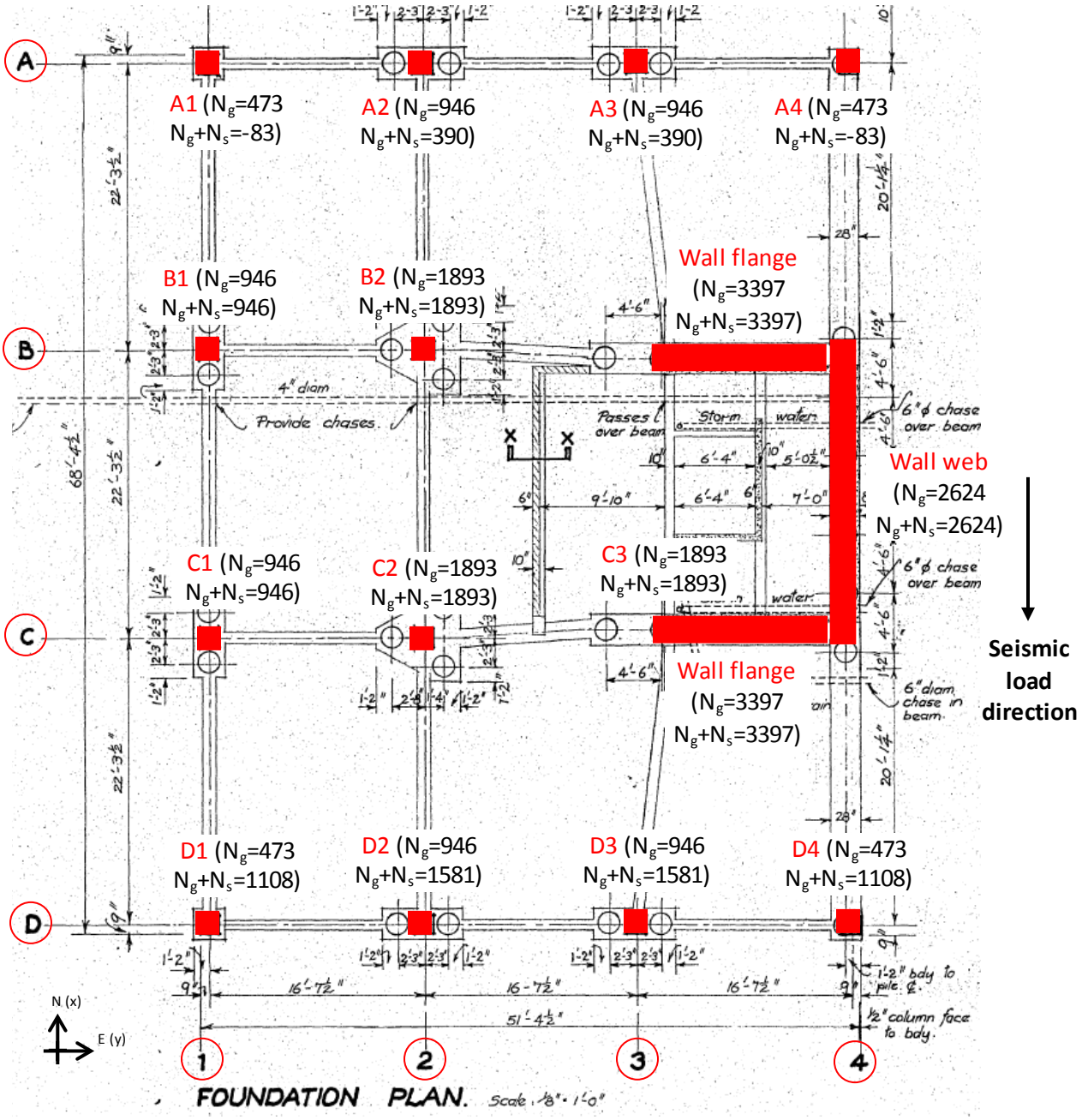

Figure 73: Foundation plan and acting loads in kN (earthquake Y direction N-S).

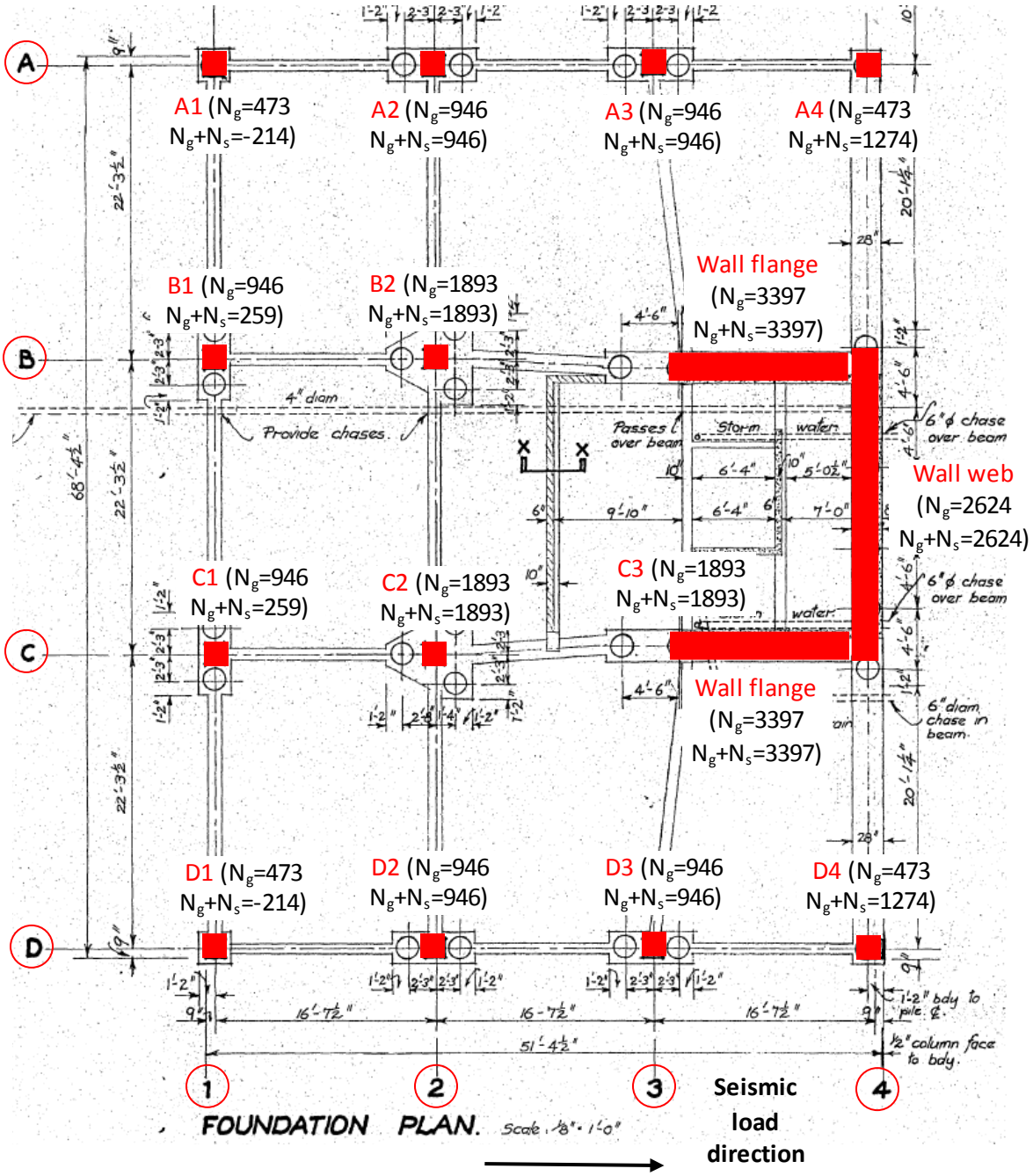

Figure 74: Foundation plan and acting loads in kN (earthquake X direction W-E).

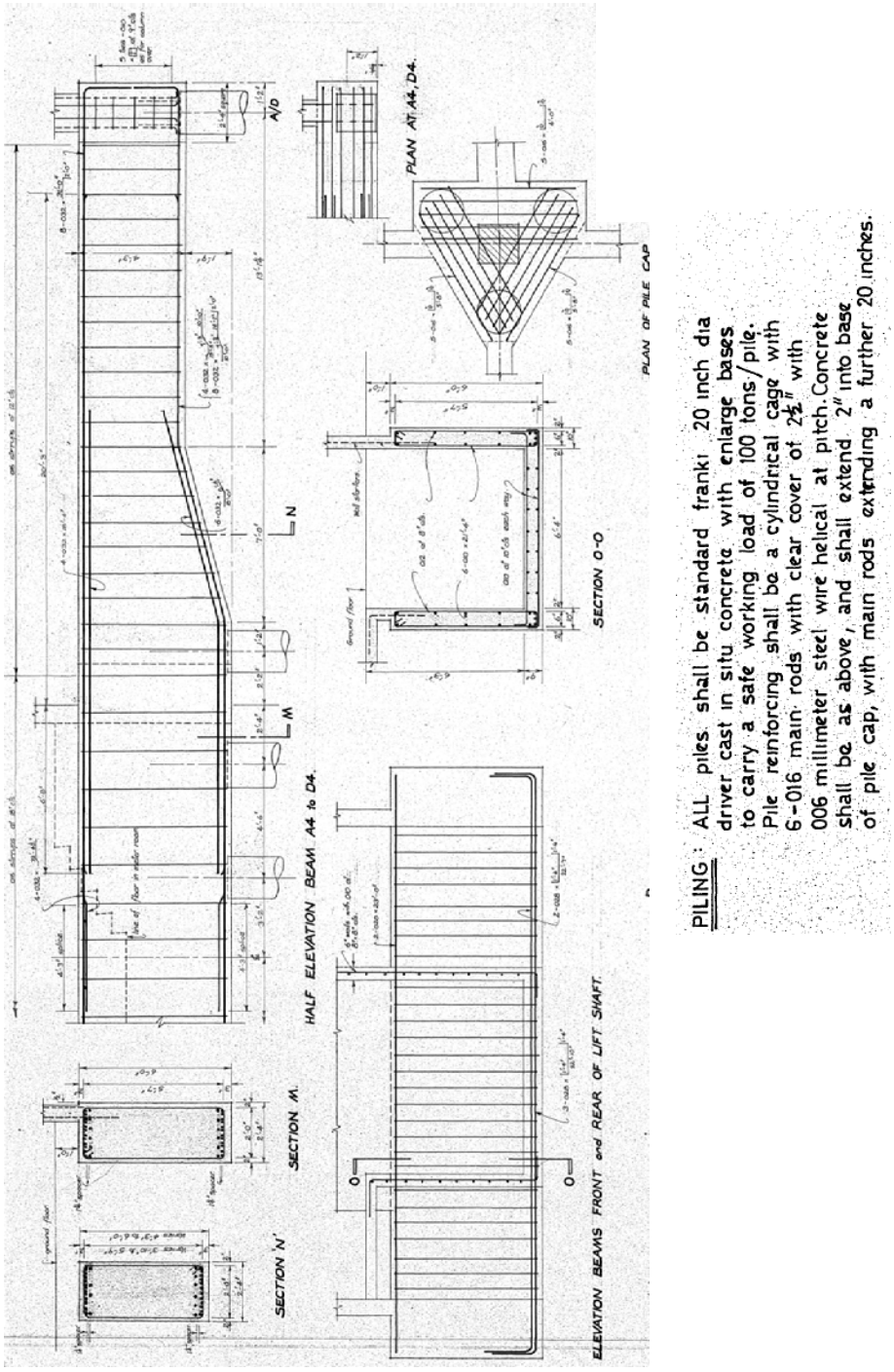

Figure 75: Structural details of the foundation system.

11. CONCLUSIONS

This report presents an example of the implementation of the simplified seismic assessment of a case study reinforced concrete (RC) building following the NZSEE/MBIE guidelines (NZSEE/MBIE 2016c, draft 10 October 2016). The Detailed Seismic Assessment procedure is showed following an overall description of the step-by-step diagnostic process.

The Simple Lateral Mechanism Analysis (SLaMA) is used from component level (beams, columns, wall elements) to subassembly level (hierarchy of strength in a beam-column joint) and to system level (frame, C-Wall) assuming 2D and then incorporating a 3D behaviour.

The effectiveness of the SLaMA approach, as well as the related approximations, are demonstrated through a comparison with a refined 2D numerical pushover analyses for each of the lateral resisting system.

Overall, the SLaMA method is able to well capture the inelastic mechanism and assess the seismic score and seismic rating (based on a %NBS, New Building Standard) with reasonable accuracy when compared to the numerical non-linear pushover analyses.

The outcomes of this study can be summarized as follows:

- The SLaMA proves to be, for this case study building, a simple and reliable tool to calculate the capacity curve representing the lateral response of the lateral resisting systems;

- The predicted capacity curves (corresponding to a mixed sidesway mechanism) and the related structural weaknesses, assessed by means of the strength hierarchy at the subassembly level, well match the observed earthquake damage detected on the case study building. Beam hinging and joint shear failures, clearly observed in the in-situ inspection in the aftermath of the 2011 Canterbury earthquake, are predicted;

- The direct comparison between SLaMA and refined numerical models outlines a satisfactory matching in terms of the pushover curves. SLaMA allows to simply and with satisfactory accuracy predict the lateral response of the frame, the plastic mechanism and the strength hierarchy of the structural subassemblies.

- The 2D capacity curves of the lateral resisting systems are combined to represent the building lateral response. If the torsional effects and the actual eccentricity in the Y direction are neglected the building lateral capacity is taken as the sum of the 2D curves. The %NBS, resulting from the comparison between the capacity curve and the seismic demand, is about 92% and 77% for the X and Y direction, respectively;

- The unbalanced stiffness/strength distribution in plan due to the presence of the C-shaped wall leads to significant torsional effect. The effect of torsion is evaluated with a simplified approach (Method C reported in the NZSEE guidelines). In this case, the %NBS in the Y direction significantly reduces to 59%. However, due to the key role of the strength eccentricity in the assessment of the overall building performance, more refined analysis, are suggested;

- The refined numerical analyses lead to a seismic score of 98%NBS in the X direction and 65% in the Y direction (see Figure 72b). SLaMA leads to more conservative predictions 92% and 59% in the X and Y direction, respectively;

- The step-by-step SLaMA procedure allows to clearly identify the structural systems/members which limit the building seismic capacity. In this example, the seismic performance is limited by the lateral capacity of Frame 1 in the Y direction. In particular, the joint panel extensive cracking is detrimental for the building seismic performances. This may allow to design efficient retrofit solutions targeting the improvement of the seismic capacity of weak members.

Acknowledgments

This study was performed in the framework of the "SAFER Concrete" project, funded by the New Zealand Natural Hazard Research Platform (NHRP) and PE 2014–2018 joint program DPC (Italian Department of Civil Protection) - ReLUIS (Laboratories University Network of Seismic Engineering).

References

Akguzel, U., and S. Pampanin. 2010. Effects of variation of axial load and bidirectional loading on seismic performance of GFRP retrofitted reinforced concrete exterior beam-column joints. *Journal of Composites for Construction* 14: 94–104. doi:1090-0268/2010/1-104.

Akguzel, U., and S. Pampanin. 2012. Assessment and design procedure for the seismic retrofit of Reinforced Concrete beam-column joints using FRP composite materials. *Journal of Composites for Construction* 16: 21–34. doi:10.1061/(ASCE)CC.1943-5614.0000242.

ASCE/SEI 41. 2013. *Seismic Evaluation and Retrofit of Existing Buildings*. American Society of Civil Engineers, Reston, Virginia, US. doi:http://dx.doi.org/10.1061/9780784412855.fm#sthash.ltq5ePWm.dpuf.

Berry, M. P., and M. O. Eberhard. 2005. Practical Performance Model for Bar Buckling. *Journal*

of Structural Engineering 131: 1060–1070. doi:10.1061/(ASCE)0733-9445(2005)131:7(1060).

Bradley, B. A., and M. Cubrinovski. 2011. Near-source strong ground motions observed in the 22 February 2011 Christchurch earthquake. *Bulletin of the New Zealand Society for Earthquake Engineering* 44: 181–194. doi:10.1785/gssrl.82.6.853.

Calvi, G. M., G. Magenes, and S. Pampanin. 2002. Relevance of beam-column joint damage and collapse in RC frame assessment. *Journal of Earthquake Engineering* 6: 75–100. doi:10.1080/13632460209350433.

Carr, A. 2009. Ruaumoko 2D, Nonlinear FEM Computer Program. University of Canterbury, Christchurch, New Zealand.

CEN. 2005. *Eurocode 8: Design of structures for earthquake resistance - Part 3: Assessment and reofitting of buildings*. Brussell: European Committee for Standardization.

Chen, Y. 2015. Evaluation of Simplified Seismic Vulnerability Assessment Procedures for Reinforced Concrete Buildings. ME Thesis, University of Canterbury, Christchurch, New Zealand.

Department of Building and Housing. 2011. *Compliance Document for New Zealand Building Code Clause H1 Energy Efficiency – Third Edition*.

Del Vecchio, C., M. Di Ludovico, A. Balsamo, A. Prota, G. Manfredi, and M. Dolce. 2014. Experimental investigation of exterior RC beam-column joints retrofitted with FRP systems. *Journal of Composites for Construction* 18. doi:10.1061/(ASCE)CC.1943-5614.0000459.

Del Vecchio, C., M. Di Ludovico, A. Prota, and G. Manfredi. 2015. Analytical model and design approach for FRP strengthening of non-conforming RC corner beam-column joints. *Engineering Structures* 87: 8–20. doi:10.1016/j.engstruct.2015.01.013.

Del Vecchio, C., M. Di Ludovico, A. Prota, and G. Manfredi. 2016. Modelling beam-column joints and FRP strengthening in the seismic performance assessment of RC existing frames. *Composite Structures* 142: 107–116. doi:10.1016/j.compstruct.2016.01.077.

Elwood, K. J., and J. P. Moehle. 2005a. Axial capacity model for shear-damaged columns. *ACI Structural Journal* 102: 578–587.

Elwood, K. J., and J. P. Moehle. 2005b. Drift Capacity of Reinforced Concrete Columns with Light Transverse Reinforcement. *Earthquake Spectra* 21: 71–89. doi:http://dx.doi.org/10.1193/1.1849774.

Galli, M. 2005. Evaluation of the Seismic Response of Existing R.C. Frame Buildings with Masonry Infills. IUSS, Pavia.

Kam, W. Y. 2011. Selective Weakening and post-tensioning for the seismic retrofit of non-ductile RC frames. University of Canterbury.

Kowalsky, M. J., and L. A. Montejo. 2007. *CUMBIA—Set of codes for the analysis of reinforced*

concrete members. Raleigh, NC, USA. doi:Tachnical Report IS-07-01.

Kowalsky, M. J., and M. J. N. Priestley. 2000. Improved analytical model for shear strength of circular reinforced concrete columns in seismic regions. *ACI Structural Journal* 97: 388–396. doi:10.14359/4633.

Magenes, G., and S. Pampanin. 2004. Seismic response of gravity-load design frames with masonry infills. *13th World Conference on Earthquake Engineering*.

Mander, J. B., M. J. N. Priestley, and R. Park. 1988. Theoretical stress-strain model for confined concrete. *ASCE Journal of Structural Engineering* 114: 1804–1826. doi:ASCE, ISSN 0733-9445/88/0008-1804.

MI. 2008. *D.M. 14 Gennaio 2008 (D.M. 2008). Technical codes for structures (in Italian)*. GU n°29, F. Rome, Italy.

MOW. 1968. *Ministry of Works, "Code of Practice, Design of Public Buildings."* Office of Chief Structural Engineer, New Zealand.

MOW. 1976. *Ministry of Works and Development New Zealand: "Code of Practice for Seismic Design Public Buildings."* Wellington, New Zealand.

NZS 1170.5. 2004. *Structural design actions, Part 5: earthquake actions—New Zealand - Commentary*. *Standards New Zealand*. Vol. 5. New Zealand.

NZS 3101P. 1970. *Code of practice for the design of concrete structures*. Wellington, New Zealand.

NZSEE. 2006. *Assessment and Improvement of the Structural Performance of Buildings in Earthquakes,*. New Zealand.

NZSEE/MBIE. 2016a. *The Seismic Assessment of Existing Buildings Technical Guidelines for Engineering Assessments. Part A : Assessment Objectives and Principles*. semi-final draft 10 October 2016. New Zealand.

NZSEE/MBIE. 2016b. *The Seismic Assessment of Existing Buildings Technical Guidelines for Engineering Assessments. Part B – Initial Seismic Assessment*. semi-final draft 10 October 2016. New Zealand.

NZSEE/MBIE. 2016c. *The Seismic Assessment of Existing Buildings Technical Guidelines for Engineering Assessments. Part C: Detailed Seismic Assessment*. semi-final draft 10 October 2016. New Zealand.

Pampanin, S., G. M. Calvi, and M. Moratti. 2001. Seismic Behavior of R. C. Beam-Column Joints Designed for Gravity Loads. In *12th European Conference on Earthquake Engineering*, ed. Elsevier Science Ltd, 726:1–10.

Pampanin, S., G. Magenes, and A. Carr. 2003. Modelling of Shear Hinge Mechanism in Poorly Detailed RC Beam-Column Joints. In *fib 2003 Symposium "Concrete Str. in Seism. Reg.", May 2003. Paper n. 171*.

Pampanin, S., W. Y. Kam, U. Akguzel, A. S. Tasligedik, and P. I. Quintana Gallo. 2012. *Seismic Performance of Reinforced Concrete Buildings in the Christchurch CBD in 22 February 2011 Earthquake Part II : Damage Observation*. Christchurch, New Zealand.

Paulay, T. 2001. Some design principles relevant to torsional phenomena in ductile buildings. *Journal of Earthquake Engineering* 2469. doi:10.1080/13632460109350395.

Paulay, T., and M. J. N. Priestley. 1992. *Seismic design of Reinforced Concrete and masonry buildings*. U.S.A.: John Wiley & Sons, Inc.

Priestley, M. J. N. 1997. Displacement-based seismic assessment of Reinforced Concrete buildings. *Journal of Earthquake Engineering* 1: 157–192. doi:10.1080/13632469708962365.

Priestley, M. J. N., R. Verma, and Y. Xiao. 1994. Seismic shear strength of reinforced concrete columns. *ASCE Journal of Structural Engineering* 120: 2310–2329.

Priestley, M. J. N., G. M. Calvi, and M. J. Kowalsky. 2007. *Displacement-Based Seismic Desing of Structures*. IUSS press. Pavia, Italy.

Tasligedik, A. S., U. Akguzel, W. Y. Kam, and S. Pampanin. 2016. Strength Hierarchy at Reinforced Concrete Beam- Column Joints and Global Capacity Strength Hierarchy at Reinforced Concrete Beam-Column Joints and Global Capacity. *Journal of Earthquake Engineering* 0. Taylor & Francis: 1–34. doi:10.1080/13632469.2016.1233916.